Predictive Quality Modelling of Polymer and Metal Parts Fabricated by Laser-Based Manufacturing Processes

Hamed Sohrabpoor B.Sc. (Hons.)

A thesis submitted for the degree of

Doctor of Philosophy

from

Dublin City University,

School of Mechanical & Manufacturing Engineering,

Supervisor: Prof. Dermot Brabazon of Dublin City University

Co-supervisor: Dr. Inam UI Ahad

September 2019

Declaration

I hereby certify that this material, which I now submit for assessment on the programme of study leading to the award of PhD, is entirely my own work, and that I have exercised reasonable care to ensure that the work is original, and does not to the best of my knowledge breach any law of copyright, and has not been taken from the work of others save and to the extent that such work has been cited and acknowledged within the text of my work.

Signed: _____ (Candidate) ID No.: 15211674 Date: 26/09/2019

Publication Declaration

Supplementary to the previous declaration, I hereby declare that this thesis contains information from three original manuscripts published in peer-reviewed journals and one currently under preparation for submission. The theme of this thesis is the modelling and optimization of laser based in additive manufacturing processes. To that end, investigations into the polymer processing via laser ablation were performed first, which formed a preliminary process modelling basis for the work.

The ideas, direction and implementation of the research, and authorship of the manuscripts were entirely the work of myself while a student in the School of Mechanical and Manufacturing Engineering under the supervision of Prof. Dermot Brabazon.

The inclusion of co-authors reflects the fact that this work was produced while working in a dynamic, multi-disciplinary research group with input from the various group members at all stages. This inclusion does not prejudice my contribution but rather highlights the collaborative spirit of the members of the Advanced Processing Technology Research Centre, Irish Separation Science Cluster and National Centre for Plasma Science and Technology.

With regards to Chapters Two, Three, Four and Five, my contribution to the resulting publications were the following:

Chapter	Publication Title	Publication Status	Candidate's Contribution
2	Development of Laser Processing Technologies via Experimental Design	Published, Chapter book in Advances in Laser Material Processing, Elsevier,	First author, literature data collection and analysis, primary manuscript author.

		Woodhead Publishing (2017)	
Chapter	Publication Title	Publication Status	Candidate's Contribution
3	Optimizing selective laser sintering process by grey relational analysis and soft computing techniques	Published, Optik - International Journal for Light and Electron Optics 174 (2018) 185–194	First author, data collection and analysis, primary manuscript author.
4	Improving precision in the prediction of laser texturing and surface interference of 316L assessed by neural network and adaptive neuro-fuzzy inference models	Published, The International Journal of Advanced Manufacturing Technology (2019)	First author, experiment design, data collection and analysis, primary manuscript author.
5	Selective laser melting: an alternative approach for the manufacturing of 316L stainless steel press-fits	Under submission,	First author, experiment design, data collection and analysis, primary manuscript author.

Signed: _____ (Candidate) ID No.: 15211674 Date: 26/09/2019

Mr hamed sohrabpoor

Signed: _____ Date:

Prof. Dermot Brabazon

List of Publications

1. H. Sohrabpoor, S. Negi, H. Shaiesteh, IU. Ahad, D. Brabazon, Optimizing selective laser sintering process by grey relational analysis and soft computing techniques, Optik 174, 185-194.
2. H. Sohrabpoor, A. Issa, A. Al Hamaoy, IU. Ahad, E. Chikarakara, K. Bagga, D. Brabazon, Development of Laser Processing Technologies via Experimental Design, Woodhead Publishing (2017).
3. H. Sohrabpoor, RT Mousavian, M. Obeidi, IU. Ahad, D. Brabazon, Improving precision in the prediction of laser texturing and surface interference of 316L assessed by neural network and adaptive neuro-fuzzy inference models, The International Journal of Advanced Manufacturing Technology, 1-10.

Acknowledgments

First and foremost, thank you to Prof. Dermot Brabazon for your guidance and encouragement throughout the last four years. You constantly pushed me to be a better student, and I have learnt much about how to be a researcher, a scientist and an engineer from you for which I am very grateful.

Besides my supervisor, I would like to thank all of members in APT and I-Form group, for the excellent research atmosphere. Their insightful comments incentivized me to widen my research from various perspectives.

Also, I would like to thank the technical staff in DCU workshop and labs especially Mr. Michael May, Mr. Liam Domican, Mr. Christopher Crouch, Barry O'Connell and Mr. Eoin Touhy for their support to facilitate the experimental work.

I would also like to acknowledge that this research was part funded from Science Foundation Ireland (SFI) under Grant Number 16/RC/3872 and co-funding from the European Regional Development Fund, and by the Irish Research Council Government of Ireland Scholarship.

Table of Contents

List of Figures

List of Tables

Predictive quality modelling of polymer and metal parts fabricated by laser-based manufacturing processes

Hamed Sohrabpoor

Laser processing techniques are widely used in industrial applications for their repeatability and reliability. However, the optimization of a laser process for a specific application is challenging and require detailed experimental investigations to determine the input processing conditions and parameter values that deliver high repeatability and reliability. The objective of this doctoral work was therefore to develop prediction models for laser-based processing techniques to understand the laser processing parameter relationship with the output properties and to forecast events not observed experimentally. The important techniques of Selective Laser Sintering (SLS), Laser Surface Texturing (LST),and Selective Laser Melting (SLM) were selected for development of the predictive models.

For SLS of glass filled polyamide parts, an Adaptive Neuro-Fuzzy Inference system using Simulated Annealing method (ANFIS-SA) and Grey Relational Analysis (GRA) were utilised to determine processing parameters (laser power and scan speed, spacing and length) delivering best mechanical properties (tensile strength and elongation). ANFIS-SA system outperformed the GRA in finding optimal solutions for the SLS process applied for glass fiber reinforced part production.

For LST study, Artificial Intelligence (AI) models were developed to predict the properties (diameter increase, insertion force and pullout force) of laser processed stainless steel 316 samples used for interference fit. Artificial Neural Network (ANN) and ANFIS were used to predict the characteristics of laser surface texturing. The models based on feedforward neural network (FFNN) were used to examine the effect of the laser process parameters for surface texturing on 316L cylindrical pins. This study demonstrated that ANFIS prediction was 48% more accurate compared to that provided by the FFNN model.

Stainless steel 316L cylindrical pins with defined surface structures for interference fit application were manufactured by the Selective Laser Melting Additive Manufacturing technique. The fabricated pins were assessed for resulting bond strength within interference fit joints. The effects of texture profile on the insertion and removal forces were investigated using Box-Behnken design of Response Surface Methodology (RSM) and results are presented and discussed. ANalysis Of VAriance (ANOVA) was used to check the adequacy of the developed empirical relationships. Two quadratic models were generated. One for correlation between profile geometry and insertion force and second for relating the profile geometry to removal force. The models were validated using experimental results and demonstrated good agreement with less than 10% error.

Chapter 1

Introduction

1.1. Introduction of laser and its application in industry

The term “Laser” is the abbreviation of Light Amplification by Stimulated Emission of Radiation. Laser technology is at the centre of the vast area of photonics, due mainly from its many specific features including well-guided light emission allowing the heating of a targeted area. Unlike most lamps which emit light beams with a wide optical spectrum, lasers have narrows optical wavelengths.

Lasers can be operated as continuous or pulsed beam emission with pulse width commonly variable form femtoseconds to microseconds. The intensity of laser beam can be controlled more easily compared to other sources of energy. These features make the laser vey functional compared to traditional manufacturing process.

The laser has great variety of applications in manufacturing such as drilling, texturing, machining, welding, cladding, cutting and recently in fabrication of sophisticated parts via metal Additive Manufacturing.

1.2.Introduction of SLS and SLM

In the Selective Laser Sintering (SLS) process, the laser employed to melt polymer powders. In order to reduce the thermal distortion, the polymer powder bed should be heated to below the melting point of the material. After that, each layer is sintered with the laser for binding the material. The melted powder shapes the part produced and the un-sintered powder can act as a support to the built parts.

In Selective Laser Melting (SLM), with the use of a Nd:YAG or fibre laser, metal parts are produced. The process is almost same as SLS except instead of polymer, metal powder has been used and higher energies are required for melting the metal. SLM can be used to manufacture samples with very complex designs. This technology represents a realistic alternative to many conventional manufacturing techniques. It has been well shown that SLM allows the fabrication of near full-density high-resistance metallic components via fusion and re-solidification of the fine metallic powders.

1.3. Challenges in laser-based additive manufacturing from modelling perspective

Although the laser-based additive manufacturing process is considered as a new industrial revolution of fabrication of parts, there are some challenges in regard to modelling and optimization. Some common challenges contain inaccuracy in the geometry, and undesirable surface texture. All these disadvantages can be significantly address by better understanding the limitations of this process.

In development of SLS and SLM, controlling of output parameters is very challenging. Because of the inferencing of many input parameters and process noise, finding the most important factors is difficult. Achieving an approximate model/ equation for each process can play a significant role in reducing the process cost and in saving time and energy. The next challenge is to select the most accurate model for each specific process. Hence, in order to determine the laser-based manufacturing process parameters which are suitable for specific needs in terms of material, tightness level, applied and removal force, and reliability, artificial intelligence approaches can be further examined and investigated.

Also, different types of optimisation need to match with the specificities of laser-based manufacturing process. As this process generates a complex network of 3D geometries, numerical and intelligent models need to combine the results from fabricated parts in the analysis.

1.4. Use of predictive modelling techniques in industry

Artificial intelligence technology is now making its way into manufacturing, and the machine-learning technology could hold the key to transform factories in the near future. While AI is poised to radically change many industries, the technology is well suited to manufacturing. AI will perform manufacturing, quality control, shorten design time, and reduce materials waste, improve production reuse, perform predictive maintenance, and more

Approximation methods which are related to artificial intelligence are secondary tools which use data generated through experiments for estimation of the manufacturing process outputs

In this thesis work, various type of simulations was employed to generate a mapping relationship between the process factors and the experimentally observed responses. In order to achieve the best mechanical characteristics, the acquired model was developed with the simulated annealing algorithm as an objective function. Grey relational analysis (GRA) as a multi-response optimization technique was also applied to evaluate which modelling technique could perform best for defining the process elements to obtain the highest mechanical properties.

1.5.Motivation

This doctoral project was focused on the development of predictive models for the laser sintering and texturing process. Laser processing is a mature method, developed over several decades and used widely in industry due to the reliability and repeatability of the process. However, laser mater interaction in the SLS/melting and texturing processes is a more complex phenomenon and involves a number of physical and chemical processes such as heat transfer, breaking and building of chemical bonding, plasma creation, melting and solidification occur.

In order to predict the behaviour of the laser sintering process for future or unknown conditions, the existing laser sintering results must be examined in detail to generate

new information. This information can be further processed by different machine learning and artificial intelligence techniques. Predictive modelling techniques can be used to understand different patterns available within large sets of data.

Due to inherent non-linear relationship between the laser sintering/melting processing parameters and final part properties, standard empirical functions cannot be used to develop predictive models.

The development of predictive modelling defines the process of developing a model in a way that we can understand and quantify the model's prediction accuracy on future, yet-to-be-seen data [1].

The prime motivation of this doctoral project was to develop accurate predictive models for the laser sintering and texturing processes. Beside accurately predicting the further results, the developed predictive models should also help to interpret the process and behaviour of different output parameters and their dependencies on input processing parameters. The developed models should also help to better and further understand the overall laser sintering/melting and texturing processes.

However, in order to develop models with higher accuracies, the models inherently became more complex and it becomes more difficult to interpret them. The simulation runs of these models then require higher processing capabilities and longer run times. [2].

In the product design phase, the tolerances in the geometry of the produced part are set according to manufacturing process capability and final part functionality requirements.

In Additive Manufacturing (AM), the automation and digital control of physical processes currently still results in geometrical inaccuracies of the produced parts. This problem of geometry control in AM is a significant challenge in designing of AM produced products, particularly in setting required and achievable tolerance levels. Predictive modelling can be used to address shape deviation problem which is critical and challenging in AM. [4].

Unlike other manufacturing processes, AM defects' analysis and modelling are not mature yet [5]. The research field is still in its infancy, but it benefits from the maturing age of data mining and analytics and machine learning techniques and their successful applications in many engineering domains. With increasing volumes and varieties of data, machine learning has gained extraordinary popularity due to its ability to explore complex patterns in observed data and make data-driven predictions or decisions on new data.

1.6. Research objectives

The aim of the thesis was achieved through a number of objectives:

1. The identification of best method for the optimization of the SLS process of glass filled polyamide parts.

2. Finding the best soft computing technique which can predict the results of the laser surface texturing process.

3. Finding the effect of the input parameters on responses of laser surface texturing of 316L stainless steel press-fits.

4. Fabrication of press-fit texture with new manufacturing approach with better output specification compared to traditional methods.

5. Finding the highest insertion and removal forces through mathematical modelling method.

1.7. Overview of work and thesis structure

This thesis is comprised of six chapters: chapter 1 introduced this work and provides context for the following chapters. Chapter 2 will present an introduction to the theory and core-concepts of modelling and optimization techniques, including Design of Experiments (DoE). Chapter 2 will present an introduction to theory and basic definition of laser surface modification. The reason behind utilising of optimization

approaches are also presented. Then, general guidelines for conducting the DoE explained. Finally, some approaches related to non-conventional methods are presented.

Chapter 3 is focused on advanced modelling and optimization methods developed for obtaining the best mechanical properties of and additive manufacturing process, selective laser sintering, which manufactured glass filled polyamide parts. In order to achieve best mechanical characteristics, the acquired model was used by simulated annealing algorithm as an objective function. Grey relational analysis (GRA) as a multi-response optimization technique was also applied to evaluate which modelling technique could perform best for defining the process elements to obtain the highest mechanical properties.

In chapter 4, two machining learning approaches, artificial neural network and adaptive neuro-fuzzy inference system were used to predict the characteristics of laser surface texturing of interference fit joints. The reliability of the aforementioned models for the output prediction of the laser surface texturing system were investigated by using the data measured from experiments.

In chapter 5, following up to previous chapter, a new approach for the first time introduced for the fabrication of 316L stainless steel press-fit by an additive manufacturing technique, selective laser melting. Also, mathematical models derived from Box-Behnken designs were extracted in order to model the process and investigate the effect of texture geometry on the insertion and removal forces.

References

1. Z. Zhu, N. Anwer, Q. Huang, L. Mathieu, Machine learning in tolerancing for additive manufacturing, CIRP Annals - Manufacturing Technology 67 (2018) 157–160.

2. Cheng L, Wang A, Tsung F (2018) A Prediction and Compensation Scheme for In-plane Shape Deviation of Additive Manufacturing with Information on Process Parameters. IISE Transactions 1–13.

3. Shao C, Ren J, Wang H, Jin JJ, Hu SJ (2017) Improving Machined Surface Shape Prediction by Integrating Multi-task Learning with Cutting Force Variation Modelling. Journal of Manufacturing Science and Engineering 139(1):011014.

4. Huang Q, Nouri H, Xu K, Chen Y, Sosina S, Dasgupta T (2014) Statistical Predictive Modelling and Compensation of Geometric Deviations of Three-dimensional Printed Products. Journal of Manufacturing Science and Engineering 136(6):061008.

5. Moroni G, Petrò S, Polini W (2017) Geometrical Product Specification and Verification in Additive Manufacturing. CIRP Annals — Manufacturing Technology 66(1):157–160.

Chapter 2

EXPERIMENTAL DESIGN AND PREDICTIVE MODELLING OF LASER PROCESSING TECHNOLOGIES – LITERATURE REVIEW

Related book chapter published:

Hamed Sohrabpoor, Ahmed Issa, Ahmed Al Hamaoy, Inam Ul Ahad, Evans Chikarakara, Komal Bagga, Dermot Brabazon, Chapter 24, Development of laser processing technologies via experimental design, In: Advances in Laser Materials Processing, 2nd Edition, 2018, pp. 707-730, Ed. J. Lawrence, Elsevier, Woodhead Publishing, ISBN 978-0-08-101252-9.

Published status: Published

2.1. Introduction

Laser light can be monochromatic, focused and coherent. This means photons with single wavelength, in a coherent beam shape can be focused (diverge) to a small area. These three major properties of laser light make it attractive for material processing with high degree of repeatability and reliability. The laser light sources are widely used in manufacturing industry for cutting, drilling, welding, cladding, soldering (brazing), hardening, ablating, surface treatment, marking, engraving, micromachining, pulsed laser deposition, lithography, etc. Very high-powered optical intensity photon beams can be applied to a very small spot (few micron diameter). In this way, an intense amount of heat can be transferred to the material for melting, evaporation or plasma formation. As mentioned above, the process can be controlled by using high spatial coherence of laser light. This enables achieving a highly focused process spot. Additionally, laser light can be produced in pulsed or continuous mode, allowing for different types of laser material interaction. However, the material being processed by the laser and environmental conditions influence the laser processed part properties. Therefore, detailed investigations are needed to fully characterize and optimize any laser process for specific application and material. As laser processing parameters can be controlled to a very high degree and material and processing conditions can also be changed, both experimental and simulation-based studies can help to optimize the process, predict outcome of different conditions and help to understand the underlying physical phenomenon.

This chapter provides a comprehensive overview of design methodologies for laser processing experimental work and major modelling techniques used in the literature for prediction of outcomes for different processing conditions.

2.2. Laser material interaction

For many decades, the surface properties of materials have been enhanced by different coatings and surface modification techniques to meet component operational environments. This includes requirements for component life times when subjected to

for example defined temperature, wearing or fatigue conditions. In order to enhance the surface properties over conventional techniques, such as flame hardening and carburizing, advanced techniques such as electron, ion, plasma and laser processing have been developed. Nowadays lasers with high energy density are commonly used in surface modification techniques.

Laser Surface Modification (LSM) can be defined as any laser material process that modifies one or more of the surface properties, with or without adding additional material. These processes are employed to modify or introduce certain desired physical and chemical properties of a material such as surface chemical composition or the surface morphology [1]. Such modifications have been applied for metals, polymers and ceramics [2]–[7].

Scientists classify LSM either according to the modification type (hardening, glazing, texturing, shocking etc.) or according to the processing temperature (heating, melting, or plasma). In this chapter a review of methods for the experimental development of laser processing is presented. Specific examples are presented for Laser Cladding, Laser Surface Melting, and Laser Shock Peening.

Laser surface heat treatment is a non-melting process, whereas in laser surface melting, the melting takes place in a thin layer which therefore solidifies rapidly forming a harder structure. During laser shock peening (LSP), surface compressive residual stress is imparted to the material via the shock waves from the laser processing. In laser cladding, the laser beam melts the metal surface while a second material is introduced to the surface. Examples of optimization of each of these types of laser processing techniques will be discussed later in this chapter. Before this, in the following sections, an introduction is given to experimental design methods for laser process optimization.

2.2.1. Selective Laser Sintering

Selective Laser Sintering (SLS) is a common Additive Manufacturing (AM) technique in which the sintering of polymer powder material is performed using a laser source.

This technique utilizes two heating sources to perform 3D printing of the parts. The first source is used to preheat the powder close to the melting transition temperature of the material. Afterwards, selective (localised) laser sintering of the powder particles is performed to fuse powder together. Preheating of the powder helps to reduce the large thermal differentials that often result in part distortion and defects. SLS has decades long history of development in terms of materials and process development, challenges remain in producing parts with high dimensional accuracy that suffer from curling, distortion and warpage [8].

2.2.2. Selective Laser Melting

Selective Laser Melting (SLM) is a metal Additive Manufacturing technique used for 3D printing of metals for applications in aerospace, automation, medical and other high-tech industries. As noted in the literature, SLM is the most versatile technique that can process wide range of metallic materials comparing to any other AM technique such as Electron Beam Melting, Direct Energy Deposition, Laser Engineered Net Shaping (LENS) and Binder Jetting (BJG) [9]. Briefly, a layer of metal powder is spread on build plate and laser is focused onto the material according to 3D CAD model and laser scan strategy. The heat energy from the laser beam melts the powder and fuses the metallic powder together.

Unlike SLS process, in which powder is sintered, in SLM, the powder is fully melted, and a solid three-dimensional part is formed. The nature of SLM process is complex and a number of conditions (feedstock properties, processing environment and laser processing parameters) influence the outcome of the material. The variations in these processing conditions induce different variations and influence the part final geometry. Therefore, process optimization studies need to be perform to develop an optimized process for specific materials.

2.3. Introduction to process optimization

2.3.1. Process optimization techniques

Ever since the advent and availability of lasers, their advancement has heavily relied on experimentally examining the effect of different process parameters on the material of interest. This has allowed an in-depth understanding of the lasers' effects and interactions with the various materials.

The ultimate goal of studying the laser processing of materials is to optimise the process in terms of single or multiple objectives. **Optimization** in this context can be defined as mathematically or statistically modelling the laser process in order to obtain desired/best response based on the process parameters. Therefore, it requires identifying the process **input (control)** parameters and the process **output (response)** parameters. Optimization can be performed for single or multiple response parameters. These parameters can be either quantitative or qualitative depending on the research objectives. To this end, researchers rely on either experimental or simulation works or a combination of both to optimise laser processes.

Experiments are used extensively to optimise the process owing to the high degree of complexity in thermal mathematical models attempting to describe such processes and the multiple parameters and their possible interactions, governing the laser material interaction. Therefore the fundamental physical simulations are often time consuming and cost intensive [10], [11]. The exercise of **experimental modelling** of the laser processes is based on statistically studying the effects of varying the process input parameters on the process response parameters through conducting specifically planned experiments. This method is more commonly known as Design of Experiments (DoE). In application of this method, prior understanding of the process allows suggestion of the most appropriate process input parameters for investigation. The DoE usually starts with screening experiments aimed to identify if a suggested process input parameter has a significant effect on the response or not. During this stage, varying one parameter at a time or a factorial design of experiments can be used

for detecting the potential interactions between the parameters. Important conditions should be observed for selection of an input parameter. The input parameter should be independent, controllable, and should have a significant effect on the response. The response parameters choice also relies on prior knowledge and experiences or on the objectives of the study. The main condition of selecting the response parameter is that it should be quantitatively or qualitatively measurable [12].

2.3.2. Design of Experiments (DoE) for Laser Processing Methods

2.3.2.1. General guidelines for conducting DoE

Design of Experiments (DoE) is a systematic method for statistically modelling a process in order to get a mathematical/empirical relationship between the process parameters and the responses [13]. The process of coming up with a finalised DoE is an iterative one. It comprises of several decisions, revisions and simplifications. The experimenter must keep in mind that study conclusions or models of a process are not universal. They are, however, applicable for the investigated range of process conditions; such as process setup, parameters, study material, and model type etc. Therefore, the investigator should aim, when selecting the study objectives, to simplify these conditions as much as possible and select those that are controllable and repeatable. The investigator must spend a considerable amount of time and effort in planning for the intended DoE to ensure success. The seven stages involved in decision making, planning and performing the DoE are as follows [14]–[18]:

1- Define the objectives of the experiment. To simplify the experiments and the analysis, this list should only involve precise questions that are to be addressed. An example of that would be to determine the correlation (if any) between laser beam power and cutting speed as parameters of a laser cutting process, and whether they influence the heat affected zone [19]. Furthermore, the objectives may need to be refined a number of times as the remaining planning steps are completed.

2- Identify all sources of variation, which are basically anything that when changed could influence the “observation” or “process response”. Some variation sources have a major effect on the process response “treatment factors” or often called “process parameters”. As an example, a laser drilling process parameter could be the laser beam depth of focus [20]. The process parameters and their levels from minimum to maximum should be selected. The levels of a process parameter should be laid out equally spaced for easy retrieval of the results and conclusions. Laser processes usually involve more than one process parameter. The experiments are called, in this case, a factorial design of experiment. This implies that the process responses are measured based on some combination of the levels of the various process parameters.

On the other hand, some variation sources have minor effects on the response that are called “nuisance factors”. The effects of these factors are of no interest to the investigator. As an example, the glass sample thickness in the laser microchannel fabrication process [21]. Therefore, it is usually decided to fix the nuisance factors and perform the experiments at these fixed values. Alternatively, the nuisance factor is fixed, and the experiments are performed and repeated for a second fixed value of the nuisance factor, and a third fixed value and so on, which is called “blocking”. This could minimise the effect of these factors on the response. A noteworthy point about nuisance factors is that they are not always controllable. An example of a controllable nuisance factor could be the operator performing the experiments. Even if they are following strict procedure, in statistical terms, variability in the results may arise from changing the operator. An example of an uncontrollable nuisance factor could be variations in properties among batches of the study material. In laser processing, the surface finish of a material to be processed is a good example. If blocking is to be used in the latter case for minimizing the nuisance factors effects, enough material should be at hand for performing each block of experiments.

The third variation factor that can be considered in studying laser processes is the “study material”. This is the workpiece treated by the combinations of laser process

parameters to induce the measurable process responses. The main consideration with the selection of the material is that it should be representative of the process objectives to be concluded. This sets a limit on the scope of the study results and objectives, which may be revised.

Finally, the decision whether a variation factor is a process parameter, or a nuisance factor is made by the investigator and depending on the process under study. It is important to note during the decision-making regarding selection of parameters that more process parameters involved in the study may complicate the analysis without providing any added value or increasing the accuracy of the model.

3- At this stage the type of DoE design is selected. This means that the way and combinations of process parameters will be assigned to the selected samples for laser processing in order to obtain process responses. This influences the number of experiments needed to analyse the process and obtain an understanding of a model. The decision here includes whether the design will have the blocking factors or not. There are several types of DoE designs, such as the Factorial Design, the Fractional Factorial Design, Response Surface Methodology (RSM) such as the Central Composite Design (CCD) and Box-Behnken Design (BBD). The reader is advised to read the previous studies [14]–[18] in order to gain knowledge of which DoE design suits most of their objectives. However, many investigators start theirs studies with a simple general Factorial Design. This is suitable if investigators have a few process parameters examined at limited number of levels. At a later stage, when more knowledge about the process is acquired, a more focused investigation can be carried out. In this case, Fractional Factorial or RSM designs can be used at more parameter levels without increasing the number of experiments needed. For a given design, there is an important rule, which is to eliminate bias by randomizing the experimental runs. Experimental samples of the material should be taken and assigned randomly to each combination of the levels of the process parameters. This is required to ensure that the

responses are not subject to- or affected by- uncontrollable sources such as the experimenter bias.

4- At this stage, decisions associated with the process response parameters have to be made. These may include; the units of the response parameters, the measurement methods and the equipment, the measurement accuracy, precision and resolution, and the procedure for preparing a sample measurement. Process response parameters are usually suggested at an earlier stage. However, some difficulties may arise prohibiting/restricting the ability of data collection or measurement. This requires running a few pilot experiments to investigate some of the difficulties involved in the data collection. This may result in the need for modifying or rectifying the selection of the response parameters or the procedure of the data collection. The pilot experiments will also assist in coming up with a systematic/strict procedure to be followed by the experimenters throughout the DoE practice. This systematic procedure can take the form of a data collection sheet that shows the conditions and the sequence in which the responses are to be recorded. The study objectives may be revised at the end of this step to simplify the experimental procedures.

5- As explained in the previous steps, a pilot experiment may need to be performed. A few observations can be made without expecting any conclusions. The main idea is to practice the experimental procedures and to check for difficulties that may arise during carrying out an experiment or in data collection. Revisions and necessary changes of the all previous decisions can be made after examination of the pilot experiments results.

6- The process model type is selected, with the aim that it will best represent the extent of the relationship between the process parameters and the response parameters. The selected model should enable the investigator to mathematically define this relationship. The analysis techniques employed to derive a model are statistical in

nature. These techniques will be applied to the collected data and will depend on the selected model type. The most commonly used model is the linear model. This model attempts to describe the process response parameter in terms of a linear combination of process parameters plus an error resulting from all minor sources of variations. A quadratic or curvilinear model is preferred in order to better fit and understand the relationship between the process input and output parameters and the results obtained.

7- Finally and before proceeding to perform the full set of experiments, some final revisions of the previous decisions can be performed that are necessary to simply and increase the accuracy of the model. These revisions might be aimed to reduce the number of experiments or to narrow down the ranges of the selected parameters. Once the experimental design is ready, experiments and data collection may commence which provide the data for analysis and process model derivation.

2.3.2.2. Software used for DoE

It should be noted that several available software packages are designed to assist researchers throughout the DoE exercise including planning, analysing, and optimizing the process. These include State-Ease Inc., Design-Expert [22], SAS Institute Inc., JMP [23], and Minitab [24]. These software packages provide a user-friendly interface equipped with 2D and 3D graphical representation of the results. Once a process model (mathematical or empirical) is derived, it can be used to draw an operational map of the process in terms of its parameters. It can also be employed to predict the responses for a given combination of process parameters within the investigated range by performing the simulations of the designed model. It is advisable that the model is validated by performing some validation experiments and checking the accuracy of the model predictions. After the process model is obtained, further optimization can be performed by performing a new DoE with more closely defined zone of investigation and ranges of process parameters. The aim of optimization studies is thus to find the values of the process parameters that produce the optimal

process response. In practice, that means; output minimising, maximizing, or producing a specific multi-modal optimization of process response.

2.4. Optimization based on mathematical simulations

On the other hand, other researchers rely mainly on computerized thermal simulations to optimize laser processes and conduct some experiments to iteratively-modify or validate their models' predictions. When the simulation model is ready and validated, it provides an inexpensive opportunity for optimizing the process [25], [26]. **Simulation models** can be used to provide analytical and/or numerical solutions. The results of these simulation can be used to predict the effects of various forces and energy fields induced by the laser irradiation of the materials. These models are commonly known as Mathematical Models. These models generally treat laser as a heat source. The laser effect on the material is modelled based on a single or a combination of different processes. The energy from the laser source is transferred to the workpiece by convection, direct radiation heat transfer, or conduction or combination of all of these processes. This allows simulation and prediction of heat generation and the progression of energy transfer in the material leading to subsequent heating, melting and evaporation [13], [25], [26].

Despite the two main schools of optimization research, experiment and simulation, many researchers find it very efficient and reliable to combine both types of studies. Therefore, the experimental studies are performed in order to directly understand process parameters effects allowing control of process outcomes. The simulation models are used to support knowledge gain and give deeper understanding of the physical behaviour leading to the experimental results. These models also allow comparing and validating the experimental findings. This type of comparative/augmented studies constitutes majority of the reported studies on laser process optimization.

Response Surface Methodology (RSM) was also used in a study of laser microchannel fabrication process in the works of Issa [21], where a pulsed CO_2 laser (1.5 kW, 10.6 μm) was used to fabricate microchannels in soda-lime glass samples of a fixed 2 mm thickness. The microchannel dimensions, surface roughness and morphologies were studied in terms of the laser processing input parameters (laser beam power, pulse repetition frequency, and scanning speed) using RSM. The collected results were also used to study the effects of the process parameters on the material's volumetric and mass ablation rates. Results from the RSM model in this study were also compared to simulated results from a thermal mathematical model [21].

2.5. Experimental and simulation-based methods- A brief comparison

2.5.1. Advantages with experimental methods

- Little prior knowledge regarding laser physical interaction with the material is required.
- Quicker results for analysis.
- Model is highly relevant to results from the investigated regions of process parameters.
- Experimental results can be used directly to identify possible industrial applications.

2.5.2. Challenges with experimental methods

- Experimental model adequacy depends on the repeatability and reliability of the process setup, accuracy of process control, governance of experimental conditions, variability in batch-material properties, stability of laser source parameters, measurability of parameters and accuracy of measurement methods.
- They are not always labour- and cost-effective.
- They do not provide deep insights to the physical phenomena underlying the process.
- They are only suitable for the investigated regions of process parameters.

2.5.3. Advantages with simulation methods

- Less human resource is required, and material consumption is minimal.
- Provide more understanding of the process physical phenomena.
- Universality (not restricted to a specific range of input parameters), however, this universality is limited by the model assumption and boundary conditions.

2.5.4. Challenges with simulation methods

- Level of the details of processes and assumptions included in the model define the accuracy. Increasing the details and lowering the assumptions can make the model complicated. The adequacy of the simulation models depends on how comprehensively they account for many process parameters (such as material properties, laser temporal mode, model assumptions, boundary conditions, material shape/thickness, ambient conditions, etc.).
- Availability of accurate values of material properties at high temperatures and short irradiation periods (materials generally behave non-linearly under these conditions), therefore, some material properties (such as thermal conductivity, evaporation temperatures, latent heats) may not be available under these conditions. This leads to assumptions which may not very accurate.
- It is still challenging to model some processes that involve complex interactions between different materials such as welding and coating processes.
- Simulation modelling is also challenging for certain processes that involve complex underlying physical phenomena. For example, ultra-short laser pulses induce micro and Nano-scale modifications in the processed materials. The complexity arises due to changes occurring simultaneously in the physical and chemical properties of the processed materials.

2.6. Experimental setup requirements and relation to modelling

When it comes to conducting experiments with the lasers, accuracy and precision are key factors. Therefore, the experimental conditions must be governed and maintained throughout the entire experiment. The experimental setup is engineered in this way to

ensure the repeatability and reliability of the results. The majority of the researchers working with laser processing rely on performing measurements of responses after the sample is processed. Many techniques and instruments can be used to fulfil this requirement, based on the nature of measurements. These techniques include but not limited to Vernier scanner, profilometers, mechanical hardness measurement equipment, chemical analyses, optical microscopy, SEM and AFM [27]–[29]. Some published research work used in-situ or online setups to measure process responses in real-time. These responses can be the physical and chemical modifications in the processed material (such as transient temperature distributions, material phase transformations, optical properties, and dimensions and topography of structured zones) [26], [30]. One major advantage in using in-situ measurement setups is that they provide the ability to modify the process parameter in real-time to visualize the exact effect of input parameter variations on the obtained results.

2.7. Modelling and optimization of laser processing with non-conventional approaches

The correct selection of the process parameter values is vital in designing a successful manufacturing process. A well calculated decision on selecting the values for the processing parameters guarantee the good quality of the manufactured product and reduces the manufacturing expenditure and increases the overall productivity of the manufacturing system. In order to design a model for the process parameters of a manufacturing process and perform optimization on that model, the complete understanding of the process is required. This understanding and thorough knowledge about the several processes involved in the manufacturing can be obtained by experimental equations that are able to identify the practical restrictions, specification of machine capacities, development and implementation of an effective optimization criterion, and understanding of mathematical and numerical optimization techniques [31].

Due to the high levels of the complexity involved in the laser surface modification techniques and multiple influences of the parameters on the process response, traditional methods of designing, manufacturing and testing to control the process are generally inefficient and provide unsatisfactory results. The advanced modelling and optimization techniques have been developed and frequently used in various industrial sectors to control and optimize the manufacturing processes.

In order to design and develop these techniques, the relationship between the response of a process and input control factors should be explained objectively and numerically. This can be performed by realization of the process through appropriate mathematical equations and optimization algorithms. The optimization techniques which have been found to be particularly useful for application with laser-based manufacturing processes are given below:

2.7.1. Response Surface Methodology (RSM)/Design of Experiments (DoE)

Using RSM, the responses of a process can be optimized by understanding and calculating the quantitative influence of the control parameters. By introducing systematic variations in the input parameters, the response of the process is recorded and conclusions are drawn on the basis of the quantitative analysis of the results [32].

2.7.2. Artificial Neural Networks (ANN)

ANNs are efficient systems in data modelling and are capable to represent complex input–output relationships [32].

2.7.3. Adaptive neuro-fuzzy inference system (ANFIS)

For creating and testing connections between inputs and outputs of a system or process, ANFIS provides an opportunity to integrate both adaptive artificial neural networks and fuzzy logic to provide a feedback control system to obtain accurate process

response by adaptively changing the input control parameters [32]. The use of ANFIS provides adaptive control over the process thus optimization can be performed automatically based on the feedback received from the process response.

2.7.4. Grey Relational Analysis (GRA)

If a process involves multiple control inputs that provide influence and generate complex multiple responses and accurate information regarding the influence of control factors is unknown, the GRA can be used as an effective solution. In such cases, the multiple process response system is simplified by introducing a single grey, hazy or fuzzy relational grade output response to provide a variety of possible solutions [32].

2.7.5. Technique for order preference by similarity to ideal solution (TOPSIS)

The TOPSIS provides a rather simple but unique solution to model the relationship between input, control and output response of a process or a system by selecting different criteria to reach a decision. The approach used in this method is based on iterations in criteria on the basis of compensation in the aggregation. The accuracy of results (poor or good) suggests which criteria suits best of the process under consideration [32].

2.7.6. Meta-Heuristic optimization

Metaheuristics algorithms do not ensure a globally optimal solution however provide a sufficient solution for immediate goals with limited and incomplete data availability. The solutions produced by such algorithms are generally dependent on the set of random variables generated during a stochastic process. In combinatorial optimization, by searching over a finite set of optimal solutions, metaheuristics can often discover decent solutions with less calculation tasks than other optimization algorithms, iterative methods, or simple heuristics. For example, imperialist competitive algorithm (ICA) is a meta-heuristic optimization method. The ICA algorithm consists of eight

main steps (generating initial empires, assimilation, revolution, total power of an empire, imperialistic competition, elimination of powerless empires and stopping condition) exchanging positions of the imperialists of colony to detect best solutions [32].

2.8. Investigations on laser-based surface modifications and processing techniques

2.8.1. Laser Cladding

Sohrabpoor in 2016 presented an analysis of powder deposition factors for the laser cladding process, with ANFIS modelling and optimization [33]. In this work, an adaptive neuro-fuzzy inference system, ANFIS, was implemented to model the response of the deposition parameters based on collected experimental data for the iron-based alloy powder deposition onto mild steel substrate. It was concluded that for multi-response optimization problems of a manufacturing process where the outputs are well correlated to each other, the ANFIS-ICA method can be utilized. The structure of the ANFIS model for predicting outputs parameters is shown by Fig 2.1.

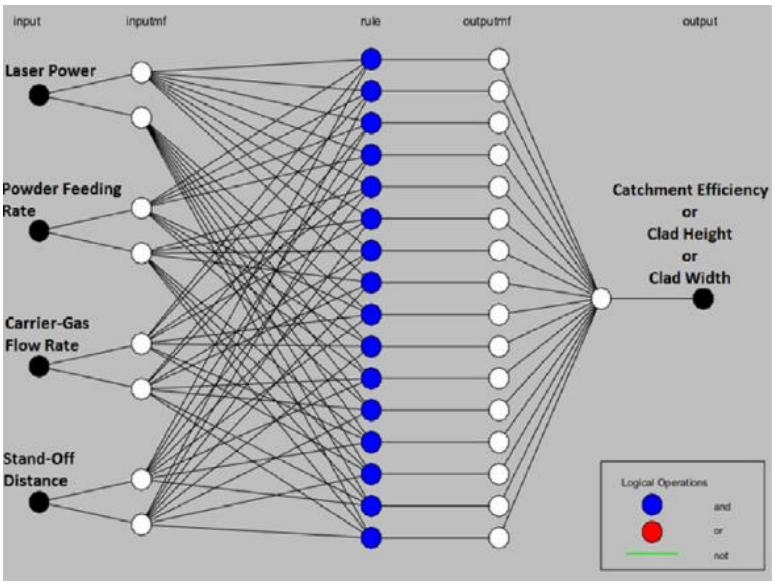

Fig 2.1. Structure of developed ANFIS model for predicting of catchment efficiency, clad height and clad width [33].

Mondal et al. in 2014 used Artificial Neural Network (ANN) for prediction of the laser cladding procedure characteristics with input date defined according to Taguchi-based design condition [34]. In this work, nickel, chromium and molybdenum mixture powder was used for laser cladding of AISI 1040 steel by CO_2 laser. Input factors examined including laser power, scan speed and powder feed rate to reach to maximum level of clad width and minimizing the clad depth. The correlation between the inputs and the outputs was implemented via the back-propagation method of ANN. It was found that the optimum condition of the cladding factors for multi-performance characteristics varied with the various combinations of weighting factors. The structure of 4-layered ANN model utilized is shown in Fig 2.2.

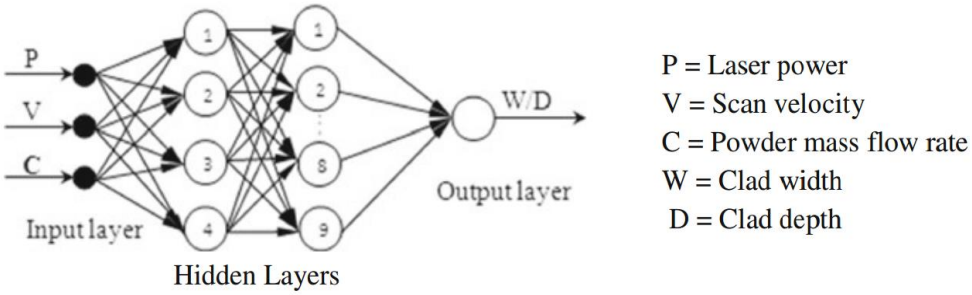

Fig 2.2. Structure of 4-layered ANN model used for prediction of the laser cladding process outputs [34].

Guo et al. [35] in 2012 studied the effects of process parameters on the quality of a laser cladding layer of Co-based alloy on 304 stainless steel with a high power diode laser (HPDL). For exploring the optimum process parameters and reducing the times of procedure experiments in practical engineering application, a back propagation (BP) neural network model was established. The calculation and predication results reveal an appropriate agreement with the experimental results. The research results have both significant reference value and provide guidance in the selection of process parameters of Co-based alloy cladding by HPDL. The structure of BP-NN model for laser cladding of Co-based alloy is shown on Fig. 2.3. The results showed that the laser scanning speed has the most significant effect on the width, height and depth of laser cladding layer, and the powder feeding rate has the most major impact on the hardness of laser cladding layer.

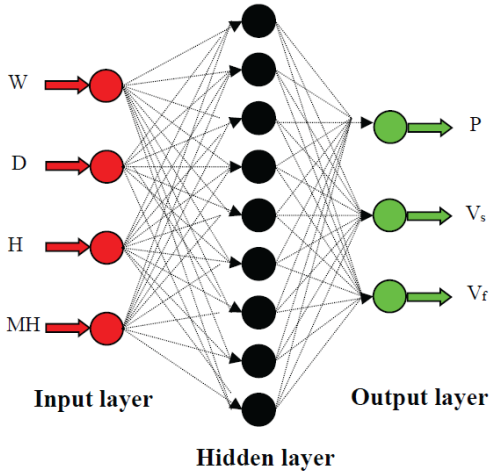

Fig 2.3. Structure of BP-NN model for laser cladding Co-based alloy by a HPDL [35].

Marzban et al. [36] in 2014 investigated optimal process parameters to increase the laser cladding process performance. The design of experiments based on L9 orthogonal array used to investigate the effects of input factors (laser power, scan speed and powder feed rate) on output factors (clad height, width and depth). As three response factors were selected, in order to investigate the multi-response optimization of the process, the Principal Component Analysis (PCA) was used in combination with TOPSIS.

The weight factors associated with the characteristics of the quality were determined by the PCA. The study found that by increasing the laser power during the processing, a positive effect on the clad width can be achieved. Concurrently a negative effect on the clad height and depth was observed. Increasing scan speed was found to have a positive effect on the clad height, width, and depth. Fig 2.4 shows the main effects of the input parameters on output response, implemented in Minitab 16 software.

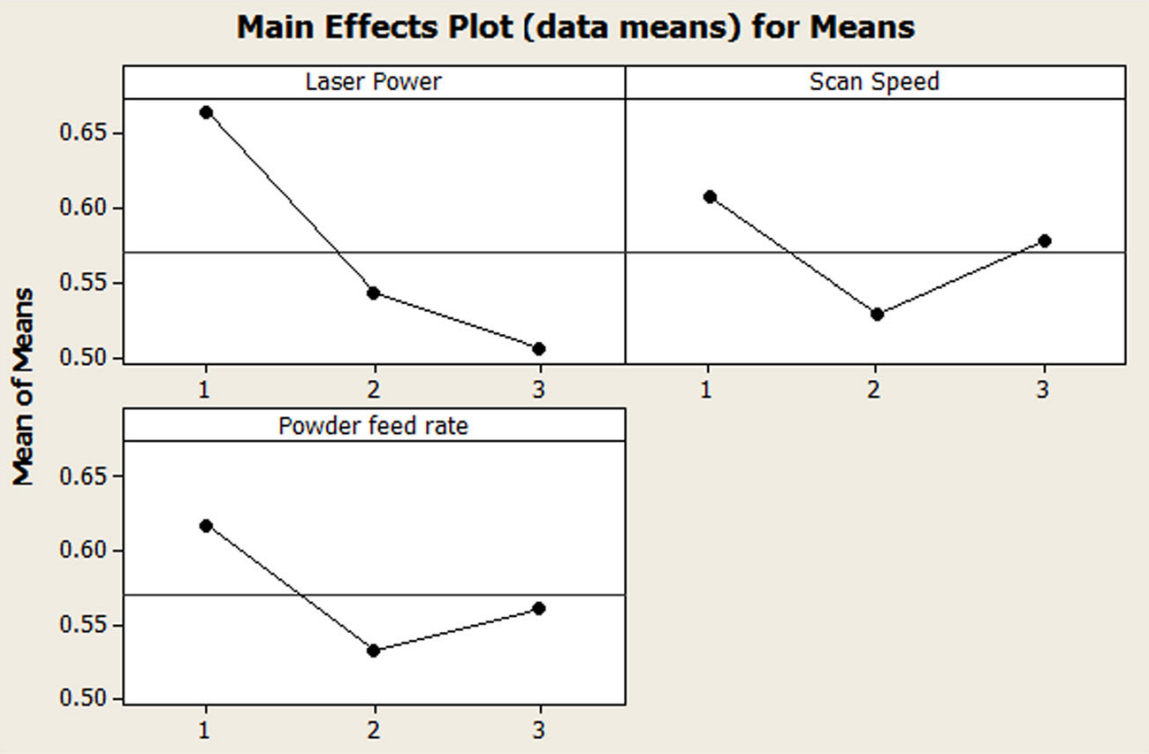

Fig 2.4. Response of process factors to relative closeness of a particular alternative to ideal solution [36].

Mondal et al [37] in 2013 used Taguchi and grey relational analysis in order to investigate optimal process parameters for the laser cladding of AIS1040 steel plane surface. The impact of different laser deposition factors on the clad bead geometry were investigated. The laser power was selected as source parameter and the scan speed and powder feed rate were selected as process condition parameters. The GRA was for the process modelling and optimization to examine the grey relation grade for each experiment. The best response of the laser cladding of AISI 1040 after optimization was obtained with the laser power of 1.25 KW, at scanning speed of 0.8 m/min while keeping the powder feed rate at 11 gm/min. Fig. 2.5 shows the grey relational grade. Also, it is concluded that for a complex multi response process such as laser cladding, the optimization problem can be converted in to single objective optimization problem with GRA.

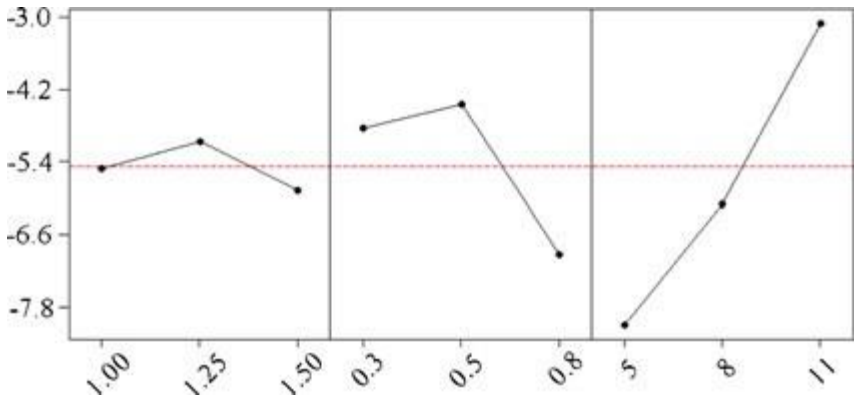

Fig. 2.5. Graph of grey relational grades determined for the laser power, scan speed and powder feed rate [37].

2.8.2. Laser Melting

During Laser Melting, a thin material surface layer melts and solidifies rapidly due to self-quenching. This results in modification of the surface microstructure. For higher solidification rates, the melting should be limited to only thin layer substrate. Therefore this technique requires lower power densities at high transverse speeds [1].

In 2013 Sun et al. [38] produced highly dense samples with Ti6Al4V alloy powders using selective laser melting (SLM) technique. Taguchi method was used to optimize the selected parameters of LSM. These selected laser parameters were laser power, scanning speed, powder thickness, hatching space and scanning strategy. The optimal parameters and a regression model were developed with design-expert software and the analysis on the results obtained was performed using analyses of variance (ANOVA) methods and the signal-to-noise (S/N) ratios. Based on the figure, higher value is better. The results indicated that powder layer thickness provides a major influence over resulting part density. The lowest powder thickness (0.02 mm) provides high density (~95%). Comparing to casting method, higher surface micro hardness was achieved by keeping the laser power at 80 W.

Calignano [39] studied the manufacturability of overhanging structures using optimized support parts. SLM technique was carried out for Al and Ti alloys overhanging structures. Taguchi L_{36} design was used for the experimental study to identify the optimal design of the self-supporting overhanging structures. Several process parameters including hatching space, teeth height and teeth base interval were optimized using Taguchi method to obtain highly accurate geometry of the build material by reducing the deformations of the overhanging surfaces.

In 2015 Read et al. [40] investigated the influence of SLM on AlSi10Mg alloy porosity development. They correlate the statistical design of experimental approach with the energy density model to study the influence of laser power, scan speed, scan spacing, and island size using a Concept Laser M2 system on the SLM process. It was reported that for AlSi10Mg alloy, by keeping the critical energy density at about 60 J/m^3, a minimum pore fraction can be achieved.

The surface modification of biomaterials is often desirable to improve the degree of biocompatibility of the implants [6]. The laser surface structuring of biomaterials has been reported extensively [7], [27], [28], [41], [42]. Chikarakara et al. [2] investigated the effect of 1.5 kW CO_2 high speed laser processing on Ti-6Al-4V surface modification for biomedical implant application. During the laser processing, argon (being an inert) gas was used to minimize any unwanted chemical modifications induced on the workpiece surface. The processing parameters studied in this work were irradiance, pulse width, residence time and sample pre-treatments. SEM was used to characterize surface topology, microstructure and melt pool depth. From this study, a 3^2 factorial design as presented below was used to provide a new understanding from the use of DoE in the laser processing of this material.

The two parameters (irradiance and residence time) were selected to make a three-level factorial design of experiment to investigate laser surface processing of Ti-6Al-

4V alloy. Continuous Wave (CW) mode laser was used to irradiate the workpiece at three levels of irradiance: 15.72, 20.43 and 26.72 kW/mm^2 and three levels of residence time: 1.08, 1.44 and 2.16 ms, see Table 2.1.

Table 2.1 Design of Experiments parameters for Ti-6Al-4V alloy laser surface processing [2].

ID	Irradiance (kW/mm^2)	Residence Time (ms)
LSM 1	15.72	
LSM 2	20.44	2.16
LSM 3	26.72	
LSM 4	15.72	
LSM 5	20.44	1.44
LSM 6	26.72	
LSM 7	15.72	
LSM 8	20.44	1.08
LSM 9	26.72	

For surface laser processing, a laser beam with 90-micron diameter was focused on the titanium alloy samples. In order to provide microstructural and compositional homogeneity to the surface, the irradiation of the samples was carried out using a raster scan with a partial overlap of 30%. The pressure of the argon gas was kept at 200 kPa. Inert gas was used to prevent metal oxidation. To ensure uniform processing conditions and maximum absorbance during laser irradiation, the laser beam was kept perpendicular to the sample.

Fig. 2.6 highlights the modifications in the microstructure, roughness and melt pool depth of the laser irradiated areas of the sample. It can be observed from the BSE images that increase in the irradiance of the laser on the sample surfaces results in modifications in the uniformity of the thickness of the irradiated area. The melt pool

depth introduced in the laser processed surface can be modelled by the equation given in Table 2.2.

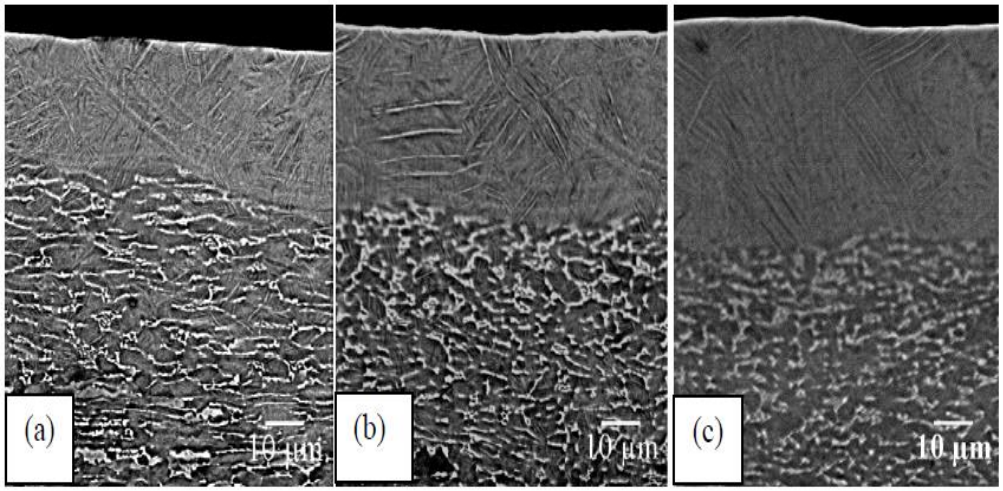

Fig. 2.6: Back scatter detector (BSE) surface morphology images of laser surface modified Ti-6Al-4V at a constant level of irradiance 26.72 kW/mm^2 and three levels of irradiance of residence time of (a) 1.08 (b) 1.44 and (c) 2.16 ms [2].

Table 2.2 Analysis for variance (ANOVA) table for melt pool depth – 2FI model.

Source	Sum of Squares	Mean Square	F Value	p-value
Model	502.786	167.595	23.268	0.0023
A-Irradiance	135.375	135.375	18.795	0.0075
B-Residence Time	366.601	366.601	50.898	0.0008
AB	0.81	0.81	0.112	0.7510
Residual	36.013	7.202		
Cor Total	538.8			

		Final equation obtained from the model
R-Squared	0.933	Meltpool depth =
Adj R-Squared	0.893	-3.93448
Pred R-Squared	0.879	+0.61818 × Irradiance
Adeq Precision	14.047	+11.26016 × Residence Time
		+0.15152 × Irradiance × Residence Time

The statistical findings from the ANOVA demonstrated that both input laser process parameters influence the melt pool depth of the irradiated surface. It was further observed that comparatively, the residence time effect more strongly on the melt pool depth of the processed material with respect to irradiance as the F-values obtained by ANOVA were 50.898 and 18.795 respectively.

By considering the interaction of both selected input factors, the statistical analysis showed low significance for influence on melt pool depth. This result from the 2FI model was further confirmed by the coded factor model equation given below. The coded factors model equation was derived from the experimental design's low and high coded levels (-1 and 1).

Melt pool Depth (μm) = 32.63 + 4.75A + 7.82B + 0.45AB

Which A refers to the irradiance and B is Residence time.

The predicted values of melt pool depth from the model were plotted against the experimental values in Fig. 2.7. The model was able to predict the output response parameter (the melt pool depth) very close to the experimental values. The signal to noise ratio was also calculated to find the adequate precision of the model which was 14.047 in the study. The ratio higher than 4 confirms that the developed model can be used to optimize the process parameters for desired output response.

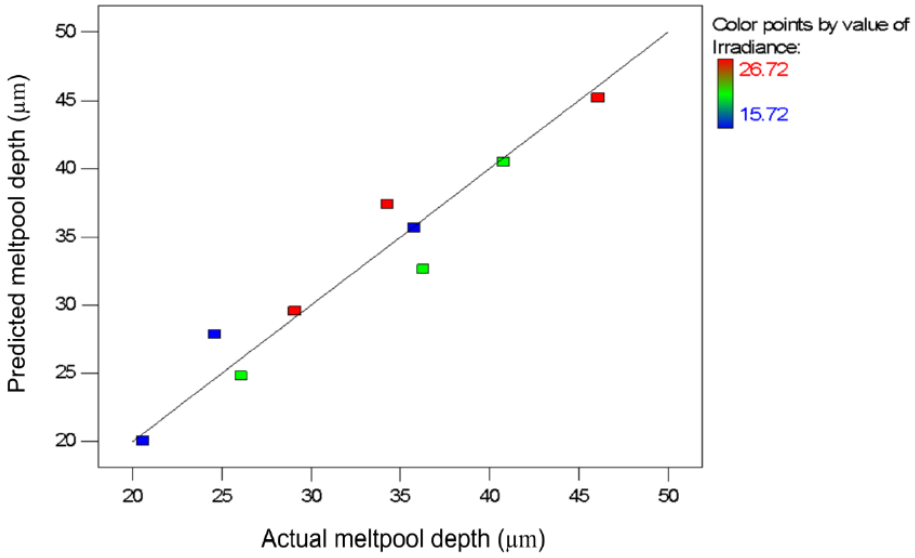

Figure 2.7. A graph of the actual melt pool depth versus the predicted values [2].

2.8.3. Laser Shock Peening

Laser Shock Peening (LSP) is an efficient surface treatment technique used to improve the fatigue performance of metals. In 2013, Sathyajith et al. [43] investigated the effect of laser shock peening without any coating on aluminium alloy Al-6061-T6 with a 300mJ infrared laser. It was shown that micro hardness and surface compressive stress were significantly improved using laser shock peening technique without additional coatings. However trivial increase in surface roughness was observed, as shown in Fig.2.8.

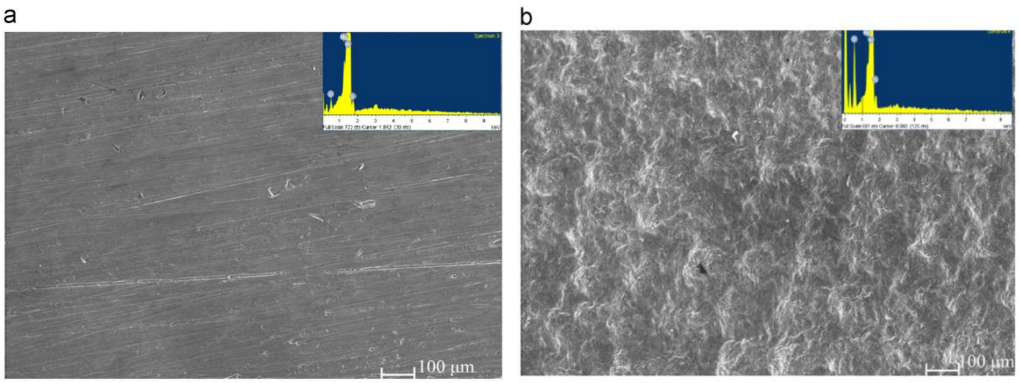

Figure 2.8. Surface SEM micrograph: (a) pristine and (b) laser shock peened surface [43].

Through this technique pulsed laser fired at the material surface, the rapid expansion of the resultant formed plasma will generate a high amplitude and short duration shock wave. The plasma by laser irradiation on the material is formed due to vaporization of an ablated layer placed on the surface of the material surface confined by water [44]. The shock wave generates stresses on the specimen surface causing a compressive residual stress field which increases the surface hardness and the fatigue life. From that we can understand that LSP is a mechanical process unlike other laser processing techniques based on thermal processing of the materials [45].

Sibalija et al. [46] varied three Nd:YAG laser parameters in laser shock peening (LSP) to find the optimum parameters. The experiment was conducted on nickel-based superalloy Nimonic 263 sheets, and the selected LSP parameters for optimization included source voltage, focus position and pulse duration. The group performed modelling and optimization using the advanced problem-independent method. Taguchi quality loss function was used first to express the responses, then uncorrelated and synthesized into a single performance measure using the application of multivariate statistical analysis. Finally, the process model was built using an artificial neural network, and simulated annealing was utilized to find the optimal process parameters setting in a global continual space of solutions. The obtained global optimum for the process parameters provided improved micro hardness along with

very fine grains and the overall surface roughness was reduced after LSP at these values. Therefore, making the surface smoother with clean microstructure as well as improved fatigue life.

2.9. Conclusion

Laser processing has a wide application range from micro/Nano fabrication techniques to surface treatment, structuring, modification, and controlled surface plastic deformation. As the laser matter interaction is a complex phenomenon, the advancements in laser processing applications require accurate mathematical models to describe the various processes that occur during the laser interaction with different materials. The models can be developed to predict the response of the laser processing for a specific application by establishing relationship between the process input parameters (laser parameters and working conditions) and output response (resulting property of the processed material). A systematic approach is required to generate data that is required for modelling and simulation of laser processing. Design of Experiments (DoE) has been extensively used to describe how the materials properties can be controlled as a result of control of processing conditions. In particular, the DoE approach has been successfully used in laser processing to establish and validate the relationship between the laser process parameters, working conditions and output responses. This allows the definition of accuracy, repeatability, and reliability from the laser process enabling the use of these techniques to be taken up and employed more widely by industries which are adopting new laser-based technologies for both material modification and fabrication.

REFERENCES

[1] E. Kannatey-Asibu, Principles of Laser Materials Processing, vol. 4. 2009.

[2] E. Chikarakara, S. Naher, and D. Brabazon, “High speed laser surface modification of Ti-6Al-4V,” Surf. Coatings Technol., vol. 206, no. 14, pp. 3223–3229, 2012.

[3] D. Karthik, S. Kalainathan, and S. Swaroop, “Surface & Coatings Technology Surface modi fi cation of 17-4 PH stainless steel by laser peening without protective coating process,” vol. 278, pp. 138–145, 2015.

[4] A. Riveiro et al., “Laser surface modification of ultra-high-molecular-weight polyethylene (UHMWPE) for biomedical applications,” Appl. Surf. Sci., vol. 302, pp. 236–242, 2014.

[5] R. S. Faeda, H. S. Tavares, R. Sartori, A. C. Guastaldi, and E. Marcantonio, “Evaluation of titanium implants with surface modification by laser beam. Biomechanical study in rabbit tibias.,” Braz. Oral Res., vol. 23, no. 2, pp. 137–143, 2009.

[6] I. Ul Ahad et al., “Surface modification of polymers for biocompatibility via exposure to extreme ultraviolet radiation,” Journal of Biomedical Materials Research - Part A, vol. 102, no. 9. pp. 3298–3310, 2014.

[7] I. U. Ahad, B. Budner, H. Fiedorowicz, A. Bartnik, and D. Brabazon, “Nitrogen doping in biomaterials by extreme ultraviolet (EUV) surface modification for biocompatibility control,” Eur. Cells Mater., vol. 26, no. Suppl. 6, p. 145, 2013.

[8] J. W. Stansbury and M. J. Idacavage, “3D printing with polymers: Challenges among expanding options and opportunities,” in Dental Materials, 2016, vol. 32, no. 1, pp. 54–64.

[9] H. Shipley et al., “Optimisation of process parameters to address fundamental challenges during selective laser melting of Ti-6Al-4V: A review,” International Journal of Machine Tools and Manufacture, vol. 128. Pergamon, pp. 1–20, 01-May-2018.

[10] A. Olabi, F. Alsinani, and A. Alabdulkarim, “Optimizing the CO 2 laser welding process for dissimilar materials,” Opt. Lasers, 2013.

[11] K. Huehnlein, K. Tschirpke, and R. Hellmann, “Optimization of laser cutting processes using design of experiments,” Phys. Procedia, 2010.

[12] S. Britten, A. Olowinsky, and A. Gillner, “Stress-minimized laser soldering of h-pattern multicrystalline silicon solar cells,” in Physics Procedia, 2013, vol. 41, pp. 153–163.

[13] A. Issa, D. Brabazon, and M. S. J. Hashmi, “3D transient thermal modelling of laser microchannel fabrication in lime-soda glass,” J. Mater. Process. Technol., vol. 207, no. 1–3, pp. 307–314, 2008.

[14] D. Montgomery, Design and Analysis of Experiments. 2000.

[15] J. L. Mason, R.L., Gunst, R.F. and Hess, Statistical design and analysis of experiments: With applications to engineering and science. 1989.

[16] K. Hinkelmann and O. Kempthorne, Design and Analysis of Experiments, Special Designs and Applications. 2012.

[17] D. Cox and N. Reid, The theory of the design of experiments. 2000.

[18] D. Angela and V. Daniel, Design and analysis of experiments. Springer-Verlag NY, Inc, 1999.

[19] K. Tamrin, Y. Nukman, and I. Choudhury, “Multiple-objective optimization in precision laser cutting of different thermoplastics,” Opt. Lasers, 2015.

[20] B. Adelmann and R. Hellmann, “Journal of Materials Processing Technology Rapid micro hole laser drilling in ceramic substrates using single mode fiber laser,” J. Mater. Process. Technol., vol. 221, pp. 80–86, 2015.

[21] A. Issa, “Computational Control Of Laser Systems For Micro-Machining,” Dublin City University, 2007.

[22] “StatEase Inc.” [Online]. Available: http://www.statease.com/. [Accessed: 12-Dec-2016].

[23] “SAS Institute Inc.” [Online]. Available: http://www.jmp.com/en_us/home.html. [Accessed: 15-Dec-2016].

[24] “Minitab.” [Online]. Available: http://www.minitab.com/en-us/. [Accessed: 15-Dec-2016].

[25] S. Sihn, L. Childers, C. Walters, and M. Forte, “Computational and experimental study on laser heating of a Ni-based metal alloy,” Int. J., 2016.

[26] C. Fu, M. Sealy, Y. Guo, and X. Wei, “Finite element simulation and experimental validation of pulsed laser cutting of nitinol,” J. Manuf. Process., vol. 19, pp. 81–86, 2015.

[27] I. U. Ahad et al., “Extreme ultraviolet (EUV) surface modification of polytetrafluoroethylene (PTFE) for control of biocompatibility,” Nucl. Instruments Methods Phys. Res. Sect. B Beam Interact. with Mater. Atoms, vol. 364, pp. 98–107, Dec. 2014.

[28] I. Ahad et al., “Extreme Ultraviolet Surface Modification of Polyethylene Terephthalate (PET) for Surface Structuring and Wettability Control,” Phys. Pol. A, vol. 129, no. 2, pp. 241–243, 2016.

[29] M. Ahmed Obeidi, E. McCarthy, and D. Brabazon, “Methodology of laser processing for precise control of surface micro-topology,” Surf. Coatings Technol., vol. 307, pp. 702–712, 2016.

[30] R. Schmitt, G. Mallmann, K. Winands, and M. Pothen, “Automated process initialization of laser surface structuring processes by inline process metrology,” Phys. Procedia, 2013.

[31] R. V. Rao, Advanced Modelling and Optimization of Manufacturing Processes: International Research and Development. 2011.

[32] T. Šibalija and V. Majstorović, Advanced Multiresponse Process Optimisation. 2016.

[33] H. Sohrabpoor, “Analysis of laser powder deposition parameters: ANFIS

modelling and ICA optimization," Optik (Stuttg)., vol. 127, no. 8, pp. 4031–4038, 2016.

[34] S. Mondal, A. Bandyopadhyay, and P. K. Pal, "Application of artificial neural network for the prediction of laser cladding process characteristics at Taguchi-based optimized condition," Int. J. Adv. Manuf. Technol., pp. 2151–2158, 2013.

[35] S. Guo, Z. Chen, D. Cai, Q. Zhang, V. Kovalenko, and J. Yao, "Prediction of simulating and experiments for co-based alloy laser cladding by HPDL," in Physics Procedia, 2013, vol. 50, pp. 375–382.

[36] J. Marzban, P. Ghaseminejad, M. H. Ahmadzadeh, and R. Teimouri, "Experimental investigation and statistical optimization of laser surface cladding parameters," Int. J. Adv. Manuf. Technol., vol. 76, no. 5–8, pp. 1163–1172, 2014.

[37] S. Mondal, C. P. Paul, L. M. Kukreja, A. Bandyopadhyay, and P. K. Pal, "Application of Taguchi-based grey relational analysis for evaluating the optimal laser cladding parameters for AISI1040 steel plane surface," Int. J. Adv. Manuf. Technol., vol. 66, no. 1–4, pp. 91–96, 2013.

[38] J. Sun, Y. Yang, and D. Wang, "Parametric optimization of selective laser melting for forming Ti6Al4V samples by Taguchi method," Opt. Laser Technol., vol. 49, pp. 118–124, 2013.

[39] F. Calignano, "Design optimization of supports for overhanging structures in aluminum and titanium alloys by selective laser melting," Mater. Des., vol. 64, pp. 203–213, 2014.

[40] N. Read, W. Wang, K. Essa, and M. M. Attallah, "Selective laser melting of AlSi10Mg alloy: Process optimisation and mechanical properties development," Mater. Des., vol. 65, pp. 417–424, 2015.

[41] H. Fiedorowicz et al., "Laser plasma sources of soft X-rays and extreme ultraviolet (EUV) for application in science and technology," 2014 Int. Conf. Laser Opt., pp. 1–1, Jun. 2014.

[42] I. U. Ahad et al., "Polycarbonate polymer surface modification by extreme

ultraviolet (EUV) radiation," in Acta Physica Polonica A, 2014, vol. 125, no. 4, pp. 924–928.

[43] S. Sathyajith, S. Kalainathan, and S. Swaroop, "Laser peening without coating on aluminum alloy Al-6061-T6 using low energy Nd:YAG laser," Opt. Laser Technol., vol. 45, no. 1, pp. 389–394, 2013.

[44] G. Tani, L. Orazi, A. Fortunato, A. Ascari, and G. Campana, "Warm Laser Shock Peening: New developments and process optimization," CIRP Ann. - Manuf. Technol., vol. 60, no. 1, pp. 219–222, 2011.

[45] W. Braisted and R. Brockman, "Finite element simulation of laser shock peening," Int. J. Fatigue, vol. 21, no. 7, pp. 719–724, 1999.

[46] T. V. Sibalija, S. Z. Petronic, V. D. Majstorovic, and A. Milosavljevic, "Modelling and optimisation of laser shock peening using an integrated simulated annealing-based method," Int. J. Adv. Manuf. Technol., vol. 73, no. 5–8, pp. 1141–1158, 2014.

Chapter 3 Optimizing selective laser sintering process by grey relational analysis and soft computing techniques

Publication Status: Published

Hamed Sohrabpoor, Sushant Negi, Hamed Shaiesteh, InamUl Ahad and Dermot Brabazon, Optik - International Journal for Light and Electron Optics 174 (2018) 185–194

DOI: 10.1016/j.ijleo.2018.08.040

Abstract

Selective laser sintering (SLS) is a novel fabrication technique with multiple industrial applications in different industrial sectors. Choosing optimum combination of elements which lead to the best component properties and lower process cost are required in the SLS process. In this study, we focused on advanced modelling and optimization method developed for obtaining the best mechanical properties of SLS produced glass filled polyamide parts. The key processing parameters examined were part bed temperature, laser power, scan speed, scan spacing, and scan length. Response output properties measured were elongation and ultimate tensile strength. Five factors with three levels according to the central composite design were trailed. Adaptive neuro-fuzzy inference system (ANFIS) was employed to generate a mapping relationship between the process factors and the experimentally observed responses. In order to achieve best mechanical characteristics, the acquired model was used by simulated annealing algorithm as an objective function. Grey relational analysis (GRA) as a multi-response optimization technique was also applied to evaluate which modelling technique could perform best for defining the process elements to obtain the highest mechanical properties. In comparing the two optimization methods, the results indicated that the ANFIS-SA system outperformed the GRA in finding optimal solutions for the SLS process applied for glass fibre reinforced part production.

Keywords: Selective laser sintering; Adaptive neuro-fuzzy inference system; simulated annealing algorithm; grey relational analysis

3.1. Introduction

The selective laser sintering (SLS) was invented in 1989 [1]. In this process, laser employed to melt polymer powders. In order to reduce the thermal distortion, metal powder bed should be melted to below the melting point of the material and at the same time assist melted fusion to the prior layer. After that, each layer is fused by laser for sintering the material. The melted powder shapes the parts and the section which is un-sintered, makes main structure of the parts. The SLS can be classified as a complicated process, as many fabricated elements must be controlled, see process schematic in Fig 3.1.

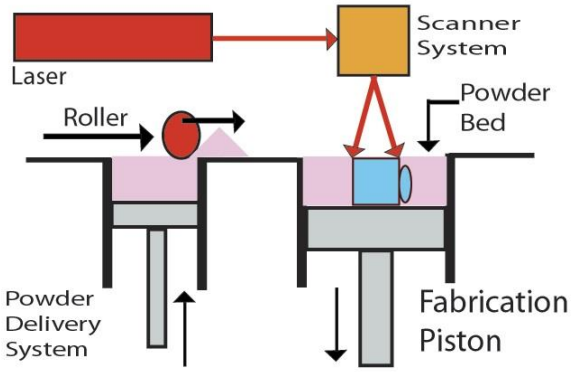

Fig 3.1. A structure of SLS process

In the case of development of empirical models, some statistical techniques and mathematical modelling such as Response Surface Methodology (RSM) has been used to correlate relationship between SLS process inputs and its main outputs. Bacchewar et al. [2] developed a new mathematical model to determine the effect of input factors on the polymer product made by SLS. They used a CCD (central composite design) as the strategy of experimental work. They found within their design of experiments that hatch distance was the most important parameter in terms of resulting mechanical properties. Sharma et al. [3] with using of dynamic mechanical analyzer, investigated the of laser sintered produced samples. They found that with increasing some input

elements like scan length, part bed temperature and laser power the storage modulus also increased; and that it was decreased with increasing scan spacing. Furthermore, they found that scan spacing was the most prominent factor amongst all parameters investigated. Design of experimental methodology is a popular method for optimization of process parameters, particularly for complex laser-based processes for which it is difficult to develop fundamental model for [4,5].

Dingal et al. [6] used a design of experiment strategy with seven elements including laser pulse on-time, laser peak power, and interval-between pulses, and responses including density, porosity and hardness. The results show that the laser peak power density had the highest impact on the laser sintering process. Design of experiments methodology has also been applied for metal Selective Laser Melting (SLM) in addition to Selective Laser Sintering [7]. Negi et al. in order to improve service life in glass-filled polyamide in SLS process, studied the impact of process factors including part bed temperature and beam speed on the dynamic mechanical properties [8]. The CCD of experiments was applied for their systematic experiment methodology. From the results, it was observed that with reducing bed temperature, dynamic mechanical characteristics were reduced [9]. The ANOVA results from this work indicated that the scan spacing, and laser power had a high level of impact on the surface roughness and that for minimizing of surface roughness, the bed temperature should be set to the lower level. The influence of some input parameters on the tensile strength, elongation and yield strength of glass filled polyamide parts produced by the SLS process was examined [10]. A CCD was implemented in this work as the design of experiments with the response equations derived from the experimental results. The results from this work indicate that the scan spacing, and scan speed were the most important parameters in terms of effecting the mechanical property outputs. The effect of same input parameters on the flexural strength of the samples was also examined.

Negi et al. [11] applied both RSM and ANN for the prediction of shrinkage in laser SLS sintered glass fiber reinforced polymer (PA 3200GF) samples. The RSM and ANN models were compared for their ability to predict shrinkage. Results indicated that ANN was better than RSM in both data fitting and estimation abilities. Munguia

et al. [12] in order to pedict build time in SLS process used an ANN with part height, volume, and bounding box considered for input parameters. The results from this work indicated good potential for the ANN-based approach to be employed for the SLS process. Boillat et al. [13] used ANN in order to optimize the SLS process for a component of circular geometry and also applied an ANFIS model which typically has lower error levels in compression ANN. Shen et al. [14] applied ANN to predict the density of SLS samples. The inputs of this ANN were laser power, scan speed and scan spacing, and an orthogonal experimental approach was applied for training and testing of the system. Verification experiments were utilized to assess the quality of the model and the results showed the high accuracy of ANN for prediction. Vijayaraghavan et al. [15] used a combination of FEM and evolutionary algorithm simulation in order to determine the relationship between inputs (laser power, scan velocity and scan spacing) and the output (density). The results from this work indicated that scan spacing, and velocity had the highest impact while scan spacing had the least effect on the density of SLS-fabricated samples. SA algorithm which is part of metaheuristic algorithm is one of the most important and prominent optimizer algorithms which is used frequently in some manufacturing process [16, 13, 17, 18, 19, 20], however there are no previous publications concerning the usage of SA algorithm for the SLS process.

There have been very few publications in regard to usage of GRA for prediction or optimization of laser processes. GRA has however been applied as an optimization technique for many other manufacturing processes [21, 22, 23, 24, 25]. The experimental results achieved from the optimal settings predicted from the GRA algorithm show that there is a significant improvement in the related manufacturing process. The benefit of this approach is that the changes in multiple output response can be linked to various input settings which hence streamlines the optimization procedure.

3.2. Methodology and experimental tools

3.2.1. Description of ANFIS

For making relationship between input and response parameters adaptive neuro-fuzzy inference system is utilized which is mixture of neural network and fuzzy logic. In this study, the model consists of five layers and each layer includes several nudes. There were fifty sets of parameters studied in the experimental work including forty data points as a training for ANFIS model ten of data points for the model evaluation. For further information about implementation of the ANFIS, interested reader is referred to the following references [15,26].

In this work, in order to make a connection between input parameters and outputs, the ANFIS model was employed. After that, for each output, a specific ANFIS model was chosen based on RMSE. For example, because of five inputs, first layer of ANFIS includes five nudes and the last layer has one nude which represent of tensile strength.

3.2.2. Optimization with SA algorithm

One of the most significant algorithms which is broadly utilized for optimization of manufacturing processes is the SA algorithm which is a metaheuristic algorithm and is derived from modelling of thermal annealing. When a metal heated in a high temperature, it will reach to molten point. In this level of temperature, as a result of energy which is given by heating, all of atoms can move easily. When the temperature drops, the atoms will be arranged in the crystalized solid which have low level of energy. Based on the annealing process explanation, SA is an algorithm which is based on accidental exploration which naturally will not be trapped in a specific area, as a result of using the probability distribution function. For further information about implementation of SA, interested reader is referred to the following reference [23].

3.2.3. Multi response optimization with GRA

GRA is a popular type of optimization method which is used for solving of multi-criteria problems. According to the experimental data, in order to find best optimal condition, tensile strength and elongation should convert to one output. In this analysis, Firstly, data need to be normalized from to zero to one. After that, grey relational coefficient is computed in order to generate a relationship between inputs and responses. Next, in order to find Grey Relational Grade (GRG), the mean of grey relational coefficient needs to be calculated in relation to outputs. Finally, the result of multiple output process is structured on GRG which is calculated in previous section. This optimization method has been presented in detail previously [23].

3.3. Material and test specimen

The data examined was recorded in experimental work was performed by Negi et al. [8] and is summarized here for clarity. The materials which are utilized for making parts in SLS process was glass filled polyamide produced by EOS GmbH. This material is including polyamide glass beads and powder. The detailed experimental methodology implemented is indicated in Fig 3.2.

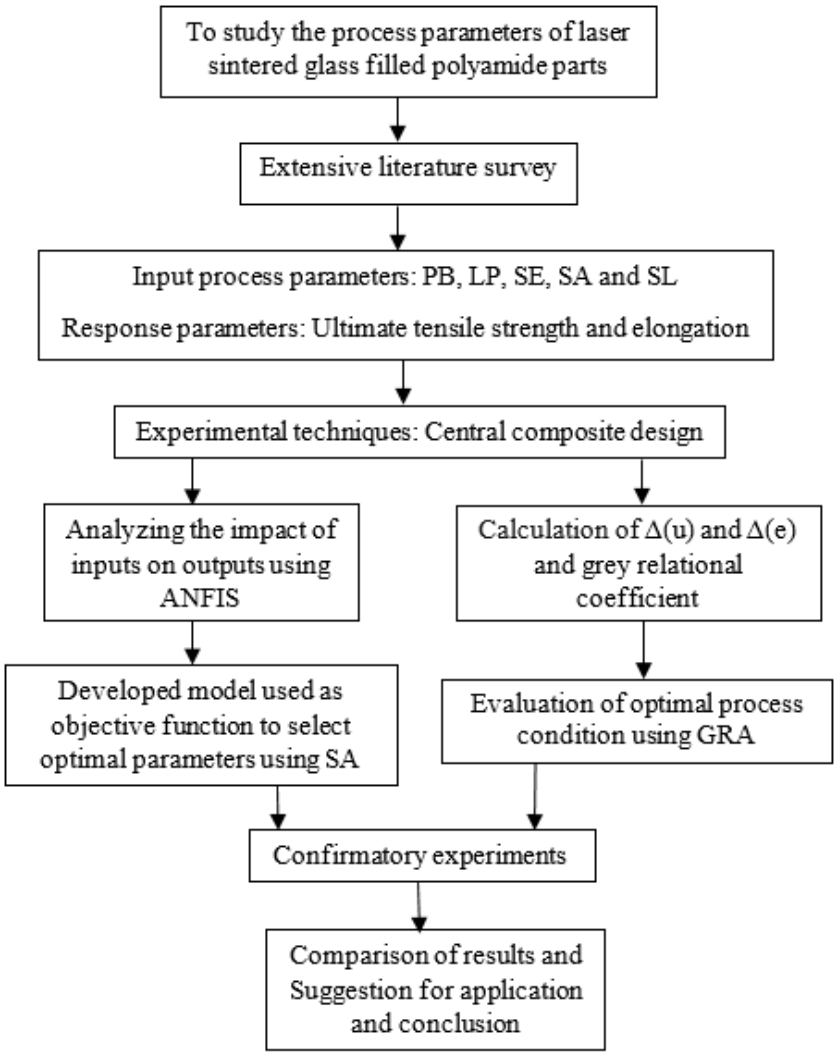

Fig 3.2. Flow chart of the implemented experimental and modelling methodology.

3.4. Selective laser sintering (SLS) parameters definition

For producing parts in SLS process several input elements are important and if they control sufficiently by the operator, parts will produce better in terms of strength. In this work, the process parameters to fabricate the test specimens are as shown in Table 3.1. Fig 3.3 presents the experimentally recorded values of tensile strength and elongation.

Table 3.1. Process variables and their levels (Negi et al., 2015)

Process parameters	Unit	Symbol	Code levels		
			0	0.5	1
Part bed temperature	ºC	T	176	179	192
Laser power	W	LP	28	32	36
Scan velocity	mm/s	SE	2500	3500	4500
Scan spacing	mm	SA	0.25	0.35	0.45
Scan length	mm	SL	100	120	140

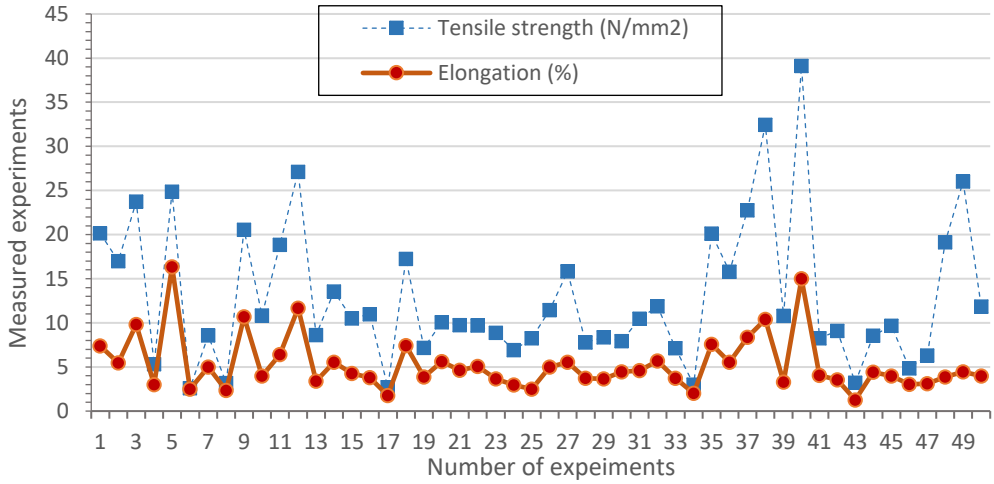

Fig 3.3. Measured ultimate tensile strength and elongation of the test specimens [9]

3.5. Results and discussion

Process optimization by ANFIS-SA has two major stages. The initial stage is to determine objective function, and next stage is to mix the objective function and SA for choosing best step setting. The implementation of each step is presented below.

3.5.1. Development of ANFIS model

For developing the ANFIS model the model needs to be trained. This involves Root Mean Square Error (RMSE) assessment between predicted and actual values after each iteration. Each combination of backward and forward propagations in ANFIS is called an epoch. The model was stopped after the RMSE fell below 0.01 or the number of epoch iteration reached 200. Next, a comparison was conducted on trial and error results and the model was selected according to precision which is estimated in related to new values in the testing section when they were checked with empirical data. By examining of different structures, ANFIS model for each of two outputs, were selected which was 32 MFs for each input data, which has the minimum of RMSE (Table 2). The basic structure of this model is indicated in Fig 3.4.

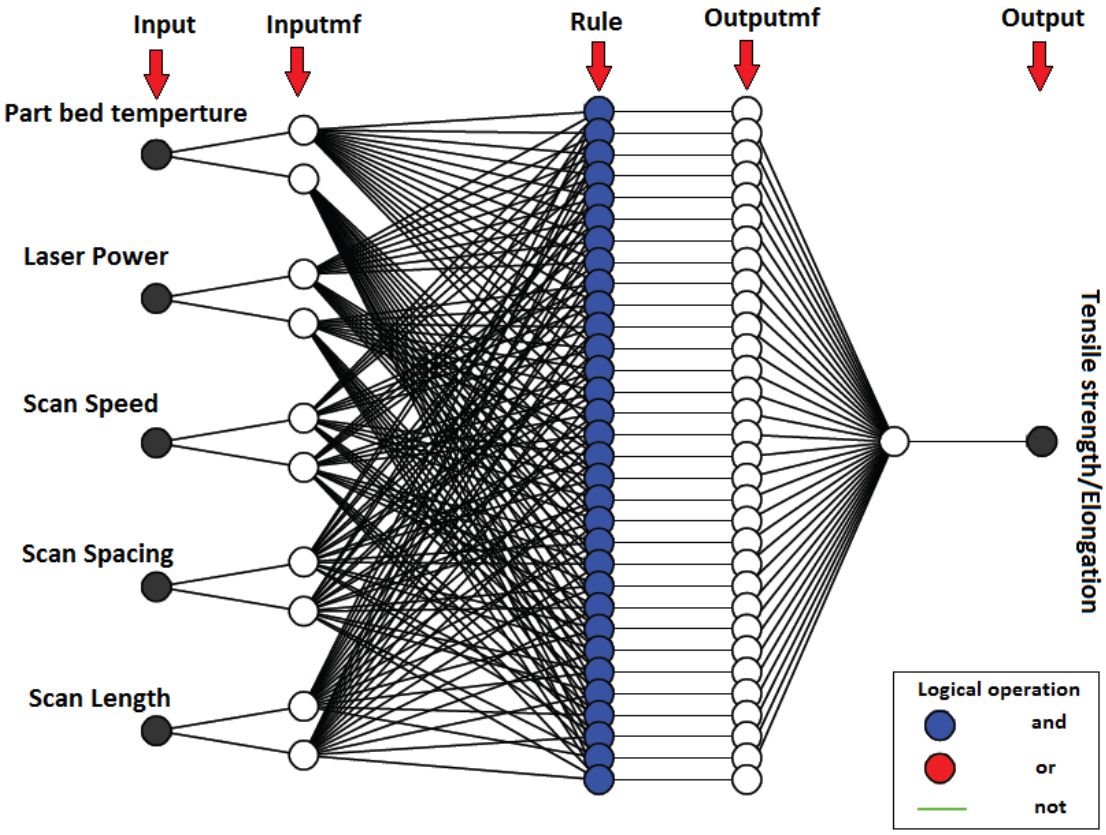

Fig 3.4. Structure of obtained ANFIS for estimation of ultimate tensile strength and elongation.

Choosing a structure of ANFIS with so many membership functions cause an overfitting and also type of MFs is considered as an essential element for accuracy of the model. In this study, different types of MFs namely generalized bell, trapezoid, triangular, Psigmoidal and Gaussian were examined. Table 3.2 indicates the RMSE of the implemented ANFIS models for tensile strength and elongation.

Eight types of membership function were examined and lowest RMSE was selected for each structure model. According to the result of ANFIS model, 2-2-2-2-2 structure with P sigmoidal function had the minimum values of RMSE based on the other MFs and other models for all two outputs. As shown in table 2, P sigmoidal is chosen for both outputs tensile strength and elongation regarding to other types of membership function. Also, Fig 3.5 and 3.6 indicates the comparison of measured values through experiments and estimated values with ANFIS for elongation and ultimate tensile strength in 10 experiments out of 50 experiments which are chosen randomly by 5 folds. It can be observed from the figures that there is good confirmation between data which measured experimentally and data which is estimated by ANFIS.

Table 3.2. Values of RMSE for tensile strength and elongation for various MFs structures.

Membership function	Tensile strength (N/mm2)	Elongation (%)
Triangular	19.8556	6.9848
Trapezoid	13.3039	7.0094
Generalized bell	14.2695	6.8417
Gaussian	13.2800	6.8756
Gaussian2	13.2688	9.9613
Pi shaped	13.2834	6.9666
D sigmoidal	13.2480	6.9632
P sigmoidal	**13.2391**	**6.9630**

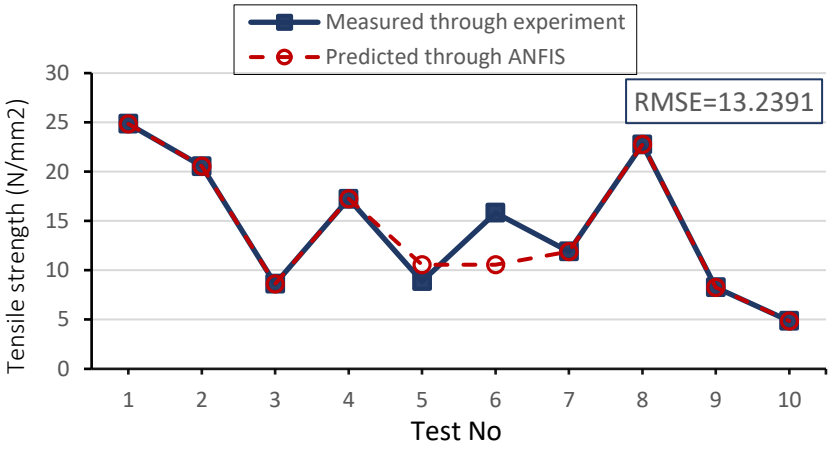

Fig 3.5. Comparison between measured and estimated data for tensile strength.

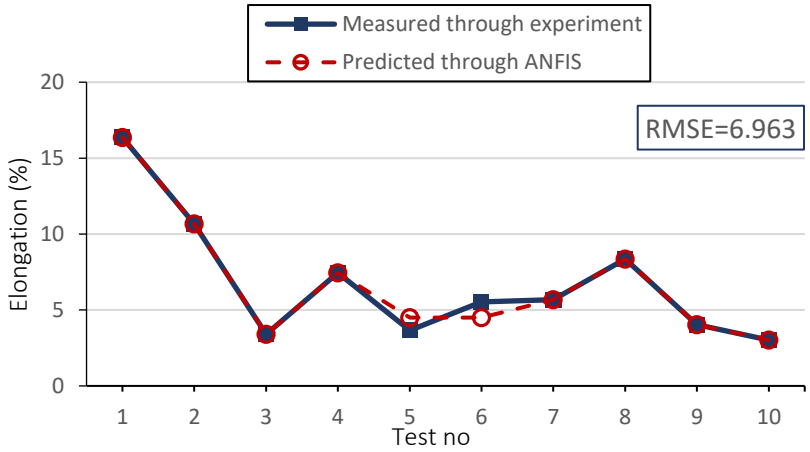

Fig 3.6. Comparison between measured and estimated data for elongation.

3.5.2. Analysis of responses: ultimate tensile strength and elongation

Figure 3.7 depicts the ANFIS response surface for tensile strength. According to RSM model, all of input factors had a significant impact on responses Fig 3.7(a-c). In particular, tensile strength and elongation were seen to increase with higher laser power (LP), and lower levels of scan speed (SE), and scan length (SL). It would be expected that with these settings, more material will be more melted and therefore greater bonding between the powder materials.

Figs. 3.7a and 3.7b show that there is an interaction between the part bed temperature and laser power for ultimate tensile strength and elongation. From the plots, it is evident that the tensile strength and elongation attained maximum values at a high level of part bed temperature (182°C) and at a correspondingly high level of laser power (36 W). These parameters would be expected to result in a higher degree of melting of the polyamide allowing it to flow and adhere better with the glass bead particles and surrounding material. This is beneficial to the densification of the glass-filled polyamide, causing increased relative density of the laser sintered parts. When the density of the part increases, tensile properties will be enhanced. When sintering takes place at a higher level of laser power and part bed temperature, the bond between the powder particles becomes stronger due to better fusion, resulting in increased ductility and strength. On the other hand, when laser power and bed temperature are on lower stage, melting the powder will be impossible due to lower temperature which is transferred to the powder, therefore, resulting lower tensile properties of sintered parts. According to the figure 3.7(a and d), temperature of part bed has a limitation, but if the temperature is increased distortion in parts will be accrued, resulting in reduced part properties.

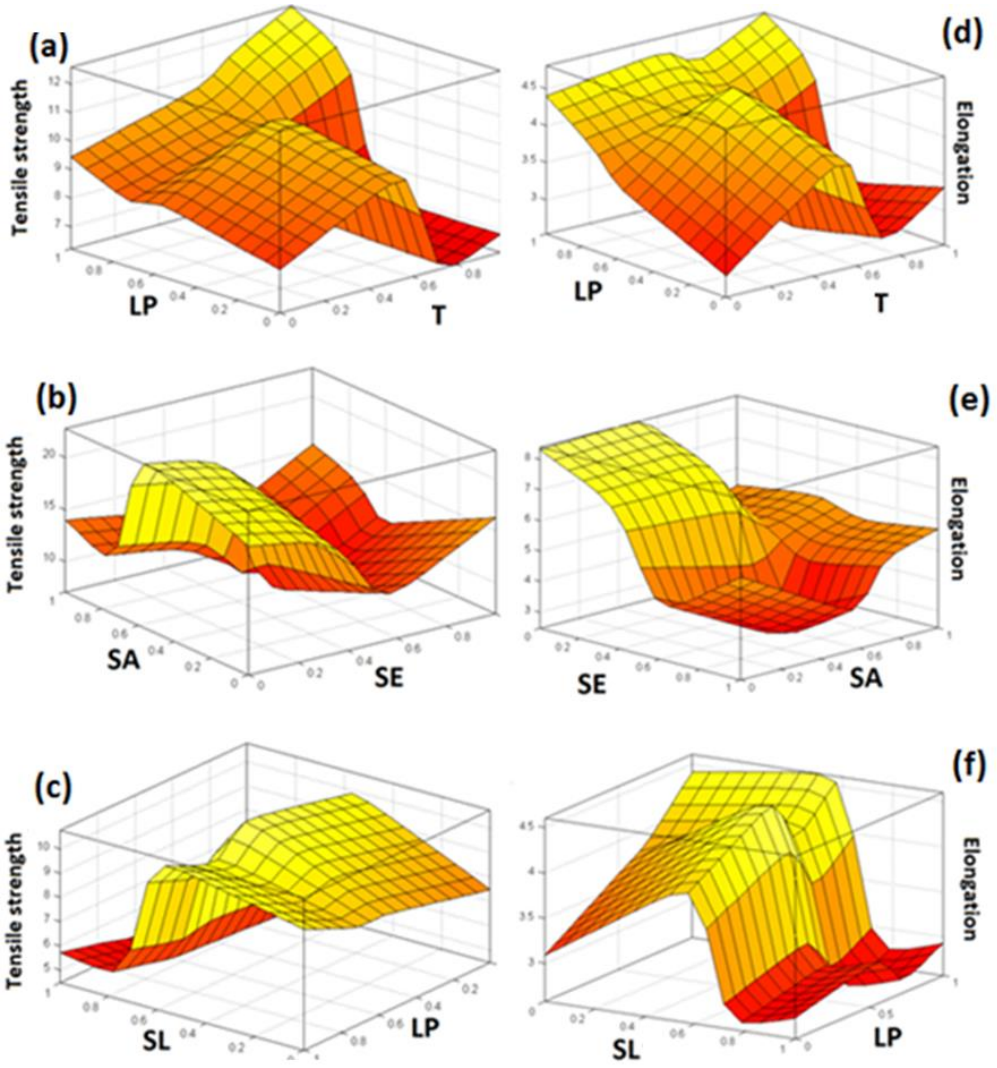

Fig 3.7. 3D response surface plots of tensile strength and elongation against (a and d) laser power (LP) and part bed temperature (T); (b and e) scan speed (SE) and scan spacing (SA); (c and f) laser power (LP) and scan length (SL).

Figs 3.7b and 3.7e demonstrate the interaction effect of scan speed and scan spacing on tensile strength and elongation. From the plots, it can be seen that the tensile strength and elongation attained a maximum value at a low level of scan speed (2500 mm/s) and scan spacing (0.25 mm). This can be described by the phenomenon that all of specimens which are made by SLS process at lower energy density phase (i.e. higher values of scan speed and scan spacing) were less well sintered.

However, very low values of scan speed and scan spacing (which means higher values of energy density) may cause over sintering of powder particles and will result in an unwanted increase in processing time.

Figure 3.7c and 3.7f show the interaction effect of laser power and scan length on tensile strength and elongation from which it is observed that the tensile strength and elongation are lowest at the lower value of laser power (28 W) and at the high value of scan length (140 mm). This was due to the lower laser power and longer scan lengths resulting in a lower level of local thermal energy input which was insufficient to completely sinter the powder particles.

3.6. Optimization of SLS process

3.6.1. Optimization of tensile strength and elongation by simulated annealing algorithm

Because of complexity of SLS against variation of input data, choosing of a value in which the procedure maximize tensile strength and elongation is a complex problem. The optimization algorithm techniques can therefore be well applied to provide solutions which can better maximize the mechanical property values from in this process.

The simulated annealing method is based on the simulation of thermal annealing of critically heated solids. When a solid (metal) is brought into a molten state by heating it to a high temperature, the atoms in the molten metal move freely with respect to each other [28]. As the temperature reduces, the atoms tend to get ordered and finally form crystals having the minimum possible internal energy. Based on the annealing description simulated annealing is a random search method which it can't trap in local minimum due to using of probability function as follow:

$$P(E) = \exp(-\frac{E}{K_B T}) \quad (1)$$

where T is temperature, k_B is the Boltzmann constant and E is the value of energy (value of objective function) at a given annealing step.

The simulated annealing algorithm is a random optimization technique which it starts minimization of annealing energy (objective function) from a single stochastic point, then the algorithm looks for minimal solutions by attempting of all points in search spaces with respect to their value of energy. In this method by selection of high cooling rate the probability of trapping in local minima is very high, so in order to escaping from local minima, choosing of appropriate slower cooling rate is recommended. The pseudo program for step by step implementation of simulated annealing procedure is expressed as follow:

Step 1: (initializing): Generate a randomly initial point x_0, setting the initial temperature $T=T_{init}$ and iteration number $k=0$

Step 2: (calculation of annealing energy): Evaluate the value of objective function at x_k, $E_1=F(x_k)$

Step 3: (generation randomly neighbor point): Create a stochastically point x_{k+1}, near to pervious one and calculate the energy at this point $E_2=F(x_{k+1})$ and determine $\Delta E=E_2-E_1$

Step 4: (inspection of first condition): If $\Delta E<0$**,** current point is acceptable and go to step 6. Otherwise generate a random number (α) belongs to [0,1] and calculate the probability $P=exp(-\Delta E/K_BT)$

Step 5: (inspection of second condition): If $P<\alpha$**,** then current point is acceptable and go to step 6. Otherwise return to step 3.

Step 6: (inspection of iteration condition): If $k<N$ (N is the maximum number of tries within one iteration) then set $k=k+1$ and go to step 3. Otherwise go to step 7.

Step 7: (stop condition): If $T<ST$, (ST is stop temperature) stop the algorithm. Otherwise set $k=1$, reduce the temperature $T=CT$ (C is cooling rate) and go to step 3.

Table 3.3 represents all set up factors and objective function of SA.

Table 3.3. Table 6 setup parameters for implementation of SA

Parameter	Value/function	Remark
X_0	[0 0 0 0]	Initial point
T_{init}	500	Initial temperature
H(X)	- evalfis(X,net)	Objective function which uses "*evalfis*" function for Simulation the ANFIS net
R	X=rand (5,1)	Random vector *X* in the range of [0,1]
k_B	1	Boltzmann constant
ST	10e-8	Stop temperature
C	0.9	Cooling rate
N	300	Maximum number of tries within one temperature

In this part, 2-2-2-2-2 ANFIS structure which calculated from last section, will be used as an objective function in order to make maximum values of ultimate tensile strength and elongation. For the optimization algorithm, a MATLAB code was generated with Rastrigin error checking function included. In optimization of the process by ANFIS-SA, the part bed temperature of 180 °C, laser power of 28.92 W, scan speed 3410 mm/s, scan spacing 0.375 m and scan length 133.564 mm resultant in optimal solution with tensile strength of 42.883 N/mm^2 and elongation of 17.383%. Table 3.4 shows optimal results derived from simulated annealing (SA). According to the optimization these inputs would lead to maximum tensile strength and elongation. For confirmation of the obtained solution from the model, a verification experiment with values from table 3.4 will be performed. If the acquired values of tensile strength and elongation would be seen to be close to those derived from the verification experiment, the modelling and optimization would be considered implemented successfully. Table 3.5 presents a comparison between the optimal tensile strength experimental results and elongation and the ANFIS model predicted results. It is seen that percentage error is below 5% and 10% for the tensile and elongation values respectively.

Table 3.4. Optimal proposed parameters and corresponding results obtained through SA.

Process factors					Responses	
Part bed temperature (^{o}C)	Laser power (W)	Scan speed (mm/s)	Scan spacing (mm)	Scan length (mm)	Tensile strength (N/mm^2)	Elongation (%)
180.19	28.92	3410	0.375	133.564	42.8883	17.383

Table 3.5. Comparison of tensile strength and elongation of confirmatory experiments with those derived from the developed ANFIS-SA model.

Tensile strength			Elongation		
Measured	Predicted	Error (%)	Measured	Predicted	Error (%)
44.295	42.8883	3.176	15.85	17.383	-9.672

3.6.2. Optimization of process by GRA

As explained in section 3.2.3 in order to optimize the process by GRA, firstly the experimental results should be normalized. For this purpose, higher-the-better strategy was used for normalizing of material removal rate and lower-the-better strategy is used for normalizing of both tensile strength and elongation. Then the grey relational coefficients were calculated based on values of normalized data for each response. The coefficients of outputs have been collected to assess GRG that is the overall representative of tensile strength and elongation. In the present work the same weight factors ($W_1=W_2=W_3=0.333$) are considered to construction grey relational grade.

Hence, the hybrid optimization of SLS process has been converted to one equivalent objective function of the process. Figure 3.8 presents the grey value against the number of experiments for each experimental set of parameters examined.

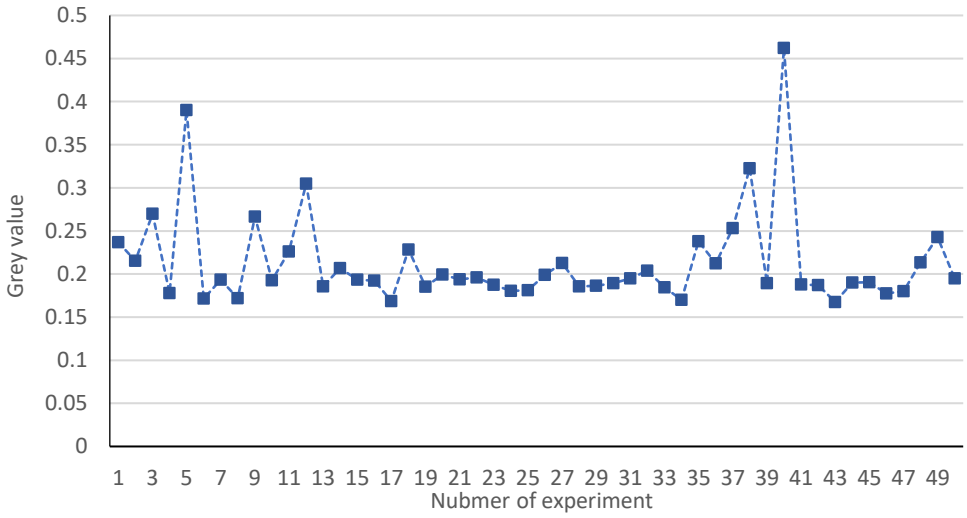

Fig 3.8. Grey relational value for each experiment run.

Fig.3.9 presents the main effect plots for the selected processing conditions such as part bed temperature, laser power, scan speed, scan spacing and scan length. The main effect plot provides a representation of the importance of each process elements on the output parameters. In the main effects chart, if the line for a specific process parameter has the biggest slop, then the parameter has the most significant effect, whereas, if the line for a specific element is closest to horizontal line, then that parameter has no significance. Therefore, from the main effects plot scan length and scan speed have slightly more significance than the other inputs on the tensile properties of the glass filled polyamide specimens. From Fig. 3.9. the optimal parametric combination can be determined. The optimal process parameter setting is 182 ºC (max.), part bed temperature, 28 W laser power (lowest), 2500 mm/s scan speed (lowest), 0.45 mm scan spacing (max.) and 140 mm scan length (max.). Furthermore, the effect of interaction between the two process parameters is shown in Fig. 3.10. From these plots, it is observed that almost all lines are intersecting with each other; that is, all process parameters have considerable interaction between each other.

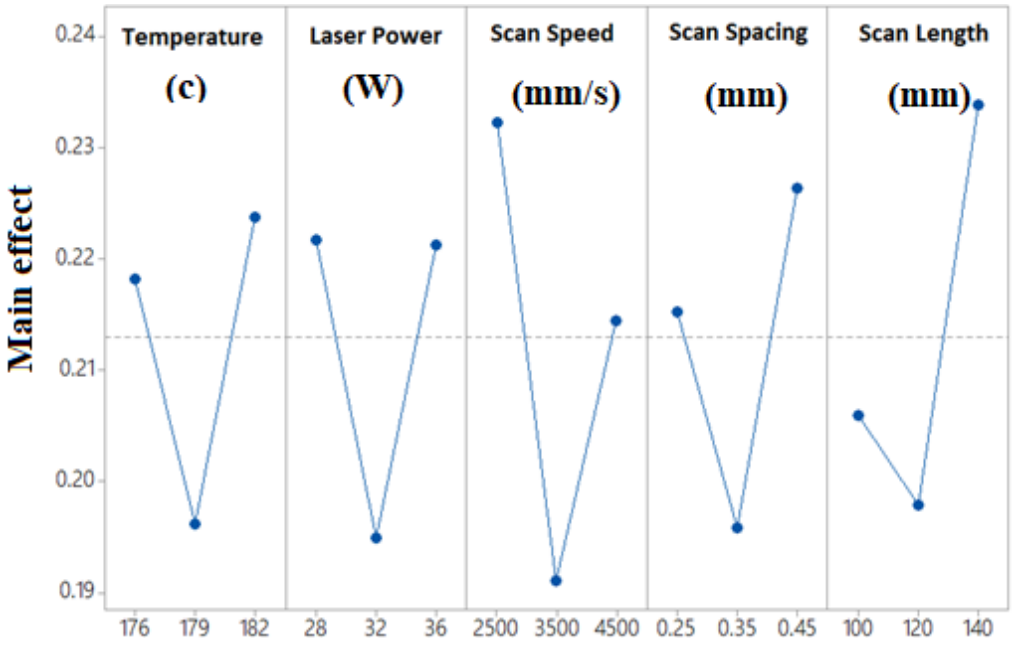

Fig 3.9. Main effects plot of the grey values for the effects of the input parameters.

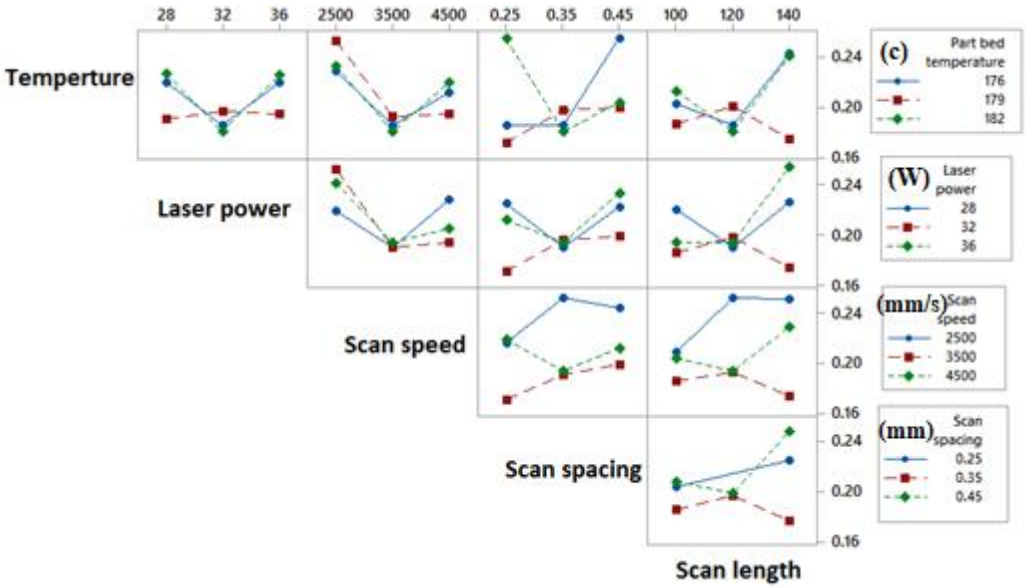

Fig 3.10. Interaction plot of the determined grey grade values for each of the input parameters.

From Table 3.6 it is seen that applying a combination of normalized grey relation coefficient of 0.2237 for temperature, 0.2217 for power, 0.2322 for scan speed, 0.2322 for scan spacing, and 0.2338 for scan length resulted in the highest value of GRA and maximum combination of tensile strength and elongation. The levels of the results which result in the maximum tensile strength and elongation correspond exactly with those found from response surface methodology.

Table 3.6. Response surface for the mean grey relational grade values.

Symbol	Sintering parameters	Level 1	Level 2	Level 3	Max-Min
PB	Part bed temperature	0.2181	0.1961	**0.2237**	0.0056
LP	Laser power	**0.2217**	0.1949	0.2212	0.0276
SE	Scan speed	**0.2322**	0.191	0.2144	0.0412
SA	Scan spacing	0.2152	0.1958	**0.2263**	0.0305
SL	Scan length	0.2059	0.1979	**0.2338**	0.0359
		Average grey relational grade=0.2125			

The following step is the verification and prediction of quality characteristics based on the new condition of inputs and outputs which is achieved by GRA. Because of that, experimental verification was performed with the achieved selected input parameters, and tensile strength and elongation. If the GRG results is acquired from the experiment was close to results from predication, the presented method can be said to be efficient in prediction of optimization process. Table 3.7 shows the difference between the predicted GRG with the actually acquired from experiments in the selected factor. It can be concluded that there is an acceptable agreement between the results from experiments and GRA. This confirms the function of the suggested method based on the multi objective optimization in manufacturing process needs to optimize the responses as the same time.

Table 3.7. Results of confirmatory test of the effects of the input factors on the output.

	Initial sintering parameters	Optimal sintering parameters	
		Experiment	Prediction
Setting level	T1, LP1, SE1, SA1, SL1	T3, LP1, SE1, SA3, SL3	T3, LP1, SE1, SA3, SL3
Tensile strength	20.14	31.04	-
Elongation	7.4	9.42	-
Grey relational grey	0.2369	0.2583	0.2765
Improvement of grey relational grade=9.033%			

Table 3.8. Optimal proposed parameters and corresponding results obtained through SA an GRA

	Process factors					Responses	
ANFIS-SA	Part bed temperature (^oC)	Laser power (W)	Scan speed (mm/s)	Scan spacing (mm)	Scan length (mm)	Tensile strength (N/mm^2)	Elongation (%)
	180.19	28.92	3410	0.375	133.564	42.8883	17.383
GRA	182	28	2500	0.45	140	28.1083	10.983

3.7. Conclusion

This work was focused on the multi-objective optimization of process elements for the SLS process of glass filled polyamide parts. The main factors examined in this process were part bed temperature, laser power, scan spacing, scan speed and scan length. The main responses were ultimate tensile strength and elongation. For performing of multi-objective optimization two methodologies have been used. The first methodology was based on modelling of tensile strength and elongation by ANFIS and optimization by SA algorithm. The second methodology was based on GRA. After performing optimization of process by these methods, the obtained results were compared together. A summary of achieved results is presented as follows:

An ANFIS based on 2-2-2-2-2 structure with Psigmoidal type of MFs led to maximum precision of modelling for tensile strength and elongation by making the minimum values of prediction error. In optimization of the procedure by ANFIS-SA, the part bed temperature of 180 °C, laser power of 29 W, scan speed 30 mm/s, scan spacing 0.37 m and scan length 133 mm resultant in optimal solution with tensile strength of 42.8883 N/mm^2 and elongation of 17.383%.

The verification experiments were also used to confirm optimal results. The results of validation experiment with GRA and ANFIS-SA approaches are Closely consistent. Due to the ability of ANFIS-SA to search the entire solution space within the process parameter settings examined, ANFIS-SA was seen to outperform the GRA model. This resulted in an increase of the overall tensile strength and elongation results obtained by 14.78 N/mm^2 and 6.4 % respectively for the output of ANFIS-SA compared to GRA. Based on our experiences, we can suggest that ANFIS-SA be an effective approach to solving a multi-objective optimization problem in manufacturing processes which responses related in a complex manner to the input parameters.

The main reason for the ANFIS-SA model's better result is the searching nature of both ANFIS and SA. With ANFIS and SA, these models consider a continues range for each parameter which leads to an extension of the search space and finding new solutions. While in optimization by GRA, only values which contribute to conducting experiments are considered. Hence, for GRA the searching space is just within the

design matrix and it is very small. The ANFIS-SA can be seen in this case to outperform on the basis that it solves the optimization as a continuous problem, and it can search all points within the solutions space.

References

1. Deckard C and Beaman J; Process and control: issues in selective laser sintering. ASME PED, 33: 191–197 (1988).

2. Bacchewar P, Singhal S and Pandey P; Statistical modelling and optimization of surface roughness in the selective laser sintering process, Part B: Journal of Engineering Manufacture, vol. 221, 1: pp. 35-52., First Published Jan 1 (2007).

3. Sharma V, Singh S, Sachdeva A and Kumar P; Influence of sintering parameters on dynamic mechanical properties of selective laser sintered parts. Int J Mater Form 8:157–166 (2015). (Sharma et al., 2007)

4. Sohrabpoor H, Issa A, Hamaoy A, Ahad I, Chikarakara E, Bagga K, Brabazon D, Chapter 24, Development of laser processing technologies via experimental design, pp. 707-730, 2nd Edition, Edited by Jonathan Lawrence, Elsevier, Woodhead Publishing, ISBN 978-0-08-101252-9 (2017).

5. Obeidi M, McCarthy E, Brabazon D; Methodology of laser processing for precise control of surface micro-topology, Surface and Coatings Technology, Vol 307, Part A, pp. 702-712; DOI: 10.1016/j.surfcoat.2016.09.075 (2016)

6. Dingal S, Pradhan T, Sarin Sundar J, Choudhury A and Roy S; The application of Taguchi's method in the experimental investigation of the laser sintering process, Int J Adv Manuf Technol, 38:904–914 (2008).

7. Arasu I, Chockalingam K, Kailasanathan C and Sivabharathy M; Optimization of Surface Roughness in 2 Laser Sintered Stainless Steel Parts, International Journal of ChemTech Research, Vol.6, No.5, pp 2993-2999 (2014).

8. Negi S, Dhiman S and Sharma R; Determining the effect of sintering conditions on mechanical properties of laser sintered glass filled polyamide parts using RSM, Measurement, Volume 68, Pages 205–218 (2015).

9. Negi S and Sharma R; Influence of Processing Variables on Dynamic Mechanical Response of Laser-Sintered Glass-Filled Polyamide, Materials and Manufacturing Processes Volume 30 (2015).

10. Negi S, Dhiman S and Sharma R; Investigating the Surface Roughness of SLS Fabricated Glass-Filled Polyamide Parts Using Response Surface Methodology, Arab J Sci Eng 39:9161–9179 (2014).

11. Negi S and Sharma R; Study on shrinkage behaviour of laser sintered PA 3200GF specimens using RSM and ANN, Rapid Prototyping Journal, Volume 22 · Number 4.645–659 (2016).

12. Mungui J, Ciurana J, and Riba C; Neural-network-based model for build-time estimation in selective laser sintering, Part B: Journal of Engineering Manufacture, vol. 223, 8: pp. 995-1003 (2009).

13. Boillat E, Kolossov S, Glardon R, Loher M, Saladin D and Levy G; Finite element and neural network models for process optimization in selective laser sintering, Part B: Journal of Engineering Manufacture, vol. 218, 6: pp. 607-614 (2004).

14. Shen X, Yao J, Wang Y and Yang J; Density Prediction of Selective Laser Sintering Parts Based on Artificial Neural Network, Advances in Neural Networks, pp 832-840 (2004).

15. Vijayaraghavan V, Garg A, CHWong K, Regalla S and Tsai M, Density characteristics of laser-sintered three-dimensional printing parts investigated by using an integrated finite element analysis–based evolutionary algorithm approach, Proc IMechE Part B: J Engineering Manufacture Vol. 230(1) 100–110 (2016).

16. Teimouri R and Shrabpoor H; Application of adaptive neuro-fuzzy inference system and cuckoo optimization algorithm for analyzing electro chemical machining process, Front. Mech. Eng. 8(4): 429–442 (2013).

17. Yanga S, Srinivas J, Mohana S, Leea D and Balaji S; Optimization of electric discharge machining using simulated annealing, Journal of Materials Processing Technology 209 4471–4475 (2009).

18. Sohrabpoor H; Analysis of laser powder deposition parameters ANFIS modelling andICA optimization, Optik 127 ,4031–4038 (2016).

19. Chen H, Lin J, Yang Y and Tsai C; Optimization of wire electrical discharge machining for pure tungsten using a neural network integrated simulated annealing approach, Expert Systems with Applications 37 -7147–7153 (2010).

20. Zaina A, Haronb H and Sharif S; Optimization of process parameters in the abrasive waterjet machining using integrated SA–GA, Applied Soft Computing 11 5350–5359 (2011).

21. Zhang Z and Kovacevic R; Multiresponse Optimization of Laser Cladding Steel + VC Using Grey Relational Analysis in the Taguchi Method, JOM, Vol. 68, No. 7 (2016).

22. Azhiri R, Teimouri R, Baboly M, Leseman Z; Application of Taguchi, ANFIS and grey relational analysis for studying, modelling and optimization of wire EDM process while using gaseous media, Volume 71, Issue 1–4, pp 279–295 (2014). (Azhiri et al., 2014)

23. Amini S and Teimouri R; Parametric study and multi-characteristic optimization of rotary turning process assisted by longitudinal ultrasonic vibration, Proc IMechE Part E: J Process Mechanical Engineering 0(0) 1–14 (2016). (Amini et al., 2016)

24. Lal S, Kumar S, Khan Z and Siddiquee A; Multi-response optimization of wire electrical discharge machining process parameters for Al7075/Al2O3/SiC hybrid composite using Taguchi-based grey relational analysis, Proc IMechE Part B: J Engineering Manufacture, Vol. 229(2) 229–237 (2015).

25. Chiu S, Gan S, Tseng Y, Chen K, Chen C, Su C and Pong S; Multi-objective optimization of process parameters in an area-forming rapid prototyping system using the Taguchi method and a grey relational analysis, IMechE Part B: J Engineering Manufacture 1–12 (2016).

26. Sohrabpoor H, Khangha S, Shahraki S and Teimouri R; Multi-objective optimization of electrochemical machining process, Int J Adv Manuf Technol, Volume 82, Issue 9–12, pp 1683–1692 (2016).

27. Sohrabpoor H, Perspective of Applying Adaptive Neuro Fuzzy Inference System (ANFIS) in Laser Cladding of Graphene-Metal Alloys; Journal of Nanotechnology: Nanomedicine & Nanobiotechnology, J Nanotechnol Nanomed Nanobiotechnol 4: 017, 2017.

Chapter 4

Improving precision in the prediction of laser texturing and surface interference of 316L assessed using neural network and adaptive neuro-fuzzy inference models

Publication Status: Published

H. Sohrabpoor, R. Taherzadeh Mousavian, M. Obeidi, I. U. Ahad, and D. Brabazon, The International Journal of Advanced Manufacturing Technology, Springer 2019.

DOI: 10.1007/s00170-019-04291-z.

Abstract

Laser based surface texturing provides highly controlled interference fit between two parts. In this work, artificial intelligence-based models were used to predict the surface properties of laser processed stainless steel 316 samples. Artificial neural network (ANN) and adaptive neuro-fuzzy inference system (ANFIS) were used to predict the characteristics of laser surface texturing. The models based on feedforward neural network (FFNN) were developed to examine the effect of the laser process parameters for surface texturing on 316L cylindrical pins. The accuracy of the models was measured by calculating the root mean square error and mean absolute error. The reliability of the ANFIS and FFNN models for the output prediction of the laser surface texturing (LST) system were investigated by using the data measured from experiments based on a 3^3 factorial design, with main processing parameters set as laser power, pulse repetition frequency, and percentage of laser spot overlap. The relative assessment of the models was performed by comparing percentage error prediction. Finally, the impact of input data was examined using predicted response surface plots. Results showed that ANFIS prediction was 48% more accurate compared to that provided by the FFNN model.

Keywords: Laser texturing; artificial neural network; adaptive neuro-fuzzy inference system.

4.1. Introduction

Joining plays a significant role in manufacturing such as in automotive engineering for the assembly of parts and devices [1]. Mechanical joints for bonding parts in assembly lines can be joined via many different gluing options [2]. Press fit or interference fit are commonly used such as in clinching joints, hinge joints, and for bonding shafts and bearings. Interference fits joints bond two components together by friction, often with a single quick stroke [3]. The creation of patterned surface microstructures on interference fit joints can be achieved in many ways, for example abrasive blasting, reactive-ion etching, and ultrasonic machining [2]. However, laser technology offers more control and precision over the produced geometry [3]. Laser Surface Texturing (LST) has been used for three decades in manufacturing industry for improvement and control of tribological characteristics of materials. However, the use of this process for press fit joints is has recently been developed [2]. LST on interference joint surfaces is a complex, stochastic process and a number of variables play a significant role in the process. Therefore, the development of an appropriate model which can approximate the effects of the most important features on the resulting geometry is of significant importance.

Several studies have been reported on the application of supervised machine learning methods on predicting the output of the laser process [4,5]. Artificial Neural Network (ANN) and fuzzy logic have been applied successfully previously for prediction of some laser processes [4,6]. Approximation methods which are related to artificial intelligence are secondary tools which use data generated through experiments for the estimation manufacturing process outputs [4]. Aminian et al. investigated the performance of ANN and applied adaptive neuro fuzzy system (ANFIS) on the laser machining and welding processes [5]. In their work these authors noted that ANFIS was a better predictor compared to Response Surface Methodology (RSM) and ANN. Biswas et al. used feed forward neural network (FFNN) for estimation of characterization of micro drilling on titanium nitride-alumina composite [6]. It was observed that an ANN node structure of 5-11-3 with 11 neurons in the hidden layer provided the least model error. Sohrabpoor et al. used ANFIS to predict laser powder deposition process outputs such as catchment efficiency and height [7]. Additionally,

ANFIS was employed in selective laser sintering to correlate relationship between input parameters such as laser power and scan speed, and output factors including tensile strength and elongation [8]. The authors have also reported previously the use of ANFIS for laser processing and demonstrated the high capability and reliability of this model [9-13]. J. Pandremenos et al. used a mixture of neural network and design structure matrices for the link between clustering efficiency and interactions of products components [14]. They found that their especial algorithm is more efficient with the empirical one [14]. Karagiannis et al. applied feed forward back-propagation for approximation of yield surface magnitude in milling process [15]. They concluded that the model had a acceptable performance for correlation of inputs and results [15]. Also, some other studies have been carried out for the practicality of ANFIS and FFNN in the manufacturing process [16-19].

The experimental values are used to train a feed forward back-propagation artificial neural network for the prediction of the yield surface roughness magnitude. Laser surface texturing of stainless-steel for interference fit is a novel technique developed by the co-authors. Interference fit is no more compliant pins focused joining technique, rather it has become an enabling technique for innovations in high-tech industries, such as safety critical fueling applications. In the developed LST technique, the control of diameter increase is crucial to achieve different levels of fastening between the joining parts and this control also determines the insertion and pull out forces. Therefore, in order to provide design flexibility, increasing strength and reliability of LST for interference fits, it is desirable to fully model the laser processing input parameters and use artificial intelligence techniques to predict the results.

In this study, investigations were performed for the first time, the selection of best approach for the estimation the characteristics of LST on 316L cylindrical pins for the interference fit joint. Although there are many factors which are related to the strength of the bonding, the most important parameters of diameter increase (DI), insertion force (IF) and removal force (RF) were studied. To achieve this goal, the actual data sets were extracted from the response surface methodology equations [3]. For the LST process FFNN and ANFIS were applied separately. The validity of the developed

models was measured based on percentage error prediction (PEP). The effect of input parameters on each process outputs are analysed.

The interference fit has innovative applications in security critical components in automobile and aerospace industry where a secure joint with high level of security and reliability is required. Therefore, in order to determine the laser processing parameters tailored for specific needs in terms of material, tightness level, applied and removal force, and reliability, artificial intelligence approaches can be further examined and investigated. The development of reliable and accurate artificial intelligent solutions is required that can predict most influencing processing parameters and provide solution to approximate the resulting properties as demonstrated previously using unsupervised and supervised learning methods.

Based on the literate review, there is no study has been carried out to demonstrate difference between ANFIS and FFNN on LST. This comparison can be useful not only in modelling terms but also on practical perspective and manufacturing industries can refer to this evaluation for the prediction of results which ensure quality of product, to reduce the manufacturing cost and to increase the quality of cold joints.

4.2. Methodology

4.2.1. Development of FFNN model

Neural network (NN) is a logical structure, in which multiple processing elements communicates with each other through the interconnections between the processors. The knowledge is presented by the interconnection weight, which is adjusted during the learning stage [14]. Backpropagation (BP) learning algorithm uses a gradient search technique to minimize the mean square between the actual output pattern of the network and the desired output pattern.

In FFNN, weights were fixed, and the activation function were examined and selected based on mean absolute error (MAE). More details were reported previously [4]. Like other approximation methods, FFNN was implemented including testing (20%) and

training (80%) and MAE was utilized as the criteria of error in FFNN. The equation used for calculation of MAE is:

$$\text{MAE}=\frac{1}{T}\sum_{i=1}^{T}|t_i - a_i|$$

[5]

where T is the number of test data, t_i is the tested value and a_i is predicted value from FFNN.

4.2.2. Description of ANFIS

ANFIS is a machine learning method with the mixture of NN and fuzzy logic for deriving the connections between the input and response elements [17]. The ANFIS model for this study was made of five layers each of which consist of some nodes. Like NN, in ANFIS, nodes transform from each layer to next layer. The accuracy of trained data was examined by root mean square error (RMSE), the formula for which is:

$$RMSE=\sqrt{\frac{1}{M}\sum_{z=1}^{M}(S_z - Y_z)^2} \qquad [17]$$

where M is the training value, S_z is actual response value, and Y_z is the model response value in training.

4.3. Materials

The data used for validation of the designed models was obtained from Design of Experiment (DoE) study on laser surface texturing for interference fit technique. This study was performed by the co-authors and reported previously [2,20]. Briefly, cylindrical 316L stainless steel pins of 10 mm in diameter and 60 mm length were laser textured. The laser process as shown in Fig. 4.1 was carried out using a computerized numerical control (CNC) CO_2 laser, Rofin DC- 015, with 1.5 kW maximum average power. The focal position was set at a distance of 1 mm below the sample surface to achieve 0.2 mm diameter focal spot size over the sample surface. Hub flanges of the

same material were machined to 30 mm external diameter, and centre drilled and reamed to give the final hole diameter of 10.05 ± 0.003 mm. Table 4.1 shows the input parameters including Laser Power (LP), Pulse Repetition Frequency (PRF) and Overlap (OL) between each laser scan and their levels which were used for experimental sample preparation. Laser power is the most important input parameter which determines the amount of thermal energy delivered to the sample being laser treated. The laser power was varied from 300 W to 400 W and 500 W. In pulsed laser surface processing, the pulse repetition frequency determines the heat build-up between the pulses. The time interval between the laser pulses should be shorter than the thermal diffusivity of the material in order to build up amount of heat required for melting of the upper layer surface. Therefore, PRF was set at 100 Hz, 200 Hz and 300 Hz and the pulse width was set at 1.6 ms to examine the effect of PRF on the resulting surface properties of the laser processed samples. For interference fit application, precise control over micro-texture longitudinal and circumferential dimensions is required. To control the laser texture geometry, the laser scan overlap over the sample surface must be accurately controlled as multiple scanning of the same area will result in different surface texture. Three different overlap scenarios were studied including negative, positive and zero overlap to examine the effect on microstructure. The overlap was controlled by controlling the rotational and translational speeds of the sample such that the laser spots were overlapped to the same extent in the circumferential and longitudinal directions. Detailed mathematical relationships used to calculate overlap percentage for all three scenarios according to sample geometry, laser processing parameter (PRF), and rotational and longitudinal speeds have been reported previously [20].

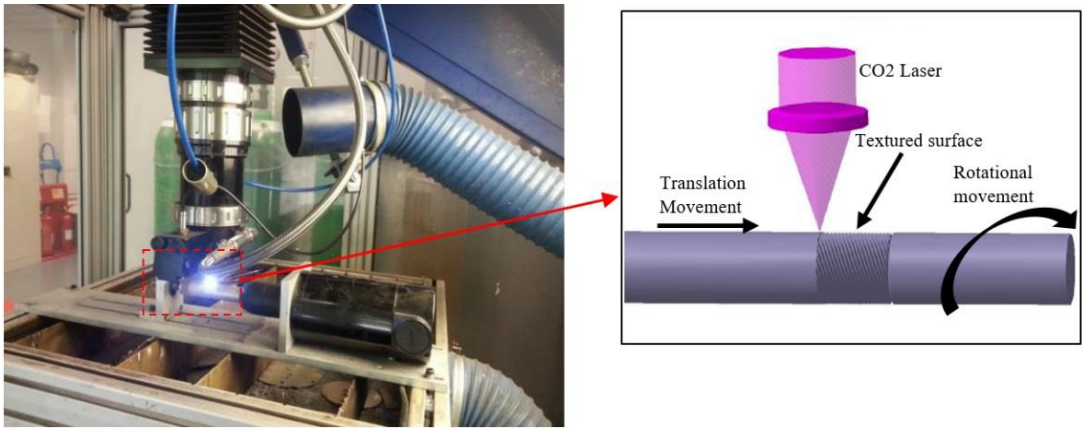

Fig. 4.1. Schematic of scanning process on an interference fit sample with CO_2 laser.

Table. 4.1. Laser surface texturing set DoE process factors and their levels.

Process factors	Units	Symbols	Levels		
			-1	0	1
Laser Power	W	LP	300	400	500
Pulse Reputation Frequency	Hz	PRF	100	200	300
Overlap	%	OV	-20	0	20

For the current study, Diameter Increase (DI), Insertion Force (IF) and Removal Force (RF) were selected as output parameters from the previous study [2]. Details on methods used to obtain these results have been reported [2]. Details on selection of these parameters for the current study and methodologies used to measure these parameters previously are as follows. The creation of microstructures on the surface of the laser processed stainless steel pins resulted in the increased diameter. The change in the microstructure from austenite to large volume martensite phase also contributed to increased pin diameters [2,1]. Diameter of the pin is directly related to amount of interference. The control over diameter increase provides control over tightness of the fit. Therefore, DI was selected as output parameter in this study. Diameters of the laser processed pins were measured by 0.05 mm resolution Vernier. Each measurement was taken 10 times and average values were obtained. The ratio of insertion and pull out forces determines the efficiency of the interference fit. The reduction in insertion force makes the process economical and the removal force determines the tightness of the interference. Being the crucial factors determining the

interference fit, IF and RF were selected as output parameters in the current study. The insertion and pull-out forces were measured using a Zwick Z-50 testing machine with the Zwick TestXpert simulation software. The insertion and pull-out tests were performed at speed of 5 mm/min (for further details, see [2]).

4.4. Results and discussion

The approximation methods including FFNN and ANFIS were used to approximate the output of the laser surface texturing of stainless-steel pins for interference fit application. In FFNN and ANFIS models in order to increase the reliability and validity of the data, each run repeated three times and average of them are reported.

4.4.1. Development of FFNN model

As the measured values of the three selected output parameters were largely different, the models were divided into 4 networks to achieve maximum efficiency separately for each parameter.

4.4.1.1 k-Fold Cross-Validation

In order to avoid overfitting and having lower bias, 4-fold Cross-Validation approach applied. Cross-validation is a resampling procedure used to evaluate machine learning models on a limited data sample [21]. In K-Folds Cross Validation we split our data into k different subsets (or folds). We use k-1 subsets to train our data and leave the last subset (or the last fold) as test data. We then average the model against each of the folds and then finalize our model. After that we test it against the test set. The procedure has a single parameter called k that refers to the number of groups that a given data sample is to be split into. As such, the procedure is often called k-fold cross-validation. When a specific value for k is chosen, it may be used in place of k in the reference to the model, which in this case data is divided to 4 folds (Fig 4.2). For the cross-validation process, first we picked 4 separate learning experiments which included one testing test and remaining for training sets. This process is repeated 4 times and finally we got the average test results from those experiments.

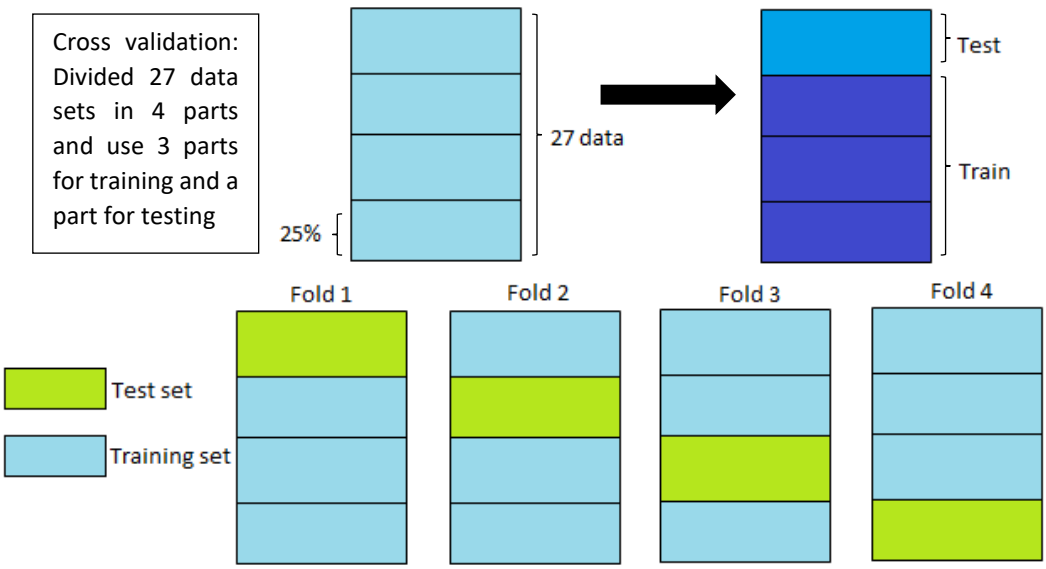

Fig. 4.2. Structure of cross validation for 4 folds.

Table. 4.2. Obtained MAE for various FFNN topographies under various training function.

Outputs	Structure	Mean absolute error (MAE)				
		Fold #1	Fold #2	Fold #3	Fold #4	Average
DI	3-4-1	0.1214	0.1303	0.286	0.1709	0.1771
	3-5-1	**0.102**	**0.1254**	**0.1903**	**0.1363**	**0.1391**
	3-6-1	0.1768	0.1227	0.2207	0.2762	0.1991
	3-7-1	0.1359	0.259	0.2031	0.1053	0.1758
	3-8-1	0.245	0.2772	0.1729	0.1605	0.2139
	3-9-1	0.1446	0.2636	0.2039	0.1336	0.1864
IF	3-4-1	9.5422	7.681	11.8953	10.9615	10.02
	3-5-1	**9.6862**	**6.4945**	**6.3013**	**14.3468**	**9.2072**
	3-6-1	12.2945	6.3225	9.5408	10.4056	9.6408
	3-7-1	8.761	8.3664	12.3194	9.5307	9.7218
	3-8-1	9.5366	10.9437	13.0343	10.094	10.9021
	3-9-1	13.6917	9.2882	12.7691	10.2411	9.2475
RF	3-4-1	1.5413	1.4407	3.6875	3.3059	2.4935
	3-5-1	4.2451	2.541	2.6988	3.2035	3.1721
	3-6-1	2.5167	2.5392	2.7247	3.847	2.9069
	3-7-1	**1.4931**	**2.8258**	**2.2417**	**3.9129**	**2.6183**
	3-8-1	2.3913	2.325	3.28	3.0497	2.7615
	3-9-1	2.8758	2.6281	2.2546	3.1993	2.73945

For developing the FFNN model, the initial step was training. Out of 27 datapoints available from the experiments performed previously [2], 21 datasets were selected arbitrary for training and the remaining (6 datasets) were kept for testing the FFNN

model (i.e. fold #1). In order to select the FFNN model which provides most accurate approximation, 9 training functions and 6 structures were tested. In hidden layers, the number of neurons should be higher than inputs [22]. Therefore, the examination should be started from 4 neurons were selected for the first hidden. Minimum MAE was selected for each output. From the table 4.2, a network with 3-5-1 structure, for DI and IF, and 3-7-1 structure for RF are the modest accurate model due to lowest values of MAE. Figs. 3, 4 and 5 present the comparison between the actual datasets and predicted datasets from the FFNN and ANFIS models fold #4 (i.e. fold with highest MAEs). As can be seen from these figures, the optimized models predicted well with the actual experimental recoded data.

Table. 4.3. Obtained RMSE for various ANFIS topographies under various training function.

Output	Structure	Root mean square error (RMSE)				
		Fold #1	Fold #2	Fold #3	Fold #4	Average
DI	**Triangular**	**0.12436**	**0.11419**	**0.10628**	**0.112**	**0.1142**
	Trapezoid	0.18483	0.4081	0.1834	0.1598	0.2325
	Generalized bell	0.14131	0.3682	0.2551	0.2551	0.2549
	Gaussian	0.14004	0.3845	0.2528	0.5851	0.3407
	Pi shaped	0.1732	0.4866	0.2722	0.2972	0.2972
	Di sigmoidal	0.25378	0.5035	0.2972	0.2597	0.3285
IF	**Triangular**	**6.9956**	**5.05**	**6.469**	**11.3502**	**7.4662**
	Trapezoid	25.2873	5.9037	7.469	13.2208	12.9702
	Generalized bell	13.7131	5.7618	13.64	13.5973	11.6780
	Gaussian	13.0184	12.1689	7.66	14.237	11.71
	Pi shaped	25.2873	5.7916	7.466	13.745	13.72
	Di sigmoidal	25.1845	5.7454	7.469	14.1162	13.1287
RF	Triangular	7.788	4.701	4.701	4.8747	5.5391
	Trapezoid	**3.8171**	**2.6461**	**1.6461**	**2.2684**	**2.59322**
	Generalized bell	7.7969	4.831	4.8431	5.3683	4.9598
	Gaussian	7.7831	4.7128	4.7128	4.2635	5.518
	Pi shaped	7.8219	4.8796	4.8796	5.0876	5.6637
	Di sigmoidal	7.8141	4.9152	4.9151	5.4665	5.7777

4.4.2. Development of ANFIS model

For approximation of the results with ANFIS for the LST process, like FFNN, testing and training datasets need to be selected and. Testing and training datasets from the FFNN model were selected for ANFIS model. In this way, a direct comparison between the models could be performed. To implement cross-validation on modelling of DI, IF and RF, four data sets were identified (based on fig. 4.2). For choosing the best and most accurate model, the structure of ANFIS was varied and different structures such as 3-3-3-3, 4-4-4-4 etc were examined. It was observed that a 2-2-2 model with 200 epochs and Sugeno type of Fuzzy-based rule had the lowest RMSE. Also, 8 Membership Functions (MF) in the ANFIS model were examined for finding the most appropriate model. It was found that Triangular type of MF for Diameter Increase and Insertion Force, and for Removal, Force trapezoid type of MF were the most accurate MF. Figs. 4.6, 4.7 and 4.8 present comparison of the predicted values from the ANFIS and FFNN models with the actual data. It can be observed from the figures that the predicted data extremely well fitted with the measured data recoded from the experiments.

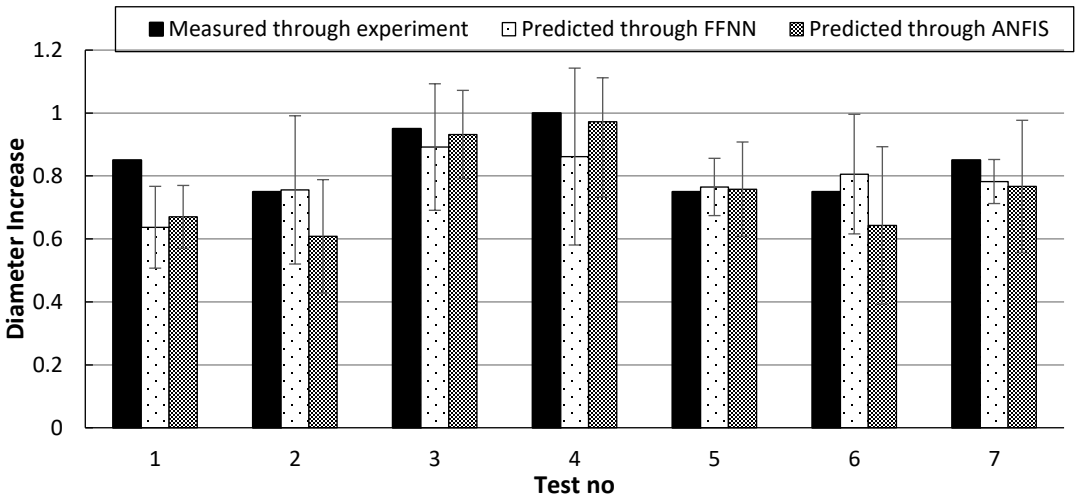

Fig. 4.3. Comparison of measured, 3-5-1 FFNN and ANFIS values of testing data for DI for fold #4.

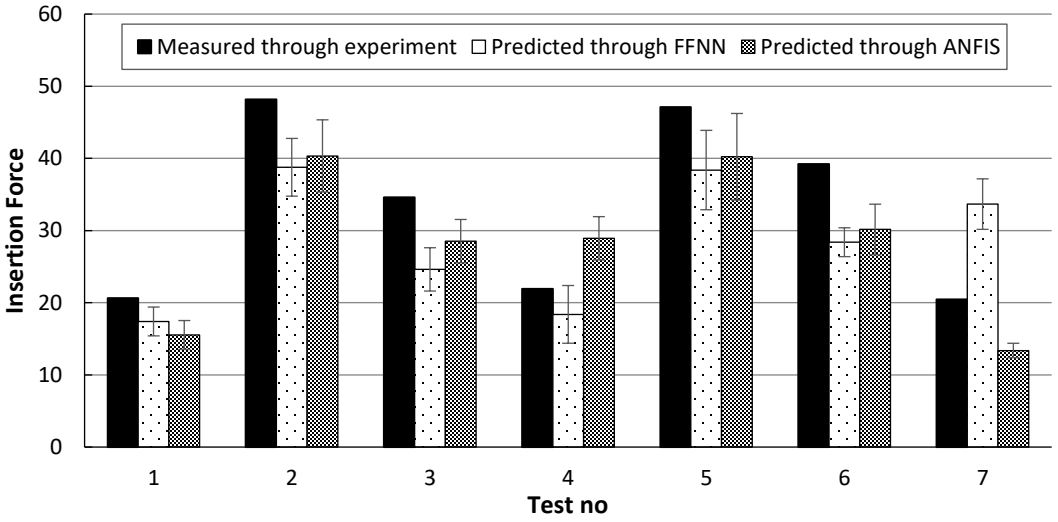

Fig. 4.4 Comparison of measured, 3-5-1 FFNN and ANFIS values of testing data for IF for fold #4.

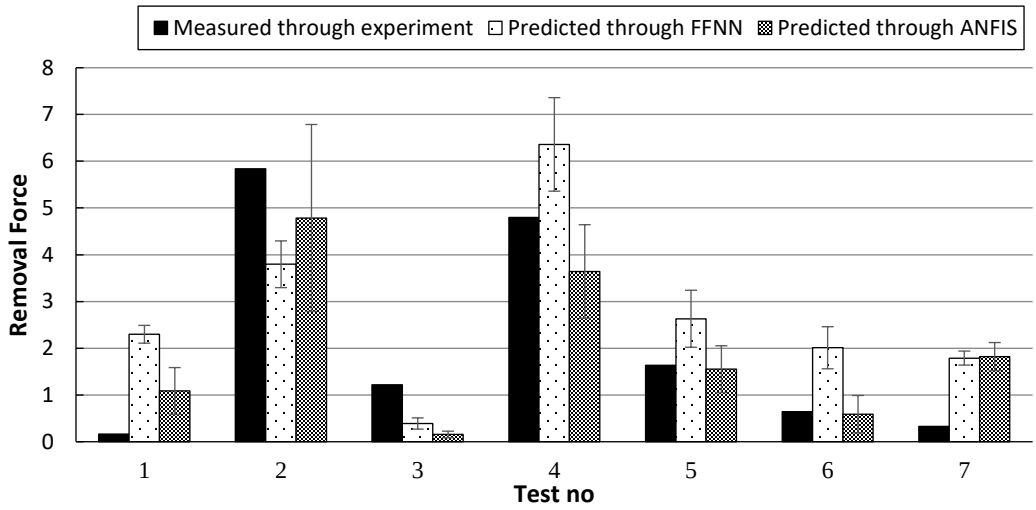

Fig. 4.5. Comparison of measured, 3-7-1 FFNN and ANFIS values of testing data for RF for fold #4.

4.4.3. Calculation of correlation coefficient percentage

Correlation Coefficient is a vital aspect used in statistics to calculate the strength and direction of the linear relationship or the statistical relationship (correlation) between the two population data sets [22]. This coefficient calculated based on relation of

FFNN and ANFIS test data to measured data in figures 4, 5 and 6 separately. This formula of is defined as:

$$R_{x,y} = \frac{\sum_{i=1}^{n}(x_i-\bar{x})(y_i-\bar{y})}{\sum_{i=1}^{n}\sqrt{(x_i-\bar{x})^2}\sqrt{(y_i-\bar{y})^2}} \qquad [22]$$

where n is sample size (here is 7), x_i and y_i are measured data points and predicted by ANFIS or FFNN and $\bar{x}$ is $\frac{1}{n}\sum_{i=1}^{n} x_i$ and analogously for $\bar{y}$. Table 4.4 shows the result of calculation of correlation coefficient. As the table 4.4 shows, ANFIS predicted significantly better compared to FFNN.

Table 4.4 Correlation coefficient for outputs

Outputs	FFNN	ANFIS
DI	62.12%	88.62%
IF	72.5%	89.7%
RF	75.2%	90.56%

4.4.4. Comparison accuracies of developed models ANFIS and ANN

To compare the prediction accuracies of the developed model, the prediction error percentage (PEP) was measured, defined as follows:

$$PEP = \frac{1}{27}\sum_{i=1}^{n}\frac{|ai-yi|}{ai} \qquad (3)$$

where a_i is the actual data and y_i is the approximated data by the developed FFNN and ANFIS models. Figs. 4.6, 4.7 and 4.8 show the PEP values from ANFIS and FFNN which were calculated for DI, IF and RF, respectively. It can be observed that ANFIS predicted more accurately the results compared to FFNN. These results are summarised in Table 4.3. Table 4.3 shows the overall comparison of PEP between the two models. As can be seen from the Table 4.3, ANFIS improved the PEP more than 45%. These results show that the ANFIS model was more reliable and resilient to noise compared to FFNN. Hence, it can be suggested that ANFIS can predict the LST

process more accurately and could serve as a precise Machine Learning method for the LST process.

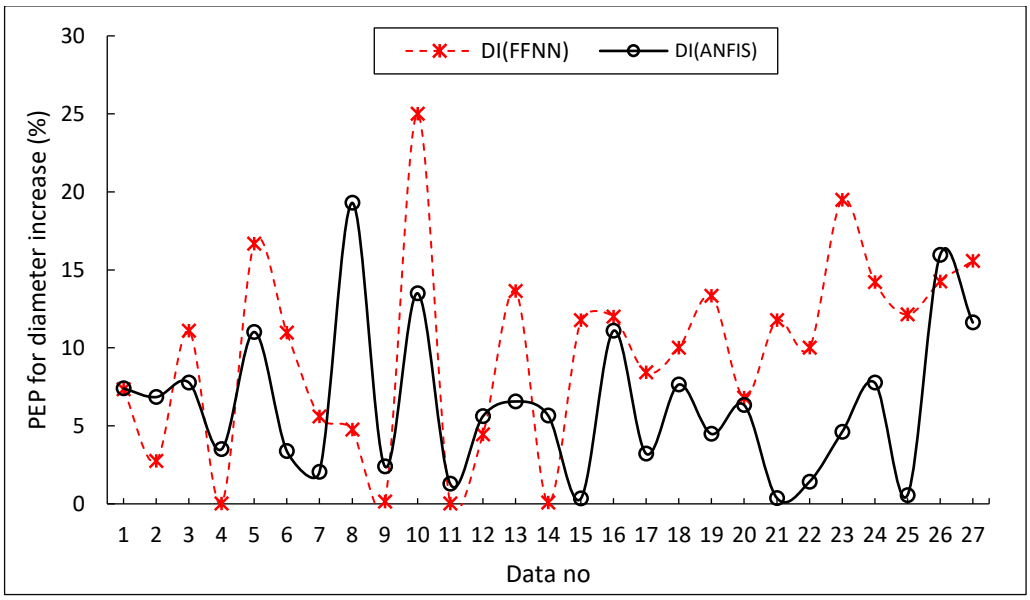

Fig. 4.6. PEP modelling of diameter increases by ANFIS and FFNN.

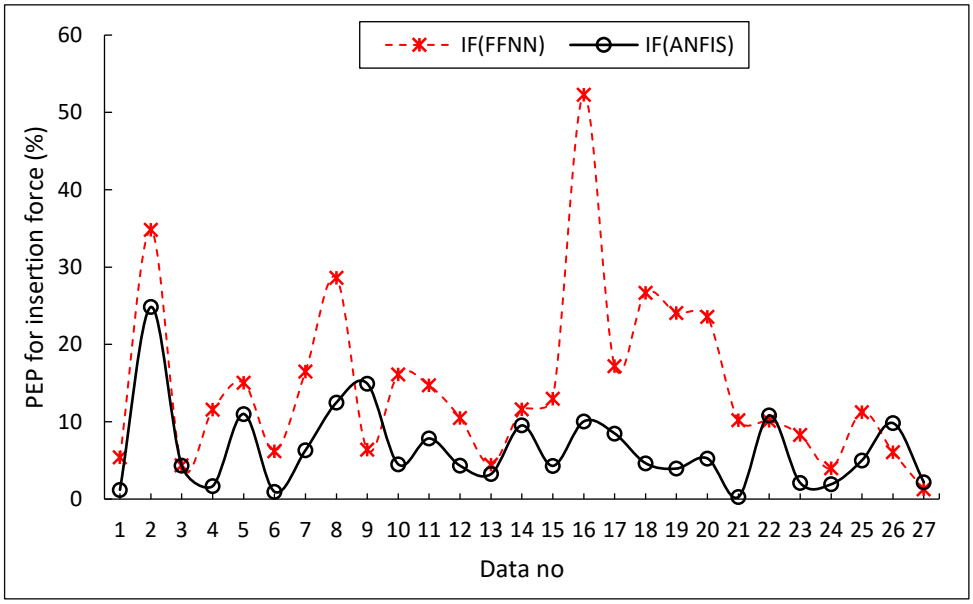

Fig. 4.7. PEP modelling of insertion force by ANFIS and FFNN.

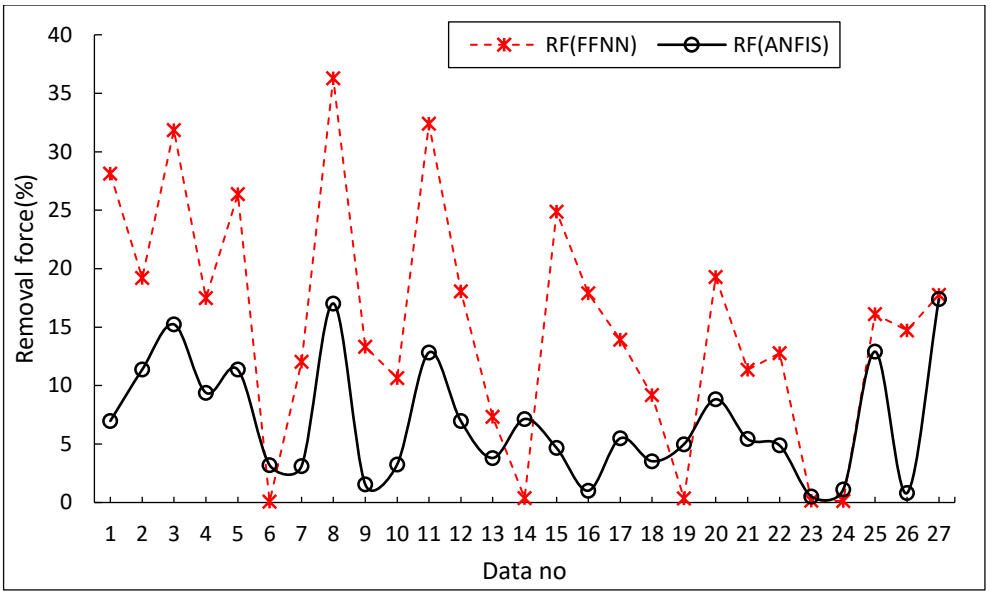

Fig. 4.8. PEP modelling of removal force by ANFIS and FFNN.

Table. 4.5. Comparison between ANFIS and FFNN for all outputs.

Modelling type	DI	IF	RF	Overall PEP
FFNN	0.097139	0.146085	0.152609	0.395833
ANFIS	0.063594	0.065152	0.068435	0.203181

4.4.5. Analysis of responses: diameter increase, insertion force and removal force

As observed from the results, ANFIS proved to be a more accurate model for prediction of DI, IF and RF. Hence, the developed ANFIS model was used for analysing in more detail the effects of laser surface texturing process parameters on the responses. The 3D plots of ANFIS prediction surfaces were constructed and the parameter effects analysed, see Fig. 4.9.

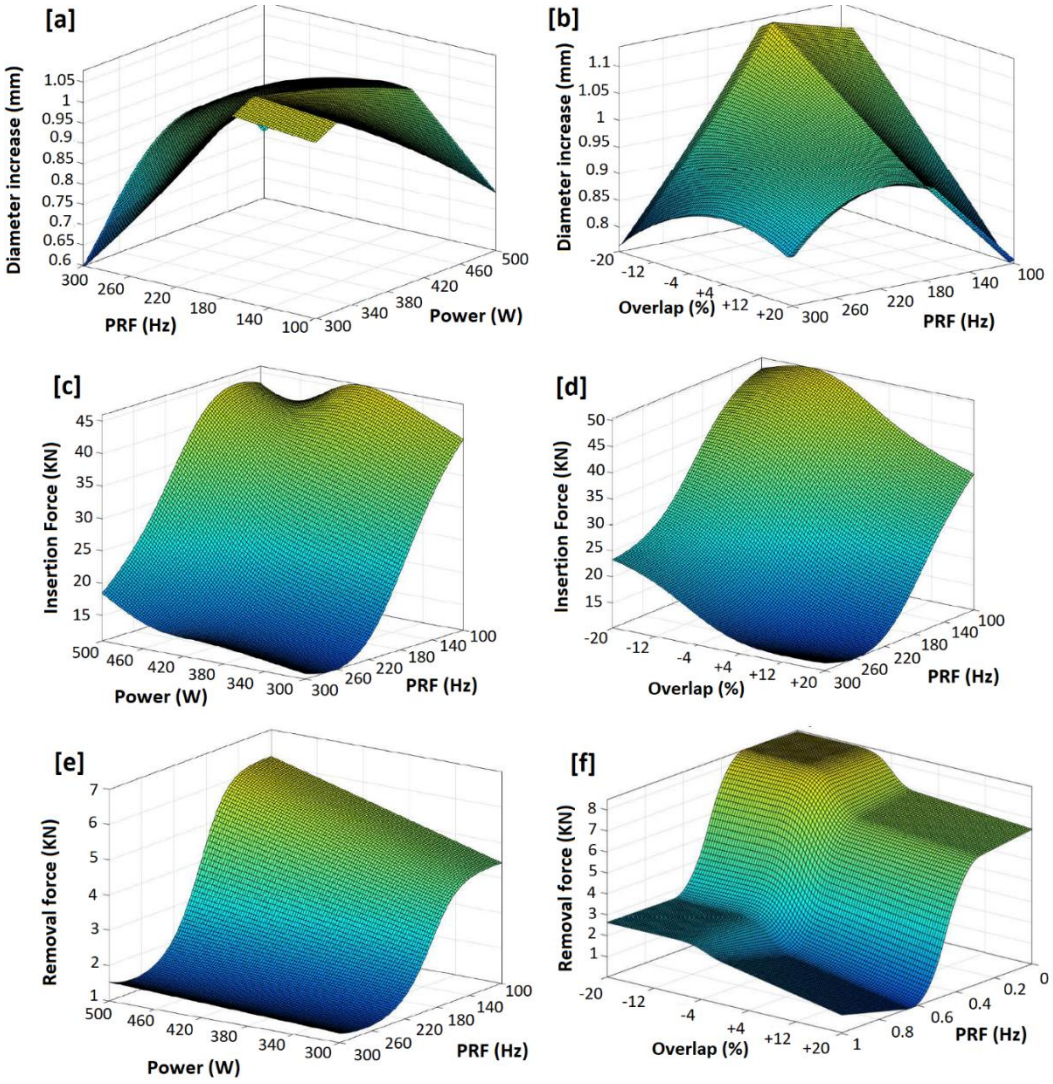

Fig. 4.9. Surface plots of diameter increase versus process inputs (a and b), insertion force versus process inputs (c and d), and removal force versus process inputs (e and f).

From figure Fig. 4.9a, the highest values of DI were obtained when the PRF was low. Due to an increased heating time (from lower PRF), a larger amount of energy was input to the surface and consequently a larger melt pool was produced, in turn resulting in a higher DI. On the other hand, by increasing the laser power from 300 to 400 W, sufficient melting should occur. However, a further increase of the power from 400 to 500 W could cause over-melting due to lower solidification time leads to reduction in diameter of texture.

Based on the results shown in Fig. 4.9b, for positive values of OV% the DI will be considerably lowered due to over-melting. By comparing Fig. 4.9a and 4.9b, it seems that when the power and OV% were minimum and negative, respectively, and over-melting occurs, then a higher value of DI can be obtained and there is an optimum range of PRF between 140-220 Hz.

Figs. 4.9c and 4.9d show the response plots of IF values obtained at various ranges of power, PRF, and OV%. Both of the plots indicated that enhancing the amount of PRF will lead a sharp decrease in IF. In fact, when the PRF is increased, due to the fast heating and cooling steps, the amount of residual stresses can be increased that may cause the formation of a brittle surface, lowering the resistance of the material under the insertion force. On the other hand, when the PRF is low, then the possibility of austenite-martensitic phase transformation occurrence will be increased, resulting in a surface hardening of the material and a higher insertion force. Therefore, by a suitable heat-treatment process during laser movement, a higher bond strength, gripping, insertion and removal force can be provided. Fig. 9d demonstrates that positive values of OV% could sharply reduce the bond strength. This could be due to the re-melting and overheating that could deteriorate the formation of martensitic phase. Also, these phase transformations are known to be sensitive to the heating/cooling cycle time and temperature.

Fig. 4.9e and 9f demonstrate the variation of RF for tested input PRF, power, and OV%. Almost, the same trend for the IF was obtained for the RF in case of power and overlap. From the bond strength point of view for having a suitable cold joint, it can be concluded that at high laser powers which brings a high thermal energy, a strong bond can be obtained if the OV% is negative and the PRF value is lower than 220 Hz, where suitable conditions for martensitic phase formation would be obtained.

4.5. Conclusion and Future Perspectives

This research dealt with the simulation and approximation of diameter increase, insertion force and removal force for Laser Surface Textured 316L interference fit joints with two supervised learning approaches. For finding the effect of a mixture of

inputs on the responses, two models FFNN and ANFIS were used. However, to determine the accuracy of the developed models, different error parameters were examined for a variety of model structures. By testing and training of various FFNN, 3-5-1 structure for DI and IF and 3-7-1 structure for RF are selected. The selection of the structures was made on the basis of the lowest value of MAE. ANFIS 2-2-2 structure with Gaussian2 MF and backpropagation optimization, D sigmoidal MF and hybrid, and Pi shaped MF showed the lowest RMSEs for DI, IF and RF, respectively. The ANFIS model produce lower values of PEP compared to FFNN. Hence, it was selected as the most powerful simulation for approximation and analysis of the responses. The effect of each processing parameters (based on interaction terms) was investigated by using response surfaces which were plotted based on the ANFIS model. With suitable laser processing parameters, higher gripping insertion and removal forces can be provided and at higher laser powers, where the OV% is negative, and for PRF values lower than 220 Hz. The ANFIS has some advantages over FFNN, including the ability to capture the nonlinear structure of a process, adaptation capability, and rapid learning capacity. ANFIS uses either backpropagation or a combination of least squares estimation and backpropagation for membership function parameter estimation. ANFIS algorithm has a hybrid learning approaches in its structure. Thus, ANFIS has the advantage to combine both ANN and Fuzzy knowledge. So ANFIS is more precise in term of prediction. Due to the fact that the laser surface texturing processing technologies are really high-cost process, the developing model can give a vision regarding to the selecting of best process parameters without needing to a high number of experiments. Otherwise stated, to reach desirable performance in each process, the developed model is beneficial to select optimal parameters without conducting extensive experiments and it has a strong economic justification.

Since ANFIS has proven a good tool for approximation of results, ANFIS model can be applied as objective function to select optimal parameters of manufacturing process, in which the process reaches to its desirable mechanical properties by using the metaheuristic algorithms such as simulated annealing algorithm, bee colony and etc.

References

1. Z, Murcinkova, P Baron, M. Pollak; Study of the Press Fit Bearing-Shaft Joint Dimensional Parameters by Analytical and Numerical Approach, Advances in Materials Science and Engineering Volume 2018.

2. M. Obeidi, E. McCarthy, L. Kailas, D. Brabazon; Laser surface texturing of stainless steel 316L cylindrical pins for interference fit applications, Journal of Materials Processing Tech. 252 (2018) 58–68.

3. H. Hüyük, O. Music, A. Koç, C. Kardogan, C. Bayram; Analysis of elastic-plastic interference-fit joints; Procedia Engineering 81 (2014) 2030 – 2035.

4. H. Sohrabpoor, A. Issa, A. Hamaoy, I. Ahad, E. Chikarakara, K. Bagga, D. Brabazon, Development of laser processing technologies via experimental design, Chapter 24, pp. 707-730, 2nd Edition, 2017.

5. M. Aminian, R. Teimouri; Application of soft computing techniques for modelling and analysis of MRR and taper in laser machining process as well as weld strength and weld width in laser welding process; Soft Comput (2015) 19:793–810.

6. A, Biswas. S. Rajat, Gu, R, Gupta; Application of artificial neural network for performance evaluation of vertical axis wind turbine rotor, International Journal of Ambient Energy 37(2):1-10, 2018.

7. H. sohrabpoor; Analysis of laser powder deposition parameters: ANFIS modelling and ICA optimization; Optik, Volume 127, Issue 8, April 2016, Pages 4031-4038.

8. Hamed Sohrabpoor, Sushant Negi, Hamed Shaiesteh, InamUl Ahad, Dermot Brabazon; Optimizing selective laser sintering process by grey relational analysis and soft computing techniques, Optik, Volume 174, December 2018, Pages 185-194

9. R. Umrao, L. Sharma, R. Singh,T. Singh; Determination of strength and modulus of elasticity of heterogenous sedimentary rocks: An ANFIS predictive technique; Volume 126, October 2018, Pages 194-201

10.R. Teimouri, H. Shrabpoor, Application of adaptive neuro-fuzzy inference system and cuckoo optimization algorithm for analyzing electro chemical machining process, Front. Mech. Eng. 2013, 8(4): 429–442.

11. A. Gholami, Hossein Bonakdari, IsaEbtehaj, M. Mohammadi, B. Gharabaghi, S. Khodashenase ; Uncertainty analysis of intelligent model of hybrid genetic algorithm and particle swarm optimization with ANFIS to predict threshold bank profile shape based on digital laser approach sensing. Measurement, Volume 121, June 2018, Pages 294-303.

12. I, Fister, M. Perc, S. Kamal, I. Fister ; A review of chaos-based firefly algorithms: Perspectives and research challenges, Applied Mathematics and Computation Volume 252, 1 February 2015, Pages 155-165.
13. J. Pandremenos, G. Chryssolouris, "A neural network approach for the development of modular product architectures", International Journal of Computer Integrated Manufacturing , Volume 24, No.10, pp.879-887 (2011).
14. S.Karagiannis, P. Stavropoulos2, C. Ziogas and John Kechagias, Prediction of surface roughness magnitude in computer numerical controlled end milling processes using neural networks, by considering a set of influence parameters: An aluminium alloy 5083 case study, Proceedings of the Institution of Mechanical Engineers, Part B: Journal of Engineering Manufacture, 228(2), 233-244.
15. V. Ojha, A. Abraham, V. Snášel; Metaheuristic design of feedforward neural networks: A review of two decades of research; Engineering Applications of Artificial Intelligence 60 (2017) 97–116.
16.H. Baseri, H. Damirchi; Prediction of the Ferrite-Core Probe Performance Using a Neural Network Approach; Materials and Manufacturing Processes 2011.
17. M. Shamsipour, Z. Pahlevani, M. Ostad, S. Mazahery; Optimization of the EMS process parameters in compocasting of high-wear-resistant Al-nano-TiC composites; Applied Physics A , April 2016.
18.M. Acı; Artificial neural network approach for atomic coordinate prediction of carbon nanotubes; Applied Physics A July 2016.
19.Obeidi, M.A., McCarthy, E., Brabazon, D.; Methodology of laser processing for precise control of surface micro-topology, Surface and Coatings Technology, Vol 307, Part A,2016.
20.I. Tsamardinos, E. Greasidou, G. Borboudakis; Bootstrapping the out-of-sample predictions for efficient and accurate cross-validation, 2018, Volume 107, Issue 12, pp 1895–1922
21.M. Yurdakul & Y. Tansel İÇ;Application of correlation test to criteria selection for multi criteria decision making (MCDM) models, Int J Adv Manuf Technol (2009) 40:403–412.
22. K. Gnana Sheela and S. N. Deepa, Review on Methods to Fix Number of Hidden Neurons in Neural Networks. Journal of Mathemtical Problems in Engineering, Volume 2013, Page 11.

Chapter 5

Selective laser melting: an alternative approach for the manufacturing of 316L stainless steel press-fits

Publication Status: Under-Preparation

H. Sohrabpoor, R. Taherzadeh Mousavian, R. Raghavendra, K. Y. Benyounis, M. Baraheni, M. A. Obeidi, I. Ul Ahad, D. Brabazon

Abstract

In this study, selective laser melting (SLM) as a novel approach was utilized for manufacturing of 316L stainless steel press-fit insertions by concentrating on the effect of texture profile geometry specifications including shape, pitch, and height on the insertion and removal forces of high-strength cold formed joints for high-end fixation application. For these purposes, the correlation between the micro-surface texture size and shape and aforementioned outputs were studied utilising a Box-Behnken of response surface methodology (RSM). The experimental results showed that the teeth height has a predominant effect. It was also found that the pitch shape of texture can effectively be set to provide enhanced control over the bonding strength of the press fit joints. The results showed that a larger pitch had a slightly positive effect on joint bond strength possibly due to higher degree of interface between the pin surface profile and the internal surface of the hub. The shape of the texture us also important. In fact, trapezoid and triangular shapes of the teeth lead to stronger bonding compared with oval texture profiles, and the traces of adhesive and abrasive wear respectively were detected on the inner surface of the hub. It is important to note that due to a limitation in the SLM process for making precise edges and the formation a rough surface, abrasive wear was also detected for the trapezoid shape. This chapter shows that the additive manufacturing (AM) process can open up a new window of opportunity for the development of metallic knurled press fit applications.

Keywords: Selective laser melting**;** interference fit joints; metal surface texturing**;** knurled pins; Response surface methodology; Box-Behnken design.

5.1. Introduction

Joining is a processing technique which is employed to assemble individual components or structures to ultimately build a larger assembly. Press-fit is a joining method which provides a relatively easy method for the joining of materials while bonding them very securely together [1,2]. It is commonly used therefore for assembly during production as well as in repair applications. In recent years, press fits have been used in many sectors including transportation, agricultural machineries and automotive industries. In many of these applications it is used for increasing the capability of the joints, including the transmission of axial force from the shaft to inner surface of hub which is assisted through the design definition of the generated plastic and friction forces [3,4]. Knurled press fits traditionally consist of two main type of pins including those of straight and helical shape of texture. With straight press fit pins, adhesion occurs as a result of the uniform shape of the interference pin and hub surfaces. In knurled fit joints the pin textured surface can be designed to cut into the hub hole surface [4]. With a single helical direction of the surface profile texture, such as a single 45° knurl, the pin is guided to turn into the hub as it enters through the hole making even tighter contact with the inner surface of the hole. Therefore, radial forces resulting from helical textures effects more the interior surface of a press fit joint compared with straight grooved pins [4]. During the creation of a press fit, both elastic and plastic deformation occurs. The extent of deformation is directly related to the texture shape and the interfering volume of material [2]. In a press-fit, the pin's texture is an important factor in bonding and adhesion of the pin to the hole in the hub region and it is crucial to know how this texture relates to the joint properties [1].

The dimensions of the texture and selection of an appropriate manufacturing technique that can provide these are therefore important considerations [5,6]. In fact, the qualification of connection insertion force (IF) and removal force (RF) are highly sensitive to the quality of the surface texture. For lower cost applications, the expense of labour and the operating process to achieve high quality interference fit components may not be economical using traditional fabrication processes [7,8].

Obeidi et al. used a CO_2 laser to produce surface textures on stainless steel pin insertions and measured the resulting insertion and pull-out forces [9]. Although, this

technique was successfully applied to manufacture pins with defined texture, the range of texture profiles could be increased using metal Additive Manufacturing (AM) [9].

Recently, additive manufacturing (AM) techniques including selective laser melting (SLM) have been used to fabricate metal parts with defined surface textures for various applications [10,11,12]. SLM can be used to fabricate samples with very complex surface textures [11,12]. This technology represents a realistic alternative to many conventional manufacturing techniques. It has been well shown that SLM allows the fabrication of near full-density high-resistance metallic components via fusion and re-solidification of the fine metallic powders [13-16].

316L stainless steel is part of the austenitic family of steels which have been used from the 19th century for interference fit joint applications [7,9]. These alloys have desirable mechanical characteristics including good corrosion resistance, elastic distortion and high ductility [17-19]. Due to the good properties, relatively low cost, and ease of use within both powder bed fusion and electron beam melting, stainless steels are commonly used in metal AM [20,21]. Based on these characteristics, SS316L steel was selected to fabricate the knurled joints and one of the aims of this study was to confirm the usability of this steel for generating textures on interference fit pins to enable interference press fit joints.

In press fit technology, the strength of joining relies on different process parameters including the size of joint hub and pin, the surface profile dimensions and the tolerance between the joining surfaces [7,9]. Some studies have been conducted to investigate the effect of different input parameters on the load bearing ability of knurled pins [22]. Investigation of process parameters and identifying the most significant factor that can be perform with different ways including machine learning and response surface methodology [23]. The limitation of modelling data with artificial intelligence model is number of experiments which is noted as requiring at least 300 data sets [24]. This other noted solution to correlate relationship between inputs and responses is response surface methodology (RSM) which for smaller data sets can result in better understanding of the impact of active factors and their interaction on the process [24]. Multiple independent variables can be examined through the RSM method which

consists of a statistical and mathematical modelling of the relationship between the inputs and outputs [26]. Box Behnken design is a great tool for investigation of the process parameters which included three levels of inputs and compared to other design matrices, requires a relatively smaller number of experiments [26]. Fig. 5.1 reveals the basic schematic of SLM process.

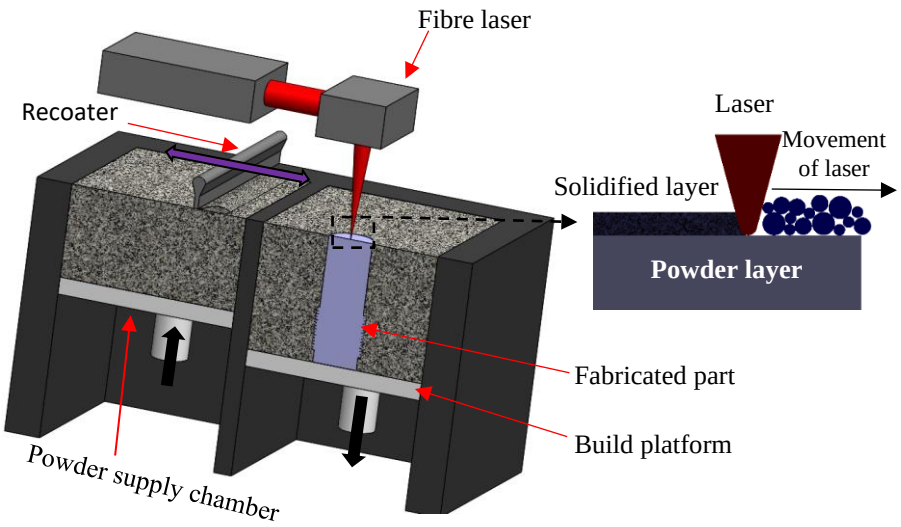

Fig. 5.1. Schematic of SLM process

To the best knowledge of the authors, no attempt has been made to manufacture knurled pins via the SLM process. In this study, the interference fit joint surfaces are accurately designed with a focus on the parameters of achievable surface profile height, pitch size, and the shape. The outputs measures including the achieved profile dimensions as well as the insertion force (IF) and removal force (RF) were assessed with RSM.

5.2. Experimental procedure

5.2.1. Material

The AM pin insertion material used was gas atomized spherical SS316L powder granules with a Gaussian size distribution sizes ranging from 15-50 µm (supplied by LPW Technology Ltd, UK) and had an average particle size of 27 µm (see Fig. 5.2). The chemical composition of the stainless-steel powders as supplied is listed in Table 5.1. The powder grains were mostly spherical in shape while a very small number of irregular shaped particles were revealed.

Table 5.1
Chemical composite of as supplied 316L stainless steel powder.

Chemical compositions	C	MN	N	P	S	Cr	Mo	O	Ni	Si	Cu
Mass fraction (%)	0.023	0.9	0.09	0.01	0.005	17.7	2.32	0.03	12.7	0.7	0.01

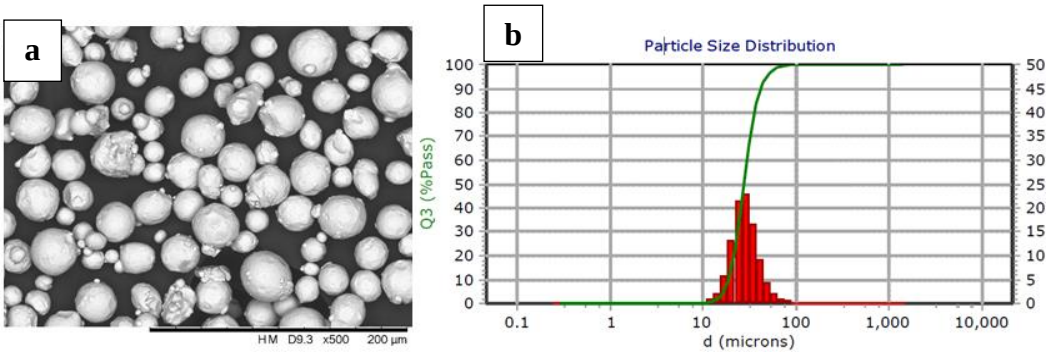

Fig. 5.2. 316L stainless steel powder. (a) SEM image and (b) particle size distribution.

5.2.2. Equipment

The laser power, scan speed, hatch space and focused spot size uses in the SLM process were 195 W, 1083 mm/s, 90 µm and 70µm respectively based on default EOS parameters for 316L. An EOS 280M AM metal printer which was used to fabricate the knurled pins. The CAD files for the pins was set as 30 mm in length and 10 mm in diameter. Various textures were added on these pin surfaces as described below. The resulting diameters which is height of texture plus diameter on the pin for the SLM

process are slightly larger than the reamed hub internal diameter. The build volume of the EOS printer was 250×250×325 mm and the layer thickness for processing was set at 20 μm. The build plate was pre-heated and maintained at a temperature of 80°C during the building process. The laser wavelength operated within the range of 1060 to 1100 nm. The inner core of the part was scanned first, followed by the outer contour. For cutting the prepared samples off from the plate, a wire EDM was used. In order to perform the insertion and removal test, the hubs were manufactured with a 30 mm outer diameter and 10.050 ± 0.003 mm internal diameter by means of a CNC lathe machine. The inner diameter of the hubs hole was reamed to the final dimension after initial rough machining in order to achieve the tolerance in diameter and eliminate non-roundness. The dimension of textures and surfaces were measured using a digital Vernier and optic microscopy. The measured accuracy of the texture printed by this SLM process was within ±50 μm in both height and pitch dimensions.

A Carl-Zeiss scanning electron microscope EVO-LS15 SEM was used to visualise the morphology of the surfaces before and after the insertion-removal testing. The experimental measurement of the texture before after the removal tests was performed via a 3D optical profiler Keyence 3D digital microscopy. The insertion and removal tests were performed at a constant speed of 5 mm/min relative to axial displacement between the hub and shaft. Fig. 5.3 reveals how strategy of the fibre laser scanning with EOS software in SLM device is. After defining all of strategy and location on the plate, 316L stainless steel samples adjusted in the powder supply chamber. Fig. 4 shows the fabricated interference fit joints samples while they are sintered on the plate. Then, a wire EDM utilized for ultra-precise cutting samples from the plate (Fig. 5.5). Fig. 5.6 represents the full instruments which was used to measure the accuracy of manufactured specimen via EOSINT M 280. Fig. 5.7 shows the insertion and removal test being performed with a Zwick Z-50 universal tensile and compression testing machine.

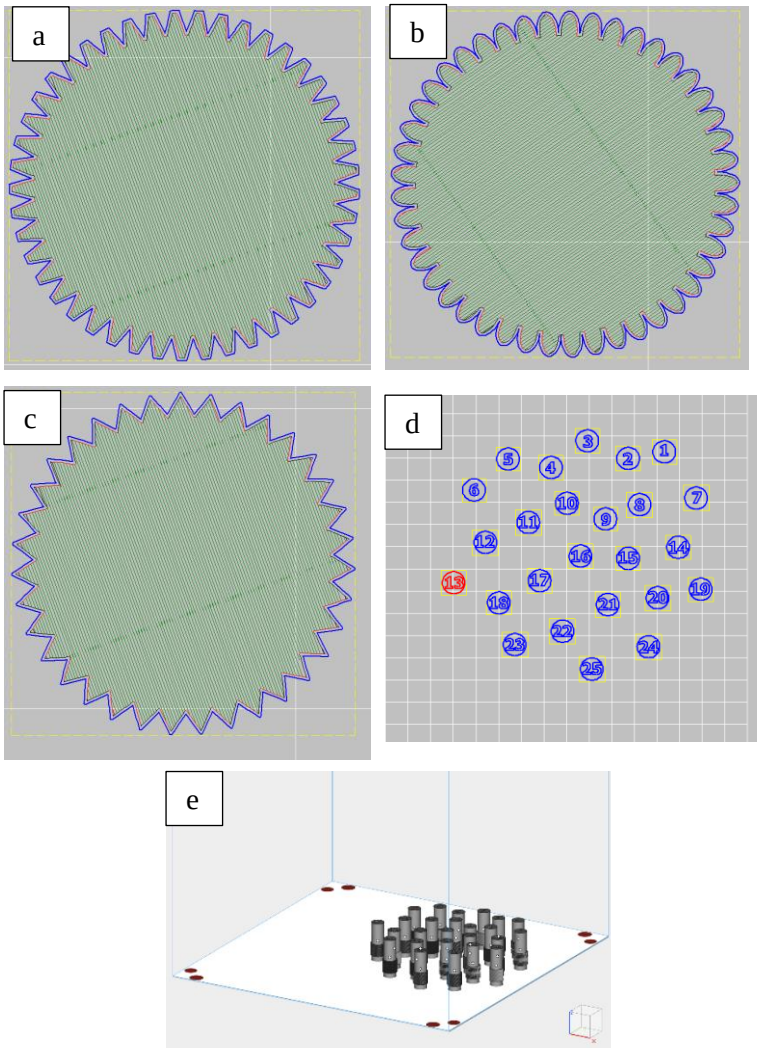

Fig. 5.3. Scanning strategy for (a) trapezoidal, (b) oval, and (c) triangular textures; and schematic of (d) pins placement as built, top view, and (e) isometric view of sample layout on build plate

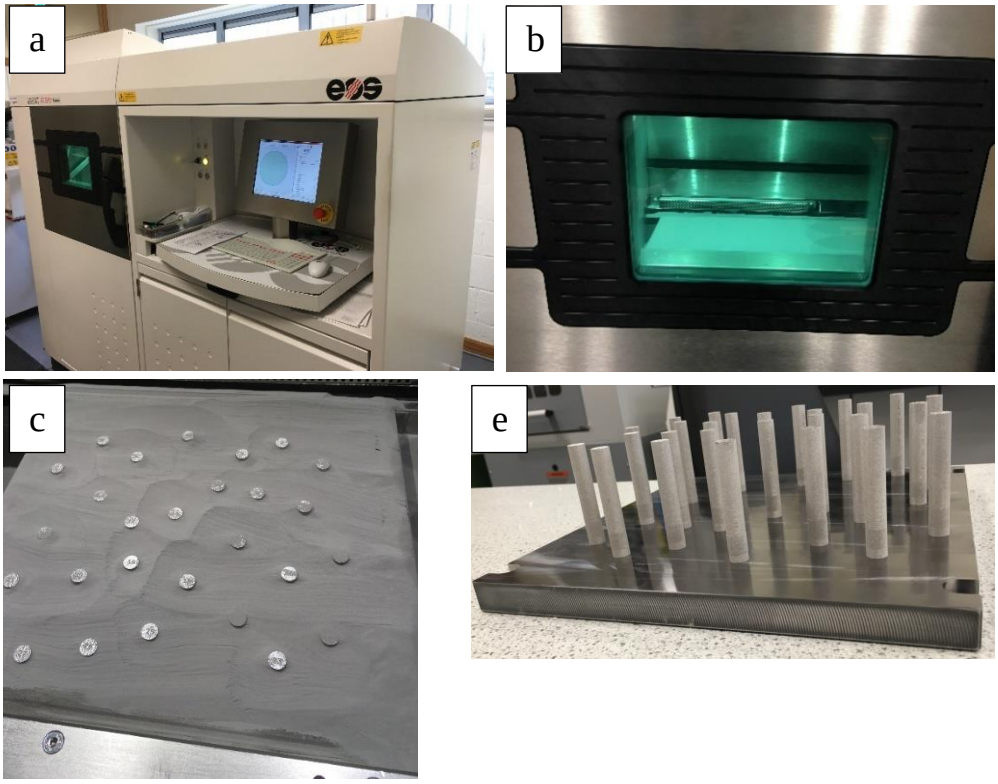

Fig. 5.4. SLM device, (a) EOS SLM machine, (b) sample location in the build plate, (c) fabricated pins in used powder, (e) samples after evacuation of powder

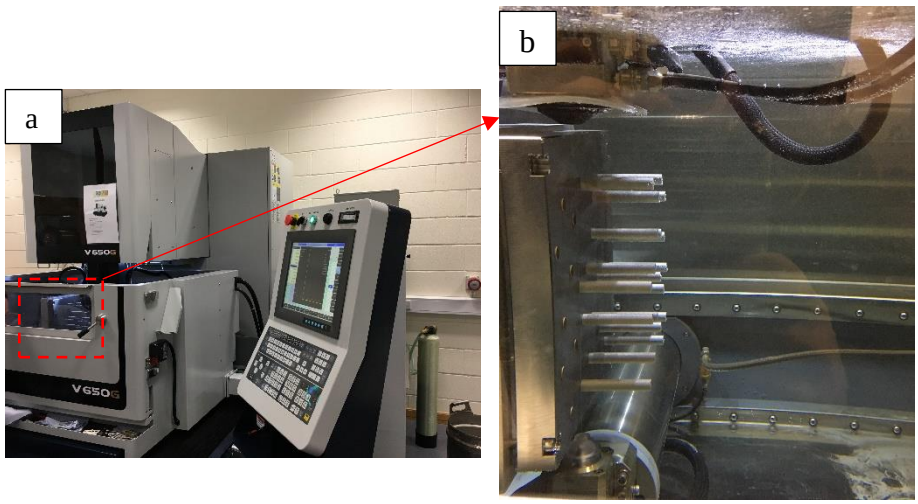

Fig. 5.5. Wire EDM for ultra-precise cutting samples from the plate, (a) V 650 G device, (b) close view of cutting samples from the plate and sink in the water

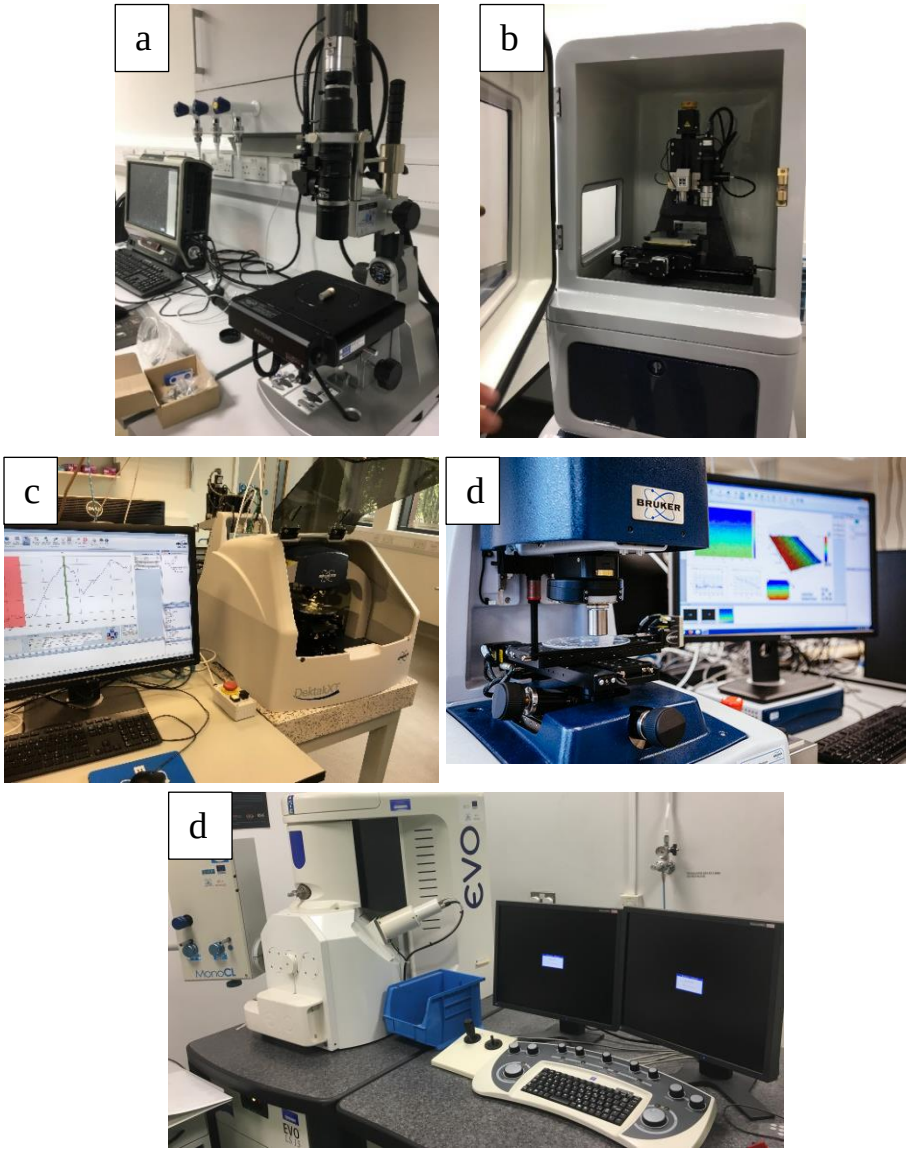

Fig. 5.6. (a) Keyenece 3D digital microscope, (b) Bruker Hysitron TI premier, (c) Bruker Dektak XT Stylus profiler, (d) Bruker contour GT 3D optical microscope, (e) EVO-LS15 SEM

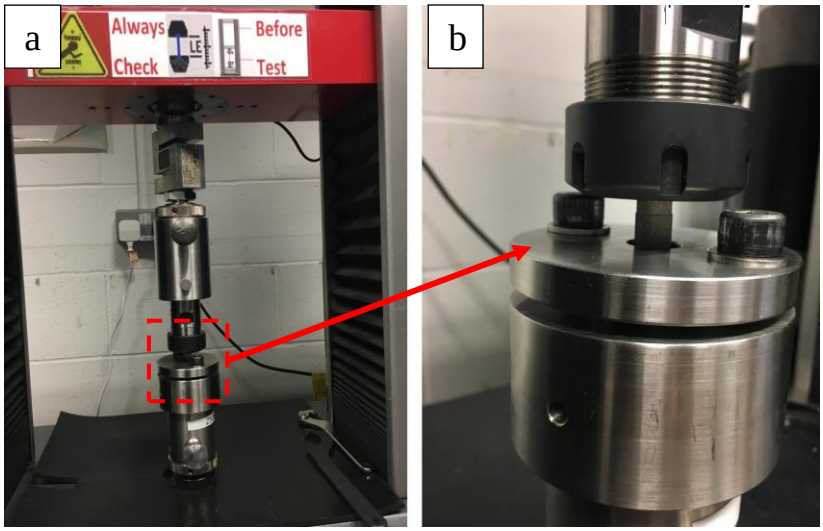

Fig. 5.7. Insertion and removal load-displacement testing showing (a) the testing machine and (b) a magnified view of pin, hub and sample clamping measurement.

5.3. Modelling Procedure

To find response of process factors with respect to process quality characteristics, second order mathematical models of the process were developed through response surface methodology. According to following equation.

$$Y = \beta_0 + \sum_{i=1}^{k} \beta_i X_i + \sum_{i=1}^{k} \beta_{ii} X_i^2 + \sum_{i=1}^{k-1} \sum_{j=i+1}^{k} \beta_{ij} X_i X_j + \varepsilon \qquad (1)$$

where Y represents the predicted response, X_i and X_j are the independent factors, β_0, β_i and β_{ii} are the intercept, the first-order constant coefficient, and the quadratic constant coefficient, respectively, β_{ij} is the linear constant coefficient for the interaction between factors, k is the number of factors, and ε is the error. To develop these models, a commercial statistical package Design Expert V9 was utilized and the validity of the quadratic models were evaluated by analysis of variances and coefficient of determination i.e. R^2.

In the present work study, the three predominate factors of surface texture chosen for analysis were profile shape of the texture, the pitch of the texture, and the height of the texture. Table 5.2 summarizes the process factors and the corresponding experimental deign set levels. Based on a Box-Behnken design, for three independent parameters at

three levels, 17 set of parameters were investigated, see Table 5.3. A step-wise regression method was used to fit the second-order polynomial Eq. (1) to the experimental data and to find the significant model terms [15,16]. Fig. 5.8 reveals the three-dimensional (3D) microscopy image of textured sample. The same statistical software was used to generate the statistical and response plots. Fig. 5.9 shows the CAD designs developed using Solid-works software version 2018 SP5 as well as SEM morphologies of the corresponding shapes. It can be observed that in trapezoid shape, due to limitation of AM process, a rough surface was formed on the smooth external surface of texture that should be exposed to a contact with the hub surface. It can be seen that triangular shape has a relatively sharp edge compared with the oval shape.

Table 5.2
Process variables and their levels.

Process parameters	Unit	Symbol	Code levels		
			-1	0	1
Shape of texture	-	A	Oval	Triangular	Trapezoid
Pitch of texture	µm	B	400	600	800
Height of texture	µm	C	300	500	700

Table 5.3
Experimental set parameters and resulting insertion and removal forces.

Std	Shape	Pitch (µm)	Height (µm)	Insertion force (kN)	Removal force (kN)	Volume (mm^2)	Overall diameter (mm^2)
1	Oval	400	500	39.5	6.5	125.8	10.89
2	Trapezoid	400	500	43.8	8.92	108.2	10.91
3	Oval	800	500	42.4	7.64	121.99	10.92
4	Trapezoid	800	500	48.1	10.2	113.27	10.93
5	Oval	600	300	16.48	0.91	72.59	10.49
6	Trapezoid	600	300	17.4	1.8	67.87	10.48
7	Oval	600	700	42.4	8.1	177.63	11.30
8	Trapezoid	600	700	49.23	10.4	157.29	11.33
9	Triangular	400	300	14.8	0.73	48.4	10.46
10	Triangular	800	300	21.7	3.8	49.7	10.49
11	Triangular	400	700	45.12	9.6	110.06	11.29
12	Triangular	800	700	54.9	10.83	115.34	11.29
13	Triangular	600	500	44.2	9.3	78.87	10.89
14	Triangular	600	500	43.2	8.8	78.87	10.89
15	Triangular	600	500	41.1	6.95	78.87	10.90
16	Triangular	600	500	44	9.12	78.87	10.90
17	Triangular	600	500	40.3	7.03	78.87	10.89

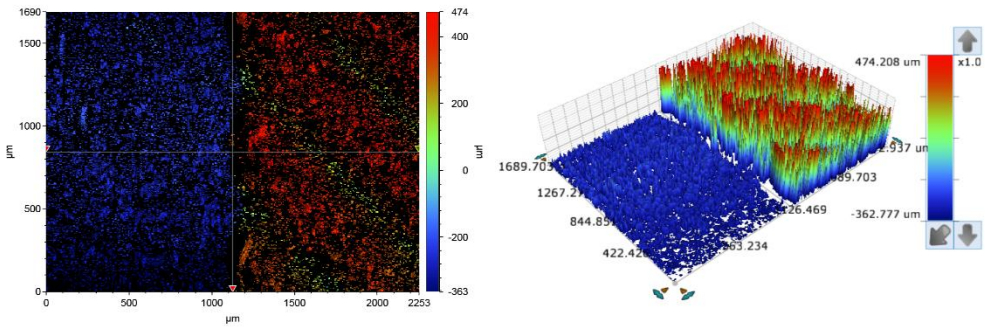

Fig. 5.8. Three-dimensional (3D) surface texture of sample 3 with contour GT 3D optical microscopy.

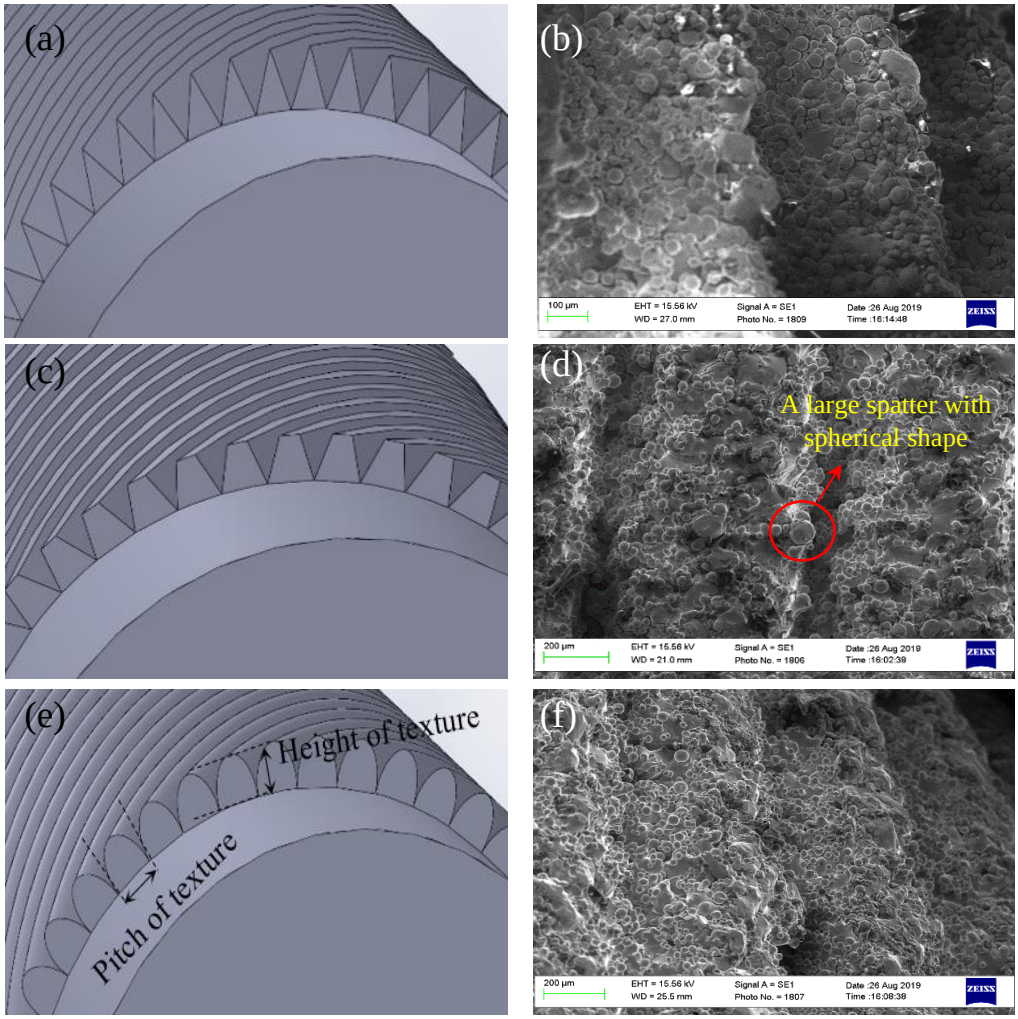

Fig. 5.9. Schematics of the CAD designs with (a) triangular, (b) trapezoid, (c) oval; and SEM images of as metal AM produced (b) triangular, (d) trapezoid, and oval textures.

5.6. Results and discussion

5.6.1. Microstructure and mechanical properties of samples

SLM samples were polished first and etched for 12 seconds with dilute aqua regia (H2O: HNO3: HCl=6: 1: 3), and then rinsed with alcohol and dried. The interfacial microstructure and fracture surface were respectively observed with the EVO-LS15 SEM at Dublin City University laboratory. The SEM microstructures revealed a martensitic and a cellular microstructure. The austenitic martensitic transformation can

be attributed to the rapid solidification rate inside the melting pool when the laser moves from one spot to another. Fig. 5.10a shows the optical microscopy images parallel to the (building direction) BD, showing the melt pool boundaries after eteching. Fig. 5.10b shows the optical microscopy images of the sample in the transvere directin to the BD, showing the solidifed melt pool boundaries with good metallurgical bonding. No evidance of a lack of fussion, unmelted powders, or porosity can be observed. Fig. 5.10c shows a high-magnification OM image of the sample transverse to the BD, showing the the different small grains with different orientation in the vicinity of (melt pool boundry) MPBs.

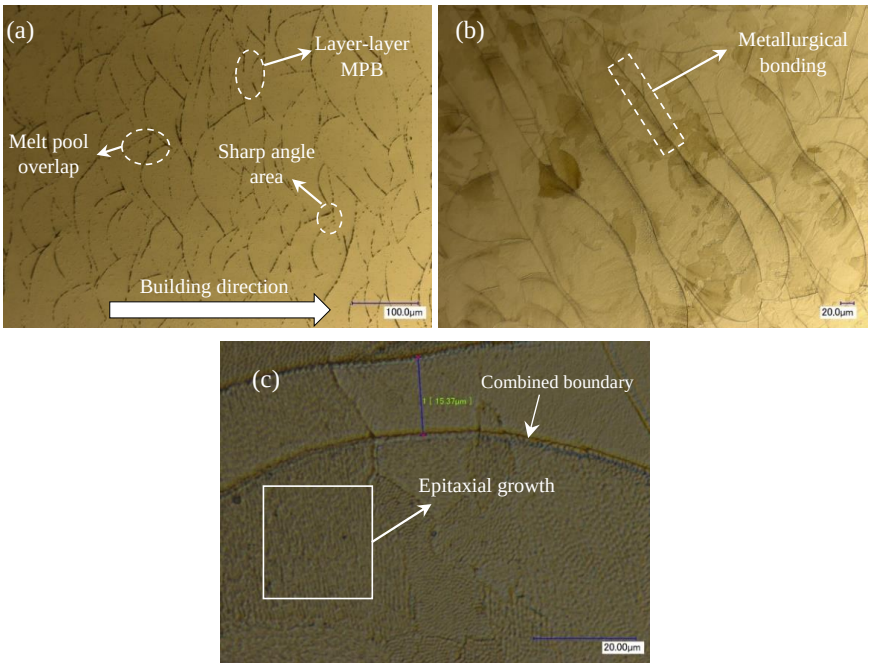

Fig. 5.10. Optical microscopy images, showing (a) melt pool parallel to building direction, (b) melt pool transverse to the build direction, and (c) a higher magnification of a gain boundary with smaller grains transverse to the build direction.

Fig. 5.11 shows two types of cellular structure from the metal AM samples. Such structures with an average size around 300nm were reported previosuly by researchers [12]. Also, nanoparticles can be observed around the cells. Based on the literature, they are rich in Cr, Mo,

and Si due to micro-segragation during fast cooling. Figure 5.12 shows diffenet types of pores in eteched sample.

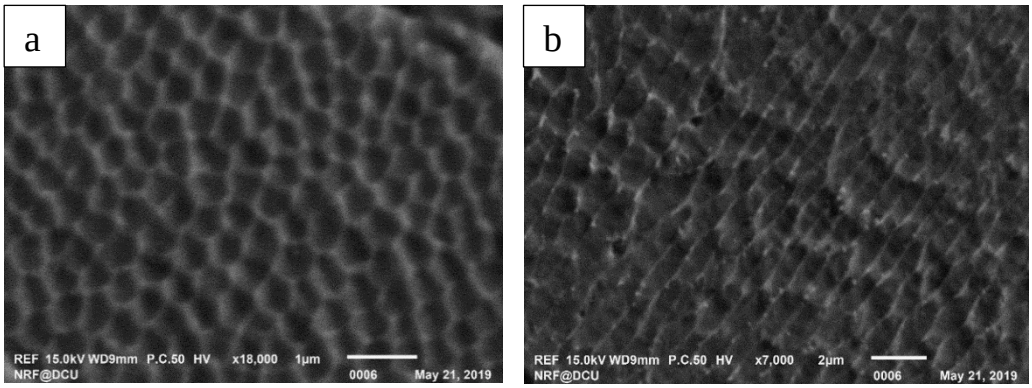

Fig. 5.11. Microstructure observation of the as built sample, (a) melt pool grain structure, (b) elongated grains

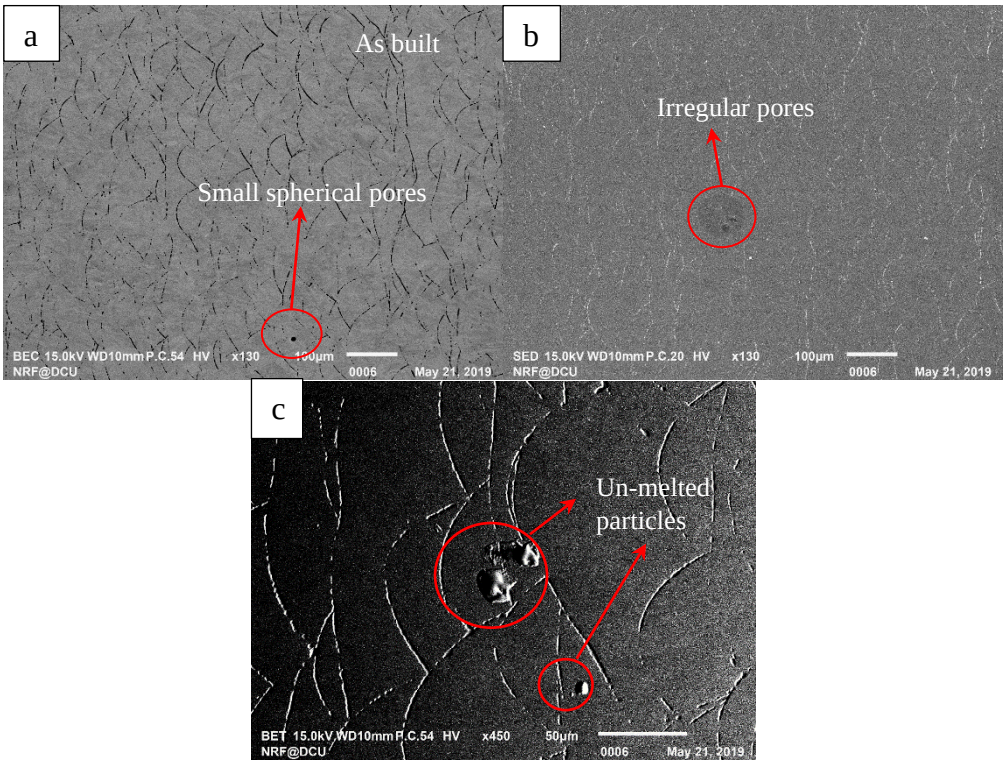

Fig. 5.12.SEM image of the as-built sample, in which some defects such as un-melted particles, small spherical pores, and irregular pores can be observed.

Fig. 5.13 shows the Nano-hardness indentation transverse to the BD. Almost, similar results were obtained after multiple indentations in a square area of 16µm×16µm. An average Youngs modulus of 195 GPa and hardness of 5.9 GPa were obtained. These results compare well with the literature, showing that regardless of the small number of defects that were observed by SEM analysis, suitable mechanical properties were observed.

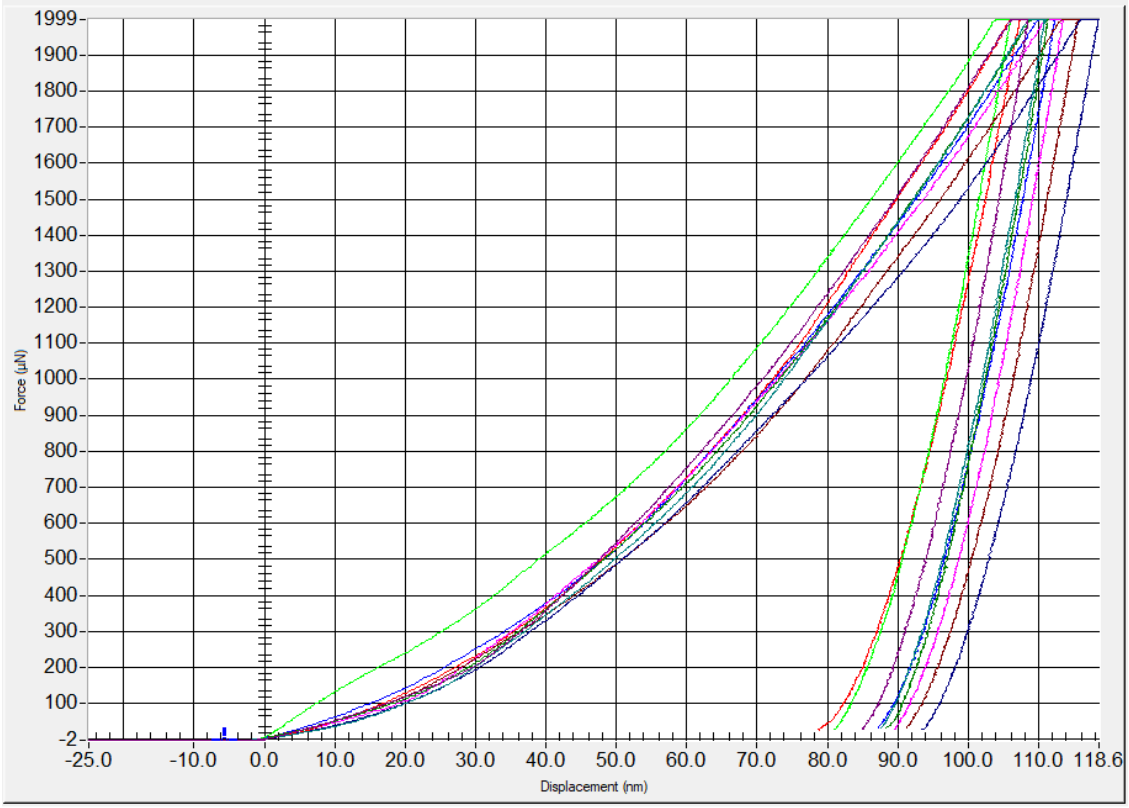

Fig. 5.13. Hardness properties of SLM samples.

Table 5.4 shows the average results of tensile test (n=3). Compared with the literature [19], it seems that such samples have a considerable ductility, while a higher UTS around 700 MPa has also been reported in the literature [20]. The break strain on average was 80% which is interesting as it is much higher than as-cast 316L and even wrought 316L alloy.

Table 5.4

The mechanical properties of the samples after the SLM process.

Sample	UTS (MPa)	Break strain (%)	YS (MPa)	Hardness (GPa)
0.001 S^{-1}	607±8	80±4	569±6	5.9±0.4

Fig. 5.14 reveals the SEM image of the surface specimen, showing two spherical pores around 5 and 3 µm that possibly caused the breaking of the sample. Fig. 15 shows extensive abrasion of sample after insertion and removal. In fact, severe plastic deformation in company with abrasion occurred which shows that such pins in press-fit application cannot be re-used. It is worth mentioning to the suitable bonding of un-melted particle that after deformation, no detachment occurred. Also, balling phenomenon was observed on the surface of the pins which is as a result of instability of melt pool (MP) attributed to the Marangoni effect which causes the higher surface tension gradients [20]. This phenomenon can increase the surface roughness. Fig. 5.16. shows some un-melted particles on the pin surfaces. Fig. 5.17 shows the surface texture of sample 4, the pin produced trapezoid shape, height of 800 µm and pitch of 500 µm. The inset shows a spherical un-melted particle in the micro groove section which is thought to be as a result of spattering and the high solidification rate. Fig. 5.18 shows a SEM image from a surface of the texture. It can be extracted from this image, as a result of friction between surfaces, some scratched materials from inner surface of hub got trapped inside the open pores which are in texture of the pins.

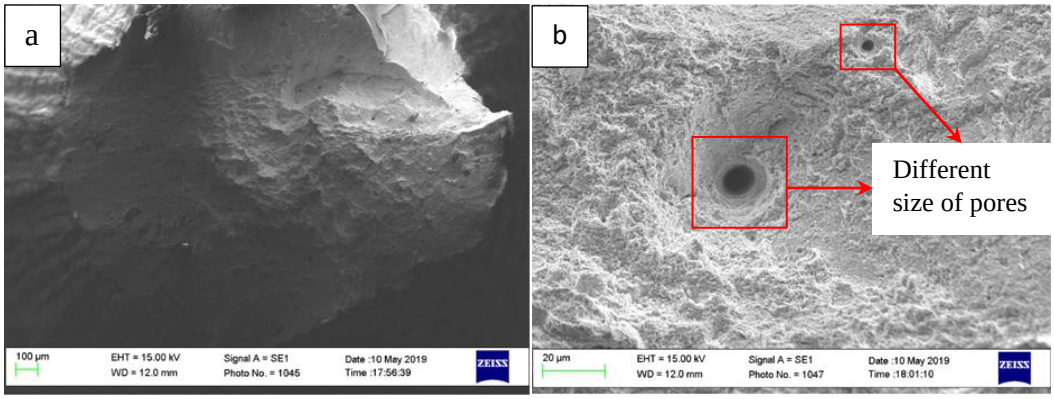

Fig. 5.14. SEM fracture surface of tensile specimen (a) fisheye, (b) high magnification of dimples

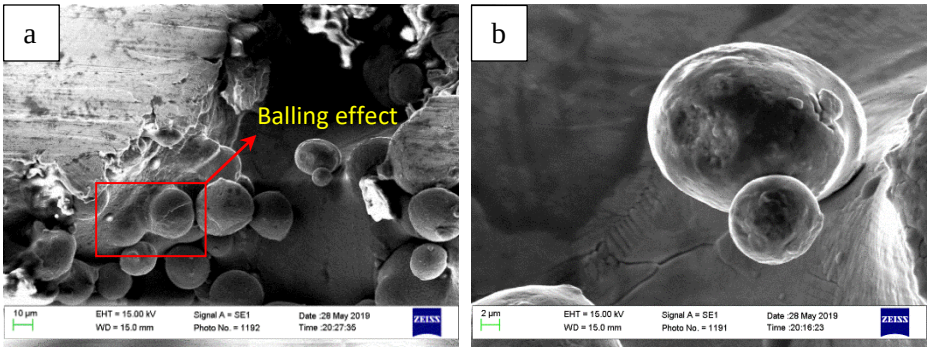

Fig. 5.15. (a) Balling effect, (b) a huge partially melted powder

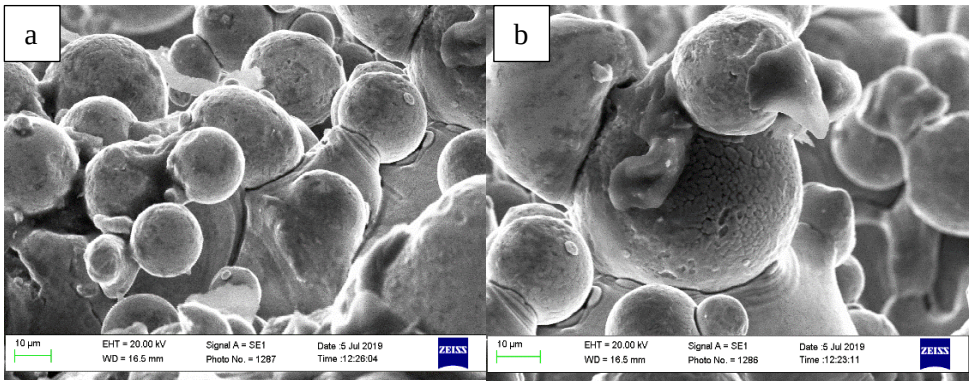

Fig. 5.16. SEM images of some un-melted particles on the surface of the texture.

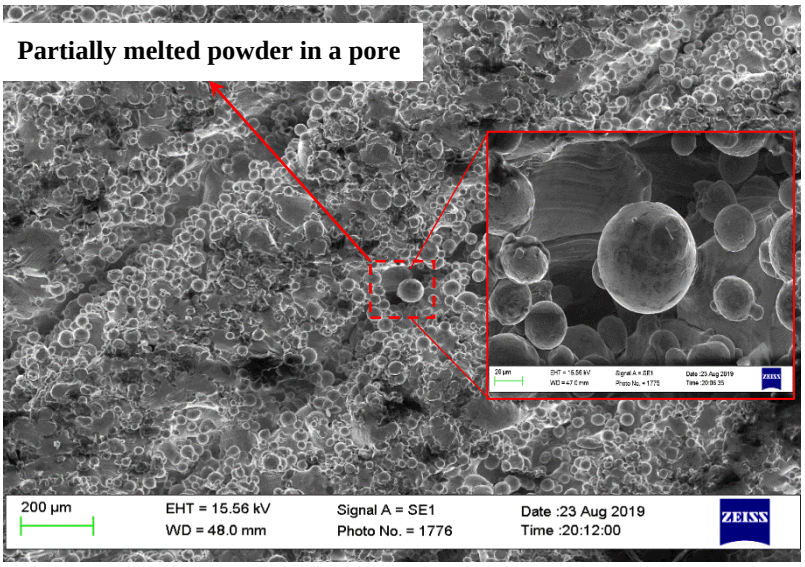

Fig. 5.17. SEM image from the texture of the pin.

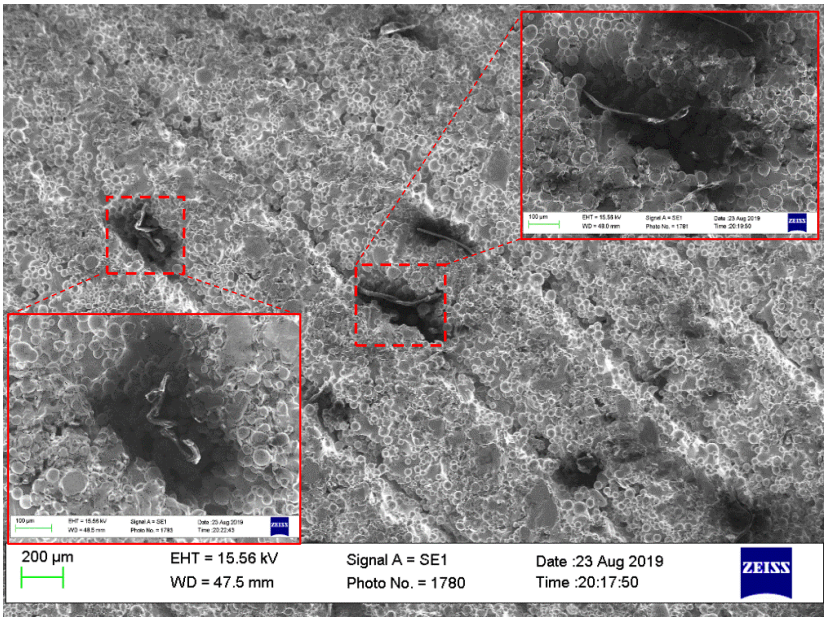

Fig. 5.18. SEM image of trapped hub materials after the insertion tests.

5.6.2. Development of mathematical models

In this work, analysis of variance (ANOVA) was used to check the adequacy of the developed empirical relationships. Two quadratic models were generated, one relating the profile geometry to the insertion and another relating them to the removal force. ANOVA test results of the responses, insertion and removal forces are presented in Tables 5.5 and 5.6. In this study, the model F value and the associated probability values P value were checked to confirm the significance of the empirical relationships. In general, if P value is below 0.05, it means that the related model is significant. From the F-value assessment, it was found that the predominant factors which have direct influence on the responses are the height and pitch of texture, followed by the shape of texture. Also, form Tables 5.4 and 5.5, the p values were less than 0.05 for the parameters and models indicating that the models are statistically significant and can be used for output prediction and that the parameters have a statistically significant effect on the output responses.

The predicted R-squared indicates how well a regression model predicts responses for new observations and the higher the R-squared, the better the model fits the data. These are presented in the Table 5.7. In all the cases, the value of the determination coefficient is close to 1 indicating that the predicted data have good agreement with the actual data. Fig. 19 shows the normal probability of the studentized residuals which prove graphically how well the predicted data are fitted to the actual data for both outputs. Although the R-squared results shows a high accuracy of the model, the other criteria are important for finding out the precision of the RSM model. The adjusted R-squared (Table 5.7) compares the explanatory power of regression models that contain different numbers of predictors. The value of the adjusted determination coefficient is also high, which indicates the high significance of the empirical relationships. The predicted R^2 values also show good agreement with the adjusted R^2 values. In addition to that, adequate precision compares the range of the predicted values at the design points with the average prediction error. Also, the values of adequacy precision for each response was calculated and presented in Table 5.7. It is seen from this table that these values for IF and RF are 25.5119 and 17.0717, respectively. In general, if the ratio is greater than 4, the equation is desirable [22]. Hence, precision of the developed

models indicates adequacy and that they can be used to navigate the design space. The mathematical relationships for correlating the mentioned responses are presented in Table 5.8.

Table 5.5
ANOVA results of insertion force.

Source	Sum of Squares	DOF	Mean Square	F-value	P-value	Importance
Model	2299.5631	5	459.9126	82.4320	< 0.0001	Sign.
A-Shape	49.5740	2	24.7870	4.4427	0.0385	
B-Pitch	71.4013	1	71.4013	12.7975	0.0043	
C-Height	1779.0613	1	1779.0613	318.8685	< 0.0001	
CA^2	396.6225	1	396.6225	71.0883	< 0.0001	
Lack of Fit	38.7322	7	5.5332	0.9776	0.5425	Not Sign.

Table 5.6
ANOVA results of removal force.

Source	Sum of Squares	DOF	Mean Square	F-value	P-value	Importance
Model	164.77	5	32.95	33.08	< 0.0001	Sign.
A-Shape	8.87	2	4.43	4.45	0.0383	
B-Pitch	5.61	1	5.61	5.63	0.0369	
C-Height	125.53	1	125.53	126.02	< 0.0001	
C^2	24.30	1	24.30	24.39	0.0004	
Lack of Fit	3.58	7	0.5111	0.2770	0.9332	Not Sign.

Table 5.7
Fit statistical measures of insertion and removal force.

Responses	R^2	Adjusted R^2	Predicted R^2	Adequate Precision
Insertion force	0.974	0.9622	0.9373	25.5119
Removal force	0.9376	0.9093	0.88	17.0717

Table 5.8
Predictive equations for the force responses in terms of actual input factors (Shape: S, Pitch: P and Height: H).

Output	Oval	Triangular	Trapezoid
IF	-66.7983+0.0149×P+0.3168 ×H-0.0002×H²	-63.9562+0.0149*Pitch +0.3168 ×H-0.0002×H²	-61.8483+0.0149×P+ 0.3168×H-0.0002×H²
RF	-20.4313+0.0041×P+0.0797×H-0.00005×H²	-19.0687+0.0041×P+0.0797×H-0.00005×H²	-18.3838+0.0041×P+0.0797×H-0.00005×H²

Furthermore, the adequacy of the models can be evaluated using diagnostic diagrams including normal probability distribution diagram of residuals and the diagram of predicted values versus real values, shown in Figs. 5.19a and b, and Figs. 5.19c and d, respectively. As can be seen in these diagrams, the points lie on a relatively straight line, suggesting the constancy of the variance and normal distribution. In the normal probability distribution diagram of residuals, the points are aligned along an almost straight line. Also, good correlations between predicted values and real values regarding IF and RF confirm the adequacy of the models in predicting the forces generated in the press fit technique using SLM fabricated pins within the investigated parameter levels. Fig. 5.20 illustrated studentized residuals vs. predicted values which revealed that all colour points representing mean If and RF had been scattered randomly and uniformly close to zero-axis and had constant range of residual across the graph which illustrated absence of constant variance. The graph in Fig. 5.21 shows a guideline for choosing the correct model. Based on the best lambda value, which is found at the minimum point of the curve generated by the auto selected. If the 95% Confidence Interval around this lambda shows one, then the software does not recommend a specific transformation.

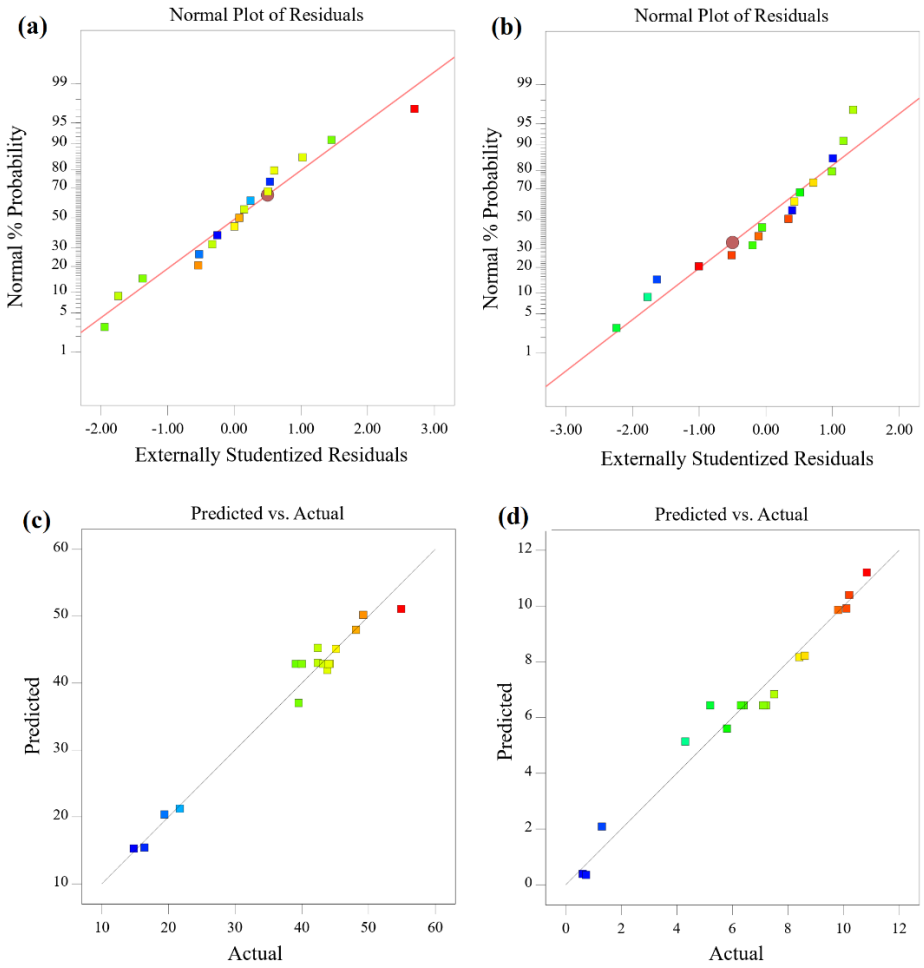

Fig. 5.19. Normal probability plots of the studentized residuals for IF and RF (a, b), predicted versus actual for IF and RF (c, d).

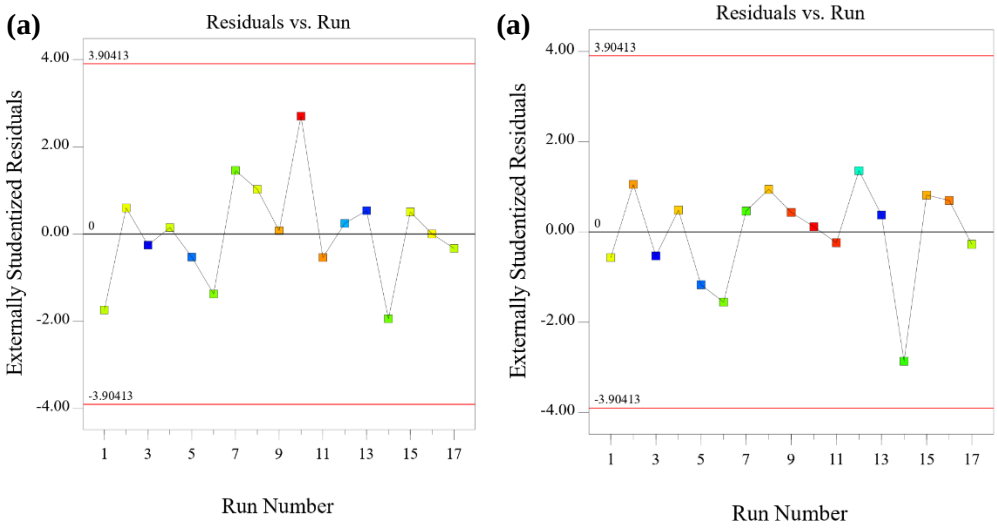

Fig. 5.20. Studentized residuals vs. predicted values plot, (a) for IF and (b) for RF

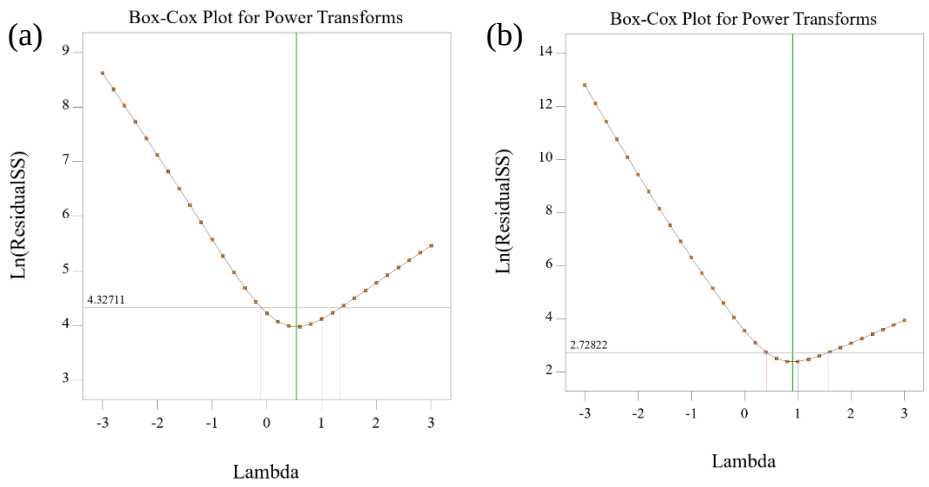

Fig. 21. Box-cox plots, (a) insertion force, (b) removal force

5.6.2. Validation of the developed models

In order to verify the adequacy of the developed models, four confirmation experiments for each texture were carried out, these experiments were randomly selected from the investigated range. Using the point prediction option in the software, all the response values can be predicted by substituting these conditions into the previous developed models. Table 5.9 presents the experiments condition, the actual experimental values, the predicted values and the percentages of error for all responses. It is clear that all the values of the percentage of the error for all the two responses are within good agreement (all errors are below 10%), indicating the validity of the models.

Table 5.9
Confirmation for randomly chose parameters within the investigated experimental range.

Exp no.	Factors			Values	Responses	
	Shape	Pitch (μm)	Height (μm)		IF (KN)	RF (KN)
1	Oval	800	500	Actual	39.745	7.6
				Predicted	43.0085	8.16375
				Error (%)	8.2112	6.9
2	Oval	600	700	Actual	43.82	8.1
				Predicted	43.0085	8.16375
				Error (%)	3.2438	6.386
3	Trapezoid	600	700	Actual	49.239	10.441
				Predicted	50.1914	9.9125
				Error (%)	1.9343	5.06
4	Triangular	800	700	Actual	47.931	10.83
				Predicted	51.071	11.8037
				Error (%)	6.5511	8.991

5.6.4. Effects of inputs on insertion and removal force

Due to the unique specifications of the AM process, stainless steel 316L pins were fabricated and characterized. In order to find the effect of shape, pitch size and height, various types of pins were prepared and tested by inserting them into hubs of defined size. The IF and RF were reported and then using RSM, the best conditions and effect of process parameters on responses for obtaining strong joints were evaluated. Fig. 5.19 shows contour plots of the effects of pitch, height and shape on the insertion and removal forces. Some important points can be drawn from this figure. First of all, as expected by increasing the height of texture IF and RF were dramatically increased. It is very important to note that before the final design of the presented texture geometries, different heights were evaluated in a set of screening experiments and it was found that a height in the range of 300-700 μm was suitable for this application. It can also be observed that when the maximum possible height is used, then there is less local response effect from the other input parameters on IF and RF.

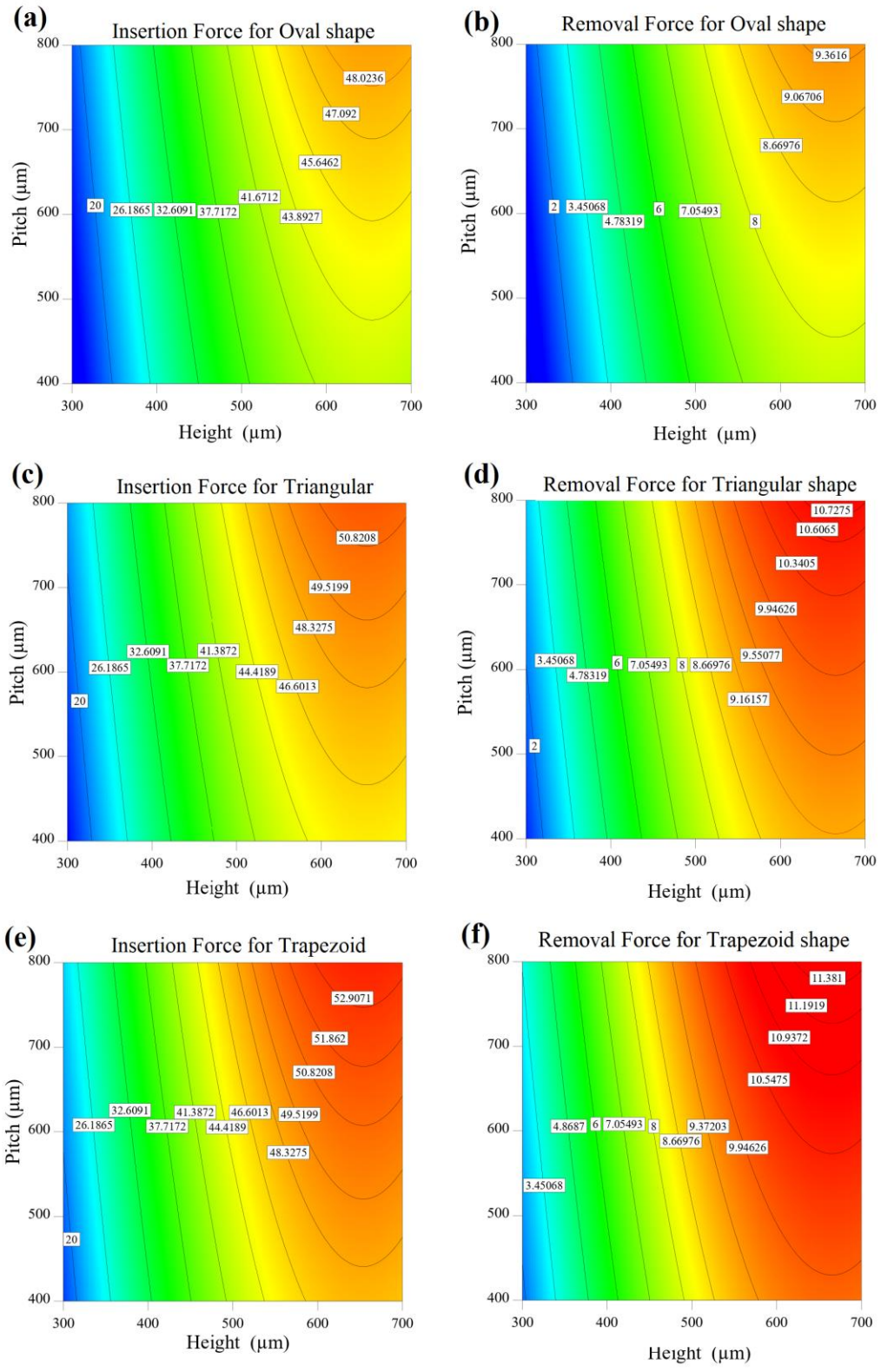

Fig. 5.22. Colour map contour plots of insertion and removal forces for the pitch, shape, and at the three different levels of height.

Secondly, from the Fig. 5.22 it is seen that that the highest values of IF and RF were obtained when the shape of texture is trapezoid, and the oval shape led to slight lower levels of joint strength. Fig. 5.23 shows the surface response morphology of some samples after insertion and removal, it can be expected that triangular shape could cause abrasive wear (see Fig. 5.23), while trapezoid shape generated more adhesion with the hub surface, while due to the limitations of AM process (see red-colored circle in Fig. 5.24b), the surface is rough and traces of abrasive wear as well was detected and shown in Fig. 5.24. Third, it was found that a higher pitch size where the height is high lead to maximum value of IF and RF.

In Figs. 5.23a and c, no considerable surface abrasion (elastic and plastic deformation) was detected for the samples 9 (triangular, pitch: 400 µm, and height: 300 µm) and 6 (trapezoid, pitch: 600 µm, and height: 300 µm). It was revealed that with the triangular texture (for example sample 10), IF and RF were at maximum values and related sample presented in Fig. 5.24b showed considerable abrasion (plastic deformation) of the surface after insertion and removal. It is interesting from the higher magnification SEM morphology of sample 6 (Fig. 5.7d) that the un-melted powders at the surface were smoothened due to the severe abrasion between the pin and hub surfaces during insertion and removal.

It can be observed that by altering the texture parameters, strong bonds can be formed in press-fit applications. Also, AM technology can be highly recommended for such applications after a suitable surface finish process. This study opens a new window for development of metal additive manufacturing for interference fit joining applications. In future, the effect of surface finishing processes after SLM also needs to be examined.

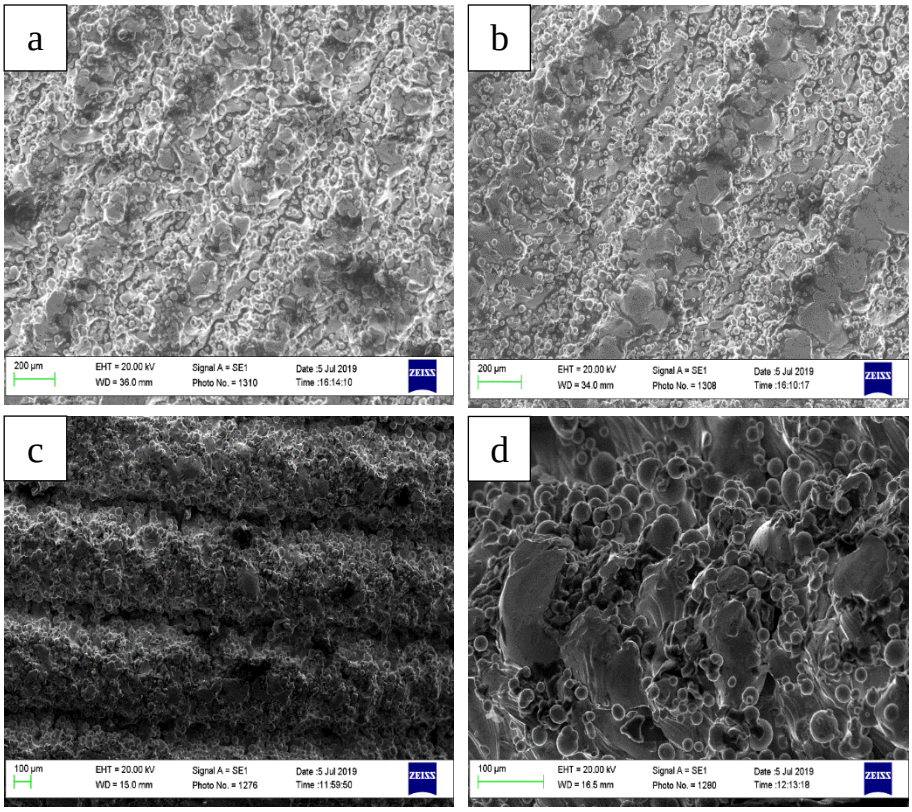

Fig. 5.23. SEM of the samples surface morphologies, after insertion and removal, of (a) sample 9, (b) sample 10, (c and d) low and high magnification of sample 6, and (d) high magnification of sample 12.

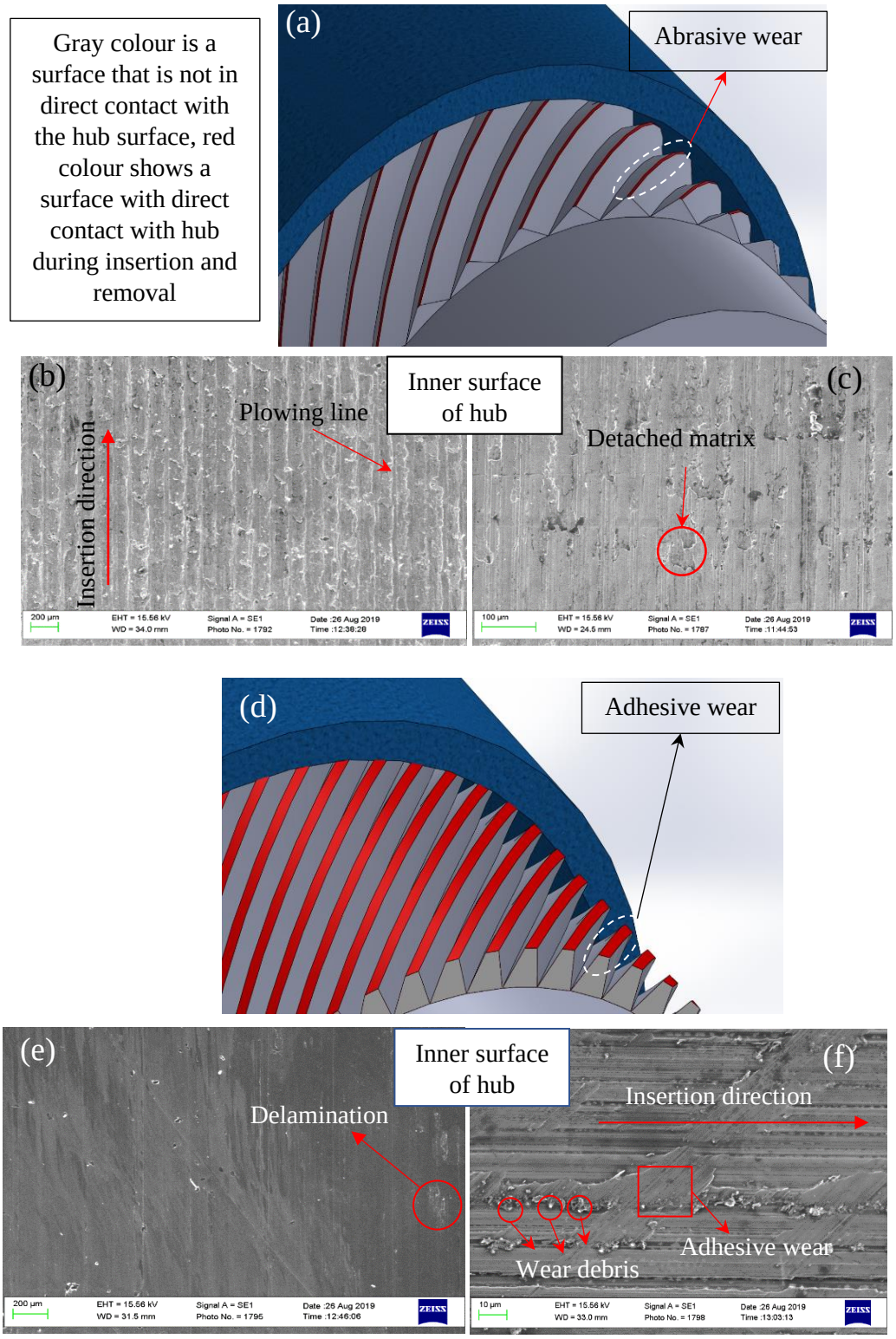

Fig. 5.24. Mechanisms of (a) abrasive wear and inner surface of pins after insertion force

5.7. Conclusion

A new approach for the manufacturing of metallic knurled press fit pins was developed in this study using the SLM process. The selective laser melted specimens with different types of texture specifications were evaluated by insertion/removal tests. A statistical and mathematical model was used to investigate the impact of input parameters on the bonding strength of press-fit joints. From the experimental and simulation results the following conclusions were drawn:

1- It was found that the texture height is the most significant impactful factor for resulting bond strength. The weakest bond strengths were obtained for the lowest profile heights of 300 µm. Insertion of pins into the hub was not possible for profile heights above 700 µm.

2- The shape of textures affects the joint bonding. The trapezoid profile had the highest positive impact on bond strength due to a large interaction area between the pin surface and the internal surface of the hub and a mixture of adhesive and abrasive wear.

3- The pitch dimension also effected the bond strength but to a much lower extent than the texture height. Larger values of pitch resulted in higher IF and RF values.

4- The RSM is an excellent technique for prediction of IF and RF from the produced texture specifications. The developed process models can be reliably used to predict the resulting insertion and removal bond strengths.

5- ANOVA analysis indicated that all inputs and their interaction terms including the shape, pitch size, height of the texture have significant effects on aforementioned outputs.

6- According to the results, the SLM process is a precise one-step method for manufacturing of such customized helical knurl metallic pins with a complex shape, although it has some limitations on the formation of smooth edges at the micrometre scale.

References

1. R.L Norton, Machine Design, 2011 (Fourth Edition) Pearson Education, New Jessey.

2. X. Wanga, Z. Loua, X. Wang, C. Xu, A new analytical method for press-fit curve prediction of interference fitting parts, Journal of Materials Processing Tech. 250 (2017) 16–24.

3. R. Mengel, J. Haberle, M. Schlimmer, Mechanical properties of hub/shaft joints adhesively bonded and cured under hydrostatic pressure, International Journal of Adhesion & Adhesives 27 (2007) 568–573.

4. P. roche*, S. Wohletz, M. Brenneis, C. Pabst, F. Resch, joining by forming—A review on joint mechanisms, applications and future trends, Journal of Materials Processing Technology 214 (2014) 1972–1994.

5. S. D. Mariottia, P. Amieuxb, A. P. Hamrib, V. Augerc, G. Kermouched, F. Valiorguee, S. Valettea, Effects of micro-knurling and femtosecond laser micro texturing on aluminium long-term surface wettability, Applied Surface Science 479 (2019) 344–350.

6. M. A. Obeidi, E. McCarthy, D. Brabazon, Laser surface processing with controlled nitrogen-argon concentration levels for regulated surface lifetime, Optics and Lasers in Engineering 102 (2018) 154–160.

7. M. A. Obeidi, E. McCarthy, D. Brabazon, Methodology of laser processing for precise control of surface micro-topology, Surface & Coatings Technology 307 (2016) 702–712.

8. A. Townsenda, N. Seninb, L. Blunta, R.K. Leach, J.S. Taylor, Surface texture metrology for metal additive manufacturing: a review, Precision Engineering 46 (2016) 34–47.

9. M. A. Obeidi, Eanna McCarthy, L. Kailasc, D. Brabazona, Laser surface texturing of stainless steel 316L cylindrical pins for interference fit applications, Journal of Materials Processing Tech. 252 (2018) 58–68.

10. F. Bartolomeua, M. Buciumeanub, E. Pintoc, N. Alvesc, O. Carvalhoa, F.S. Silva a, G. Miranda, 316L stainless steel mechanical and tribological behavior—A comparison between selective laser melting, hot pressing and conventional casting, Additive Manufacturing 16 (2017) 81–89.

11. B. Song, X. Zhao, S. Li, C. Han, Q. Wei, S. Wen, J. Liu, Y. Shi, Differences in microstructure and properties between selective laser melting and traditional manufacturing for fabrication of metal parts: A review, Front. Mech. Eng. 2015, 10(2): 111–125.

12. P. K. Gokuldoss, S. Kolla and Jürgen Eckert, Additive Manufacturing Processes: Selective Laser Melting, Electron Beam Melting and Binder Jetting—Selection Guidelines, Materials 2017, 10, 672.

13. Z. Sun, X. Tan, S. B. Tor, W. Y. Yeong, Selective laser melting of stainless steel 316L with low porosity and high build rates, Materials and Design 104 (2016) 197–204.

14. E. Liverani, S. Toschi, L. Ceschini, A. Fortunato, Effect of selective laser melting (SLM) process parameters on microstructure and mechanical properties of 316L austenitic stainless steel, Journal of Materials Processing Tech. 249 (2017) 255–263.

15. J. Metelkova, Y. Kinds, K. Kempen, C. d. Formanoir, A. Witvrouw, B. V. Hooreweder, On the influence of laser defocusing in Selective Laser Melting of 316L, Additive Manufacturing 23 (2018) 161–169.

16. Luana Bottini, A. Boschetto, Interference fit of material extrusion parts, Additive Manufacturing 25 (2019) 335–346.

17. T. Heeling, K. Wegener, the effect of multi-beam strategies on selective laser melting of stainless steel 316L, Additive Manufacturing 22 (2018) 334–342.

18. J. Suryawanshia, K.G. Prashanthb,c, U. Ramamurtya, Mechanical behavior of selective laser melted 316L stainless steel, Materials Science & Engineering A 696 (2017) 113–121.

19. C. Qiu, M. A. Kindi, A. Salim Aladawi, I. A. Hatmi, A comprehensive study on microstructure and tensile behaviour of a selectively laser melted stainless steel, SciEntific Reports, (2018) 8:7785.

20. T. Zhong, K. He, H. Li, L. Yang, Mechanical properties of lightweight 316L stainless steel lattice structures fabricated by selective laser melting, Materials & Design (2019).

21. M. Yakout, M.A. Elbestawi, S. C. Veldhuis, Density and mechanical properties in selective laser melting of Invar 36 and stainless steel 316L, Journal of Materials Processing Tech. 266 (2019) 397–420.

22. Jonathan Lawrence, Advances in Laser materials processing technology, research and applications, Woodhead Publishing, Elsevier, 2018.

23. H. Sohrabpoor, S. Negi, H. Shaiesteh, I. U. Ahad, D. Brabazon, Optimizing selective laser sintering process by grey relational analysis and soft computing techniques, Optik - International Journal for Light and Electron Optics 174 (2018) 185–194.

24. A. Y. Alfaify, J. Hughesa, K. Ridgwaya, Critical evaluation of the pulsed selective laser melting process when fabricating Ti64 parts using a range of particle size distributions, Additive Manufacturing 19 (2018) 197–204.

25. Peng Wena, L. Jauerb, M. Voshagec, Y. Chend, R. Popraweb, Johannes Henrich Schleifenbaum, Densification behaviour of pure Zn metal parts produced by selective laser melting for manufacturing biodegradable implants, Journal of Materials Processing Tech. 258 (2018) 128–137.

26. K.Y. Benyounis, A.G. Olabi, M.S.J. Hashmi, Multi-response optimization of CO2 laser-welding process of austenitic stainless steel, Optics & Laser Technology 40 (2008) 76–87.

Chapter 6
Conclusions and Future Work

This work presented in this thesis was focused on the development of predictive models for the laser sintering and texturing process. In Chapter 3, the optimisation of the SLS process with glass fibre reinforced polyamide was presented. ANFIS, SA, and Grey relational analysis was used for this work. In Chapter 4, the prediction of laser generated surface textures was implemented using neural network and neuro-fuzzy inference models. In Chapter 5, SLM produced interference fit pins were generated and tested according to a DoE and response surface methodology, for interference fit bond strength.

Laser processing is a mature method, developed over several decades and used widely in industry due to the reliability and repeatability of the process. However, laser mater interaction in the SLS and texturing processes is a more complex phenomenon and involves a number of physical and chemical processes such as heat transfer, breaking and building of chemical bonding, plasma creation, melting and solidification occur.

In order to predict the behaviour of the laser sintering process for future or unknown conditions, the existing laser sintering results must be examined in detail to generate new information. This information can be further processed by different machine learning and artificial intelligence techniques. Predictive modelling techniques can be used to understand different patterns available within large sets of data.

In this thesis, in terms of simulation, the latest AI and mathematical types of modelling and multi objective optimization methods were applied and their performances examined in the newly developed laser-based manufacturing process. In addition, for the first time, SLM was utilized as a new way of fabrication method in knurled pins with 316L stainless steel material and optimised for interference fit pin strength. An overview of the main findings from this work is presented at the end of each chapter; a summary of these are presented below.

6.1. Conclusions from chapter 3

1. An ANFIS based on 2-2-2-2-2-2 structure with Psigmoidal type of MFs led to maximum precision of modelling for tensile strength and elongation by making the minimum values of prediction error in SLS process.
2. In optimization of the SLS procedure by ANFIS-SA, the part bed temperature of 180 °C, laser power of 29 W, scan speed 30 mm/s, scan spacing 0.37 m and scan length 133 mm resultant in optimal solution with tensile strength of 34 N/mm^2 and elongation of 11%.
3. The results of validation experiment with GRA and ANFIS-SA approaches are Closely consistent and can be used for further research.
4. Due to the ability of ANFIS-SA to search the entire solution space within the process. This resulted in an increase of the overall tensile strength and elongation results obtained by 14.78 N/mm^2 and 6.4 % respectively for the output of ANFIS-SA compared to GRA in SLS process.
5. Based on our experiences, we can suggest that ANFIS-SA be an effective approach to solving a multi-objective optimization problem in manufacturing processes which responses related in a complex manner to the input parameters.

6.2. Conclusions from chapter 4

1. By testing and training of various FFNN, in LST process, 3-5-1 structure for DI and IF and 3-7-1 structure for RF were selected as a lowest MAE. ANFIS 2-2-2 structure with Gaussian2 MF and backpropagation optimization, D sigmoidal MF and hybrid, and Pi shaped MF showed the lowest RMSEs for DI, IF and RF, respectively.
2. Similar to SLS process, the ANFIS model produce lower values of PEP compared to FFNN in LST procedure. ANFIS is the most powerful simulation for approximation and analysis of the responses. The ANFIS has some advantages over FFNN, including the ability to capture the nonlinear structure of a process, adaptation capability, and rapid learning capacity. ANFIS has the advantage to combine both ANN and Fuzzy knowledge. So ANFIS is more precise in term of prediction.

3. The fact that the laser surface texturing processing technologies are really high-cost process, the developing model can give a vision regarding to the selecting of best process parameters without needing to a high number of experiments. Otherwise stated, to reach desirable performance in each process, the developed model is beneficial to select optimal parameters without conducting extensive experiments and it has a strong economic justification.

4. Since ANFIS has proven a good tool for approximation of results, ANFIS model can be applied as objective function to select optimal parameters of manufacturing process, in which the process reaches to its desirable mechanical properties by using metaheuristic algorithms such as simulated annealing algorithm, bee colony and etc.

6.3. Conclusions from chapter 5

1. It was found that the texture height is the most significant impactful factor for resulting bond strength. The weakest bond strengths were obtained for the lowest profile heights of 300 µm. Insertion of pins into the hub was not possible for profile heights above 700 µm.

2. The shape of textures affects the joint bonding. The trapezoid profile had the highest impact on the bonding due to a large interaction area between the pin surface and the internal surface of the hub and a mixture of adhesive and abrasive wear.

3. The pitch dimension also effected the bond strength but to a much lower extend than the texture height. Larger values of pitch resulted in higher IF and RF values.

4. The RSM is an excellent technique for prediction of IF and RF from the produced texture specifications. The developed process models can be reliably used to predict the resulting insertion and removal bond strengths.

5. ANOVA analysis indicated that all inputs and their interaction terms including the shape, pitch size, height of the texture have significant effects on aforementioned outputs.

6. According to the results, SLM process is a precise one-step method for manufacturing of such customized helical knurl metallic pins with a complex shape, although it has some limitations on the formation of smooth edges at the micrometre scale.

6.4. Future Work

In selective laser sintering, the proposed model from ANFIS-SA can be examined to the different material and the results can be compared with the obtained simulation. Since ANFIS has proven a good tool for approximation of results, ANFIS model can be applied as objective function to select optimal parameters of manufacturing process, in which the process reaches to its desirable mechanical properties by using the metaheuristic algorithms such as simulated annealing algorithm, bee colony and etc.

In the fabrication of 316l interference fit joins, pre-heating can be taken into the account and compare to the insertion and pull-out force of cold joints. In addition to that, in order to study the effect of adhesive and abrasive wears, different types of material can be examined. Also, various post-processing techniques can be applied to improve the mechanical properties, accuracy, and appearance of the press fit joints printed parts including annealing and sandblasting and etc.